Politecnico di Torino

Master degree of Physics of Complex Systems Master degree thesis Graduation Session October 2025



On some generalisations of the Car-Oriented approach to the Totally Asymmetric Simple Exclusion Process

Supervisors
Alessandro Pelizzola
Marco Pretti

Candidate Fulvio Bergadano

Contents

In	troduction	1
1	The TASEP Model 1.1 The Master Equation	3 5 7
2	 k-Cluster approximations 2.1 The Mean-Field approximation 2.1.1 The Mean-Field Stationary State 2.2 The Pair approximation 2.2.1 The Stationary State 2.3 The Triplet approximation 2.3.1 Comparison between the 1,2,3-Cluster approximations 	11 12 13 15 15 16
3	The Car-Oriented approach 3.1 Previous studies on the Car-Oriented Mean-Field approximation 3.1.1 The COMF approximation for the NaSch model 3.1.2 The COMF approximation for the Shuffled Dynamics 3.2 The Car-Oriented Equation 3.3 The Car-Oriented Mean-Field approximation 3.4 The Car-Oriented Pair approximation 3.5 The Car-Oriented Triplet approximation 3.5.1 Comparison between the Car-Oriented Triplet and the Triplet approximations	21 21 22 23 24 25 27 28
4 Co	The Queue-Oriented approach 4.1 The Queue-Oriented Equation	40 41 42 43
	Derivations A.1 From the Master Equation to the Continuity Equation	47 47 48
В	Notes B.1 The COTR approximation in detail	50 50 51 51

Introduction

One of the most fascinating aspects of the Physics of Complex Systems is its ability to provide connections between apparently very different fields of science by giving a minimalist mathematical description of some specific class of systems, which is often discovered only a posteriori to describe a much greater family of phenomena. One of the most paradigmatic examples is the Ising model: born in 1920 to study the behaviour of ferromagnets [1], it has been proven capable of describing a huge variety of phenomena, ranging from the liquid-gas transition in simple fluids [2] to the social opinion and voting models [3], including order-disorder transition in binary alloys (such as CuZn, i.e. brass) [4], adsorption of particles on surfaces [5] and DNA denaturation through helix-coil transitions [6], as well as many other examples. This model has become a cornerstone of equilibrium statistical physics. At a similar level, in the context of non-equilibrium statistical physics, the Totally Asymmetric Simple Exclusion Process (TASEP) has reached a paradigmatic state in the framework of driven systems. As often happens in the field of complex systems, the inspiring source was biology: the TASEP model was developed in 1968-69 by C. T. MacDonald and J. H. Gibbs [7, 8] to study the dynamics of ribosomes along mRNA filaments during protein synthesis. Then, it soon attracted growing interest and met a number of applications in various fields, way beyond the biological framework (we briefly mention a few of these applications at the beginning of chapter 1). Moreover, as a matter of history, it brought the conceptual breakthrough of boundary induced phase-transitions in a one-dimensional system (for short-range one-dimensional equilibrium systems no finite temperature phase transition is observed), which made it worthy of some purely theoretical interest going well beyond its applications. The ubiquity and appeal of TASEP come from its simplicity: it includes only the very minimal number of elements to describe the ribosomes' dynamics; nevertheless, the equations are highly non-trivial and exact solutions can be found in only a few cases. Thus, a lot of attention has been devoted, in recent years, to the development of new approximation techniques suitable for the TASEP model and its generalisations. This is also the purpose of the present thesis.

In our work, we develop some generalisations of the Car-Oriented Mean-Field approach, firstly introduced in the nineties by A. Schadschneider and M. Schreckenberg [9] in order to study the homogeneous Nagel-Schreckenberg model (a generalisation of the TASEP model which describes vehicular — rather than biological — traffic) in Periodic Boundary Conditions. We extend this approach to the case of an inhomogeneous TASEP in Open Boundary Conditions (OBC) and to different kinds of approximations, which we study mainly at the stationary state. Moreover, we generalise the spirit of the Car-Oriented variables to some new set of variables, that we call the Queue-Oriented variables, for which we develop some new, similar approximations.

The thesis is structured in four chapters, divided in the following way.

- Chapter 1 analyses the biological motivation underlying the TASEP model, discusses some of its applications and introduces the fundamental equations, summarising the main analytical results for the stationary state and some elements of the disordered TASEP.
- Chapter 2 discusses the application of the cluster approximations to TASEP, with particular attention devoted to the stationary state and to the case of inhomogeneities.
- Chapter 3 presents some generalisations of the Mean-Field-like approximation to the Car-Oriented variables and compares with the approximations shown in chapter 2.
- Chapter 4 describes the introduction of new variables, presented as a generalisation of the Car-Oriented ones and compares with the latter.

I. The TASEP Model

In this chapter we introduce the inhomogeneous TASEP model with Open Boundary Conditions, starting from the biological background and arriving at the Master Equation. The Stationary State will be presented in detail, with a discussion of the exact results for the homogeneous case and a brief review of the current state of the art for the inhomogeneous case, supported by comparisons with Monte-Carlo simulations.

Protein synthesis is a complex and fascinating polymerisation process: it lies at the heart of cellular metabolism and is required for the conversion of genetic information from mRNA into protein. The translation of the mRNA filament is carried out by multiple ribosomes and consists in four main steps: initiation, elongation, termination and recycling. The ribosomes attach to mRNA filaments at the 5' end and they sequence the filament in the $5' \rightarrow 3'$ direction, proceeding one codon at a time and binding with a probability that depends on the codon-ribosome interaction strength [10]. A ribosome cannot proceed to the following codon if the latter is already occupied. When a ribosome arrives at the 3' end, it encounters some release factors that hydrolyse the chemical bond with the mRNA filament and free the completed protein, while other factors disassemble the ribosome for reuse.

This biological framework motivated physicists to develop the TASEP model, which describes the ribosomes' dynamics in that it is totally asymmetric, one-dimensional, discrete in space, stochastic and — most importantly — it is a simple exclusion process. Particles occupy only one node at a time and can hop in only one direction, from each node to the adjacent one — provided the latter is empty — with a certain rate. In the case of OBC, particles can enter the lattice only at the first site and can leave the lattice only at the end of it, with fixed injection and extraction rates. A scheme of the TASEP dynamics with OBC is represented in figure 1.1

This is a minimalist description of the ribosomes' dynamics, and the TASEP model does not account for many aspects of it. Chief among them are the following.

- (i) Ribosomes are actually much larger than codons (approximately $10 \div 12$ times the size of a codon), so they occupy more than one site at a time [11].
- (ii) They can detach also at internal sites before the 3' end has been reached. This phenomenon is known as 'drop-off' and has some relevant biological consequences for the cell [12].
- (iii) They can bind to the filament also at specific sites called 'internal ribosome entry sites' along of it, although this phenomenon is rare in eukaryotic cells and has mainly been observed in viruses [13].
- (iv) Initiation and termination strongly depend on the environment and its evolution [14, 15], whereas in our model they are constant parameters. Moreover, they are connected one another through recycling, which in general couples the initiation of one filament to all the other filaments in the cell [16].

Some extensions of the model take into consideration these aspects. The 'TASEP with extended particles' [17] accounts for the ribosomes' size; the TASEP with 'closed-loop' dynamics takes into account recycling in that it couples the injection and extraction rates [18, 19], and in the 'TASEP with Langmuir Kinetics' particles are allowed to attach or detach from the chain at any site (although this model has actually been created to describe the motion of molecular motors on actin filaments) [20].

These are only a few of extensions of the TASEP model, and many have been formulated in order to describe a wide variety of phenomena, both in biological and non-biological contexts. For instance, in biology, it has been applied successfully — especially in its more general version, the Partially Asymmetric Simple Exclusion Process (PASEP), which relaxes the unidirectional motion constraint

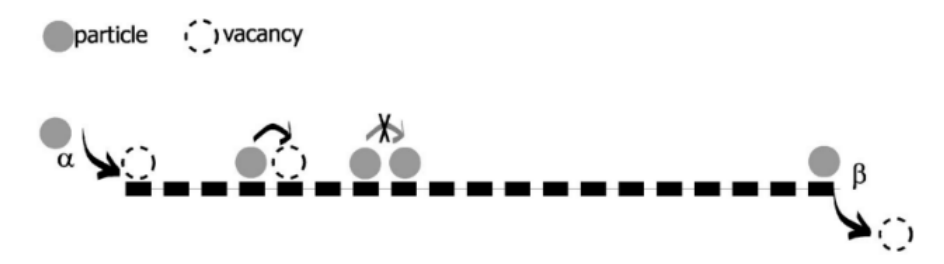


Figure 1.1: A scheme of TASEP dynamics with OBC.

[21] — to describe the biopolymerisation [22], the diffusion through membrane channels [23], the gel electrophoresis [24] and the bacterial movement [25], as well as the previously mentioned kinetics of molecular motors and protein synthesis. Outside of the biological context, the TASEP framework has found important applications in the study of vehicular traffic. For example, the Nagel–Schreckenberg model [26] (briefly reviewed in Section 3.1) allows particles to travel at variable speeds, whereas other models explicitly describe a human driver's reaction to the vehicle ahead [27]. Other interesting applications are the Exclusive Queueing Process, a model born to describe the pedestrian queueing which is equivalent to a TASEP of varying length [28], and the study of the one-dimensional surface growth in a two-dimensional dense medium [25]. Moreover, the TASEP model is amenable to a game-theoretic interpretation, particularly in the context of multi-population systems with label switching. In this setting, nodes can be interpreted as interacting agents (exchanging particles) that inhabit a two-state space: occupied/unoccupied (or, in the language of game theory, leader/follower), with certain transition rates. Some works in this direction are [29, 30].

In this thesis, we investigate only the minimalist version of TASEP with OBC and possibly inhomogeneous rates, in continuous time. At each instant of time, we can define the configuration $\underline{n}^t \in \{0,1\}^L$, that is a vector of L boolean variables, representing the occupation state of each node $\ell \in \{1,\ldots,L\}$ for a chain of length L. The central quantity of the model is

$$P^{t}[\underline{n}] := \mathbb{P}\{n_1^t, n_2^t, \dots, n_L^t\},\$$

i.e. the probability that the occupation number of nodes 1, ..., L are $n_1, ..., n_L$, at time t. It allows to introduce the density vector $\underline{\rho}^t \in [0,1]^L$, i.e. a stochastic variable whose entries are the average number of particles per site:

$$\underline{\rho}^t \coloneqq \sum_{n} \underline{n}^t P^t[\underline{n}] \coloneqq \langle \underline{n}^t \rangle.$$

We will consider, in the most general case, non-uniform hopping rates $r_\ell \in \mathbb{R}_+$ from node ℓ to node $\ell+1$ for $\ell \in \{1,\ldots,L-1\}$ and will denote by α and β the injection and extraction rates, respectively, which belong to the interval (0,1]. We assume all these quantities are non-dimensional. A crucial feature of the model is the particle-hole (PH) symmetry, as the hopping of one particle from one node to the following is equivalent to the hopping of a hole in the opposite direction. The PH transformation for a homogeneous system consists in the mappings $n_\ell^t \mapsto 1 - n_{L-\ell+1}^t$, $\alpha \leftrightarrow \beta$; while for an inhomogeneous system it also involves $r_\ell \leftrightarrow r_{L-\ell} \quad \forall \ell \in \{1,\ldots,L-1\}$. The PH symmetry comes as an invariance of the probability $P^t[\underline{n}]$ for such transformations.

1.1 The Master Equation

The evolution of the probability $P^{t}[n]$ is described by the master equation

$$\dot{P}^t[\underline{n}] = \sum_{\underline{m}} W_{\underline{n}\underline{m}} P^t[\underline{m}],$$

where the sum over \underline{m} involves 2^L terms (i.e. all possible \underline{m} configurations) and where $W_{\underline{n}\underline{m}}: \{0,1\}^L \times \{0,1\}^L \mapsto \mathbb{R}$ is an element of the transition matrix $\mathbf{W} \in \mathbb{R}^{2^L \times 2^L}$ describing the transition rate from

configuration \underline{m} to configuration \underline{n} . The normalisation of the probability yields a constraint on the columns of **W**:

$$\sum_{n} P^{t}[\underline{n}] = 1 \quad \forall t \iff \sum_{n} \sum_{m} W_{\underline{n}\underline{m}} P^{t}[\underline{m}] = 0 \quad \forall t \iff \sum_{n} W_{\underline{n}\underline{m}} = 0.$$

This constraint is normally encoded in the condition

$$W_{\underline{n}\underline{n}} = -\sum_{\underline{\nu} \neq \underline{n}} W_{\underline{\nu}\underline{n}}.$$

Although the space **W** belongs to is very high-dimensional, the transition matrix is highly sparse. Moreover — since we are considering a continuous-time model — we make allowance for at most one event (injection, hopping from one node to the next one and extraction) to modify the configuration in the infinitesimal time interval. So the only possible transitions are those between configurations that are separated by only one event. This entails that

$$W_{\underline{n}\underline{m}} = \sum_{k=0}^{L} W_{\underline{n}\underline{m}}^{(k)},$$

where $W_{\underline{n}\underline{m}}^{(0)}$ denotes the injection event; terms $W_{\underline{n}\underline{m}}^{(k)}$ for $k \in \{1, ..., L-1\}$ describe the hoppings from node k to node k+1 and $W_{\underline{n}\underline{m}}^{(L)}$ represents the extraction. Thus,

(i)
$$W_{\underline{nm}}^{(0)} = \alpha \delta_{m_1,0} \left(\prod_{i>1} \delta_{n_i,m_i} \right) (2n_1 - 1)$$

(ii)
$$W_{\underline{nm}}^{(k)} = r_k \delta_{m_k,1} \delta_{m_{k+1},0} \left(\prod_{i \neq k,k+1} \delta_{m_i,n_i} \right) (n_{k+1} - n_k)$$

(iii)
$$W_{\underline{n}\underline{m}}^{(L)} = \beta \delta_{m_L,1} \left(\prod_{i < L} \delta_{n_i,m_i} \right) (1 - 2n_L).$$

Plugging this expression into the Master Equation, it is possible to find the evolution of $P^t[\underline{n}]$ and, by marginalisation, the evolution of the probability of any cluster:

$$\dot{P}_{\ell}^{t}[n_{\ell}\cdots n_{\ell+\lambda}] = \sum_{\{n_{i}\}_{i<\ell}\cup\{n_{i}\}_{i>\ell+\lambda}} \dot{P}_{\ell}^{t}[\underline{n}] = \sum_{\{n_{i}\}_{i<\ell}\cup\{n_{i}\}_{i>\ell+\lambda}} \sum_{\underline{m}} \sum_{k=0}^{L} W_{\underline{n}\underline{m}}^{(k)} P^{t}[\underline{m}].$$

In particular, the evolution of the density $ho_\ell^t \equiv P_\ell^t[1]$ is

$$\dot{\rho}_{1}^{t} = \alpha (1 - \rho_{1}^{t}) - r_{1} P_{1}^{t} [10] := J_{0}^{t} - J_{1}^{t}
\dot{\rho}_{\ell}^{t} = r_{\ell-1} P_{\ell-1}^{t} [10] - r_{\ell} P_{\ell}^{t} [10] := J_{\ell-1}^{t} - J_{\ell}^{t} \quad 1 < \ell < L
\dot{\rho}_{L}^{t} = r_{L-1} P_{L-1}^{t} [10] - \beta \rho_{L}^{t} := J_{L-1}^{t} - J_{L}^{t},$$
(1.1)

where the vector $\underline{f}^t \in [0,1]^{L+1}$ collects the currents, with J_ℓ^t denoting the probability of a particle hopping from node ℓ to node $\ell+1$ at time t, and J_0^t , J_L^t denoting, respectively, the probability of injecting and extracting a particle at time t. The derivation of this equation is obtained in the appendix A.1. An equivalent, handy notation — which we will often use in the following — is to introduce two fictitious nodes: node 0 at the left end of the chain and node L+1 at the right end of it. These nodes are respectively always occupied and always empty and have rates $r_0 := \alpha$, $r_L := \beta$. Alternatively, one can view nodes 1 and L as if they were in contact with two infinite reservoirs: the one at the left with density α and the one at the right with density α and the one at the right with density α and the following, we will deal more often with the first description. Exploiting the fictitious nodes, we can compactify equation (1.1) in the following way

$$\dot{\rho}_{\ell}^{t} = r_{\ell-1} P_{\ell-1}^{t}[10] - r_{\ell} P_{\ell}^{t}[10] = J_{\ell-1}^{t} - J_{\ell}^{t} \quad \forall \ell \in \{1, \dots, L\},$$
(1.2)

which is the continuity equation. The quantities $P_{\ell}^{t}[10]$ evolve according to the following equation

$$\dot{P}_{\ell}^{t}[10] = r_{\ell-1}P_{\ell-1}^{t}[100] - r_{\ell}P_{\ell}^{t}[10] + r_{\ell+1}P_{\ell}^{t}[110]. \tag{1.3}$$

The characteristic feature of the TASEP dynamics already manifests in these equations and can be generalised to all marginals: the evolution of the probability of a cluster of k nodes depends on probabilities of clusters of length k+1. This generates a hierarchy of equations which grows exponentially with the size of the system and becomes infinite in the thermodynamic limit, making the model highly non-trivial. In general, it becomes necessary to close the system with some sort of approximation: this is indeed the spirit behind all the approximations presented in this work.

Another important aspect, already visible here, is that at the stationary state (which we denote by dropping the superscript t) the left-hand-sides of equation (1.2) vanish, thus implying $J_{\ell-1} = J_{\ell} \equiv J$. This has two important consequences: first, the continuity equation directly yields a form of translational invariance, at the stationary state; second, even in the stationary state, the current is non-zero, which breaks the detailed balance condition and thus makes the TASEP steady-state a non-equilibrium stationary state.

1.2 The Stationary State

Although, as previously mentioned, the system of equations is highly non-trivial, an exact solution for the stationary state has been found, firstly using recursive relations [31] in 1992 and, in 1993, using the Matrix Product Ansatz technique [32]. Here we only review some of the most fundamental features of the stationary state (in particular for the case of unit innter rates $r_{\ell} = 1 \ \forall \ell \in \{1, \ldots, L-1\}$), which will be useful to keep in mind when comparing with our results.

In the case of uniform inner rates, the density profile depends solely on the values of α and β , and different phase transitions are observed when varying these values. Indeed, the TASEP model is paradigmatic for so-called boundary-induced phase transitions [33]. When the internal hopping rates are uniform, α and β effectively act as boundary bottlenecks. The steady state phase is determined by the most restrictive element — either the injection rate, the extraction rate, or the bulk — depending on which imposes the strongest constraint on the current.

- The phase $\alpha < 1/2$ and $\alpha < \beta$ is called 'Low-Density' (LD) phase, which, for *L* large enough (with respect to the characteristic length), is characterised by a bulk region with density corresponding to $\rho = \alpha$ and by a boundary layer at the right extremum, whose features depend on the values of the injection and extraction rates.
 - In the case β < 1/2, the boundary layer is purely exponential. Indeed, in the thermodynamic limit and at distance ℓ from the right boundary, the asymptotic behaviour gives

$$\rho_{L-\ell} - \alpha \to (1 - 2\beta) \left(\frac{\alpha(1 - \alpha)}{\beta(1 - \beta)} \right)^{\ell+1} \propto e^{-\ell/\xi},$$

where ξ is the characteristic length

$$\xi^{-1} = -\ln \frac{\alpha(1-\alpha)}{\beta(1-\beta)}.$$

This subphase is called 'LD-I'.

– In the case $\beta > 1/2$, the boundary layer has an additional power-law correction:

$$\rho_{L-\ell} - \alpha \to \left[\frac{1}{(2\beta - 1)^2} - \frac{1}{(2\alpha - 1)^2} \right] \frac{4^{\ell}}{\sqrt{\pi}\ell^{3/2}} \left[\alpha (1 - \alpha) \right]^{\ell+1} \propto \ell^{-3/2} e^{-\ell/\xi_{\alpha}}$$

where ξ_{α} is the characteristic length

$$\xi_{\alpha}^{-1} = -\ln[4\alpha(1-\alpha)].$$

This subphase is called 'LD-II'.

The two endpoint densities are $\rho_1=\alpha$, $\rho_L=\frac{\alpha(1-\alpha)}{\beta}$. They can be understood considering the aforementioned reservoirs picture. The density ρ_1 reflects a local equilibrium with the left reservoir, which has density α . Taking the expression of $J_0^t=\alpha(1-\rho_1^t)$, it can immediately be seen that $\rho_1=\alpha$ implies that the value of the translational invariant current is $J=\alpha(1-\alpha)$. On the other hand, considering the expression for $J_L^t=\beta\rho_L^t$, this gives a value of the right density equal to $\rho_L=J/\beta=\frac{\alpha(1-\alpha)}{\beta}$.

• The phase $\beta < 1/2$ and $\beta < \alpha$ is called the 'High-Density Phase' (HD phase) and it is just the PH symmetric of the LD phase. Thus, it presents a bulk density corresponding to $\rho = 1 - \beta$ and two subphases called 'HD-I' and 'HD-II' where the boundary layer at the left is described by the formulas above, only PH transformed. In particular, the characteristic length ξ becomes

$$\xi^{-1} = -\ln \frac{\beta(1-\beta)}{\alpha(1-\alpha)},$$

so that an expression for ξ valid for both the LD and HD phases is

$$\xi^{-1} = \left| \ln \frac{\alpha (1 - \alpha)}{\beta (1 - \beta)} \right|.$$

The boundary layer is now at the left of the chain, due to the space inversion $\ell \mapsto L - \ell + 1$. Instead, the characteristic length ξ_{α} of subphase LD-II is mapped to

$$\xi_{\beta}^{-1} = \ln[4\beta(1-\beta)].$$

The two endpoint densities are $\rho_1=1-\frac{\beta(1-\beta)}{\alpha}$, $\rho_L=1-\beta$. These can be interpreted just as in the LD phase, with the reservoirs swapped together with the values of α and β .

• The phase $\alpha, \beta > 1/2$ is called the 'Maximal Current Phase' (MC phase), where the profile presents a double boundary layer described by a pure power-law (in the thermodynamic limit, as above), which at the left border reads

$$ho_\ell - rac{1}{2}
ightarrow rac{1}{2\sqrt{\pi\ell}} + \mathcal{O}\Big(\ell^{-3/2}\Big)$$

and at the right border is

$$\rho_{L-\ell} - \frac{1}{2} \rightarrow -\frac{1}{2\sqrt{\pi\ell}} + \mathcal{O}\left(\ell^{-3/2}\right).$$

The endpoint densities are $\rho_1=1-\frac{1}{4\alpha}$ and $\rho_L=\frac{1}{4\beta}$. They stem from the value of the current, corresponding to $J_{\text{MC}}=\frac{1}{4}$ — which is the maximum possible value of the current in the Periodic Boundary Conditions and in OBC when $L\to\infty$, hence the name of this phase — and is independent of the boundary rates.

Figure 1.2 represents the phase diagram of the stationary state. The line $\alpha=\beta<1/2$ is called the 'coexistence line' and represents a phase transition from the LD to the HD phase. This is signalled by the correlation length $\xi^{-1}=-\ln\left|\frac{\alpha(1-\alpha)}{\beta(1-\beta)}\right|$, which diverges when $\alpha\to\beta<1/2$. When $\alpha=\beta<1/2$, the system presents a density profile which is simply a straight line connecting the values of α on the left to the value of $1-\alpha$ on the right (which correspond, respectively to the bulk density of the LD phase and the bulk density of the HD phase). This phase transition is thus discontinuous in the bulk density.

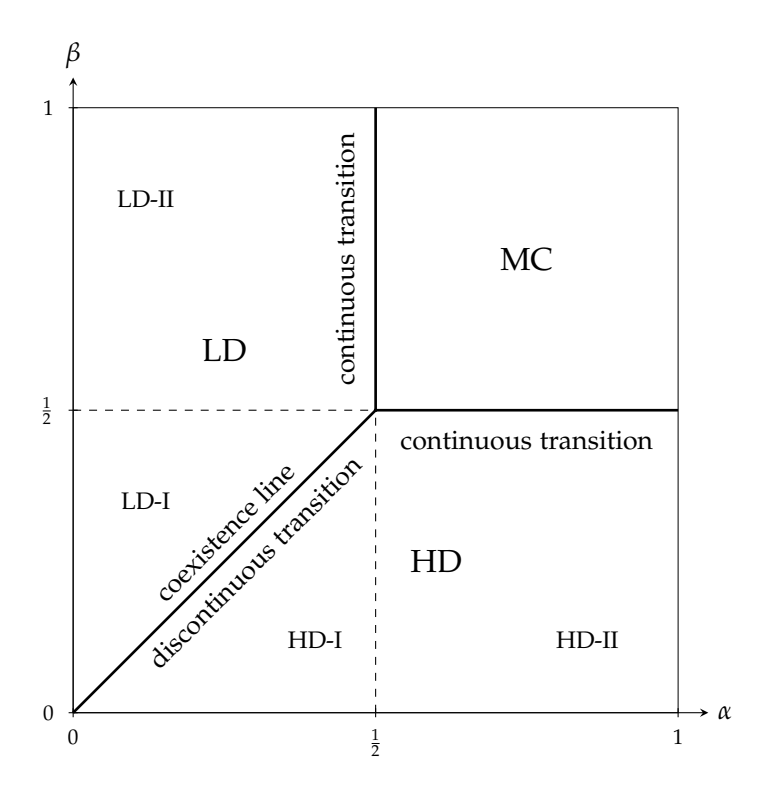


Figure 1.2: The Phase Diagram of the Stationary State, representing the values of α and β for which the stationary state is in a Low Density, High Density or Maximal Current phase. Solid lines represent phase transitions, whose order is specified next to them; dashed lines represent the border between the subphases LD-I, LD-II and HD-I, HD-II.

When the system is in subphase LD-II (respectively HD-II) a phase transition is observed at $\alpha=1/2$ (respectively $\beta=1/2$), and indeed the correlation length $\xi_{\alpha}^{-1}=-\ln\alpha(1-\alpha)$ (respectively $\xi_{\beta}^{-1}=-\ln\beta(1-\beta)$) presents a singularity for that value. This is a continuous phase transition, in the bulk density, as the bulk density of the MC phase is $\rho=\frac{1}{2}$.

It is also worth mentioning the case $\alpha = 1 - \beta$, where the characteristic length ξ diverges. Here, there are no correlations and no boundary layer is observed: the profile is flat around the value $\rho = \alpha$.

1.2.1 The Stationary State of the Disordered TASEP

The introduction of quenched disorder in the hopping rates has some dramatic consequences, as is evident from everyday experience of vehicular traffic, where jams are often originated by slow vehicles, car accidents, etc. Similarly, in biological contexts like protein synthesis, some disorder seems unavoidable: during elongation, the speed of the ribosomes is codon-dependent (for instance, in Escherichia coli, the sequencing speed varies from approximately 5 to 21 codons per second [10]). It is common to distinguish between particlewise and sitewise disorder [25]: in the former, rates are particle-dependent and site-independent (this situation represents, for instance, the slow vehicle); in the latter, rates are site-dependent and particle-independent (this represents the ribosome-codon case). Both particlewise and sitewise disorder generically induce phase separation in the sense that, for global particle densities ρ in a certain interval $[\rho^-, \rho^+]$, the system breaks up into regions of density $\rho \approx \rho^-$ and $\rho \approx \rho^+$ separated by sharp density discontinuities ("shocks") typically associated with bottlenecks, i.e. slow particles or slow sites in the particlewise and sitewise cases, respectively [34]. This implies that phase transitions are no longer governed solely by the values of the boundary rates. This is evident in figure

Many exact results have been found for the case of particlewise disorder [35], while little is known an-

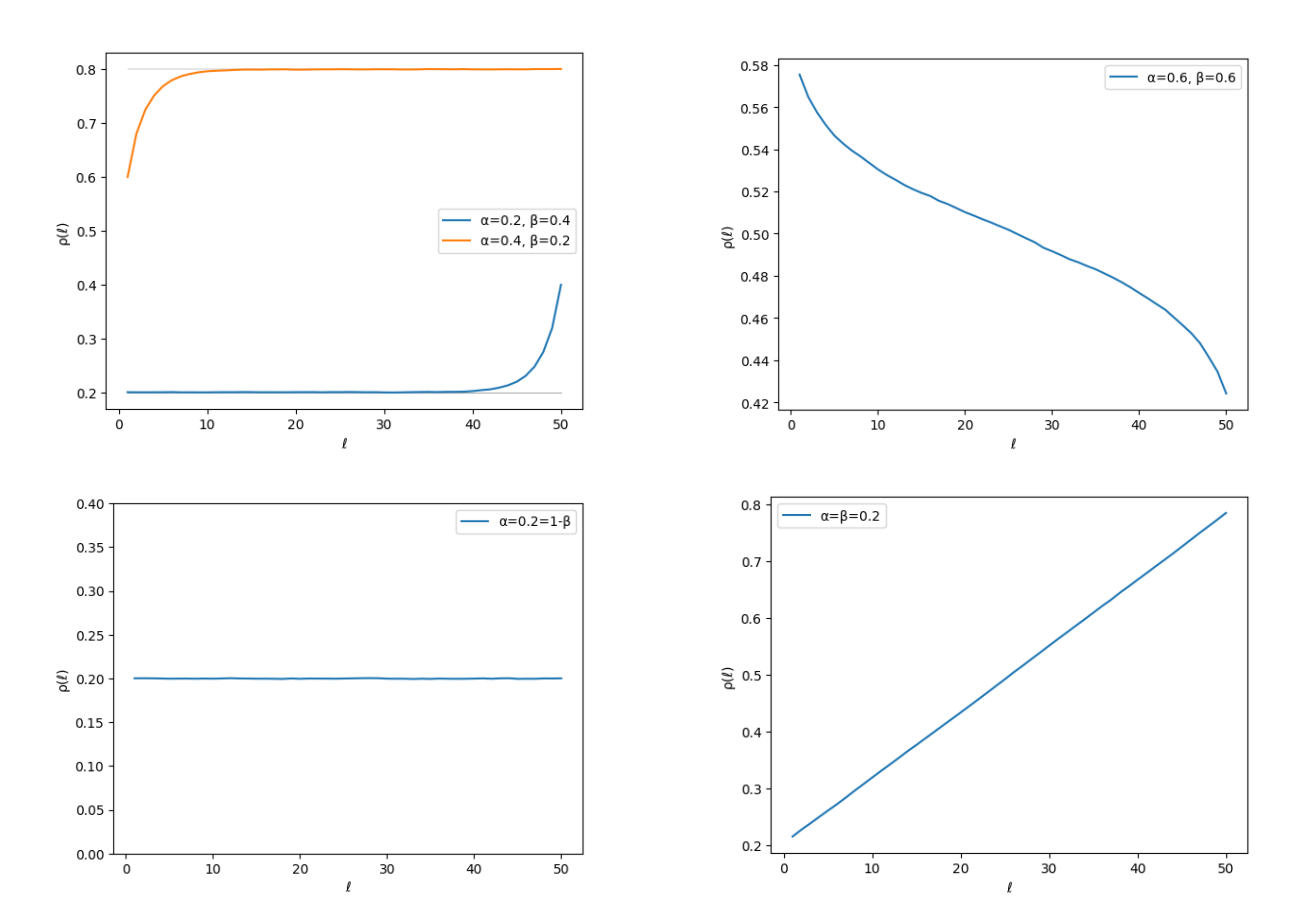


Figure 1.3: Monte-Carlo simulated density profiles for various phases and situations of interest at the stationary state, in case of uniform, unit rates for L=50 and at different values of α and β . The number of iterations is 4×10^7 (10^8 for the MC phase) and we have excluded from the average the first 10^4 generated configurations. We see that all the characteristics of the stationary state that we described above are confirmed by the simulations: on the top-left panel we have the plot of the LD and HD phases (in the subphases LD-I and HD-I, with $\alpha=1/5$, $\beta=2/5$ for the LD phase and $\beta=1/5$, $\alpha=2/5$ for the HD phase), which approach the correct bulk densities of α and $1-\beta$, respectively. On the top-right, there is the density profile corresponding to the MC phase (we set $\alpha=\beta=3/5$), where indeed the boundary layer is smoother (note the absence of a bulk, due to the finite, small size). On the bottom-left there is the trivial case of flat density profile for $\alpha=1-\beta$ (we set $\alpha=1/5$) and on the bottom-right the situation corresponding to the coexistence line $\alpha=\beta<1/2$ (with $\alpha=1/5$)

alytically for the quenched sitewise disorder [34], although it has been extensively studied numerically [36–38]. In the present work we will focus exclusively on the latter. In particular, we will mainly devote our attention to what is normally called 'type-I' disorder [34], i.e. when rates are independent random variables distributed in the interval [γ , 1], with positive γ . In figure 1.4 it can be seen that when γ is close to 1, the density profile resembles the homogeneous case, but when γ is significantly lower than 1 the boundary dependence is lost at the central nodes and a shock-like profile is observed.

Monte-Carlo Simulation of the Stationary State

The plots in figure 1.3 and 1.4 have been obtained by means of a Gillespie algorithm [39] (that is a Kinetic Monte-Carlo simulation). We will continue to employ this method to compare the numerical results presented later with the exact solution, keeping in mind that the numerical noise diminishes as the simulations are run for sufficiently long times.

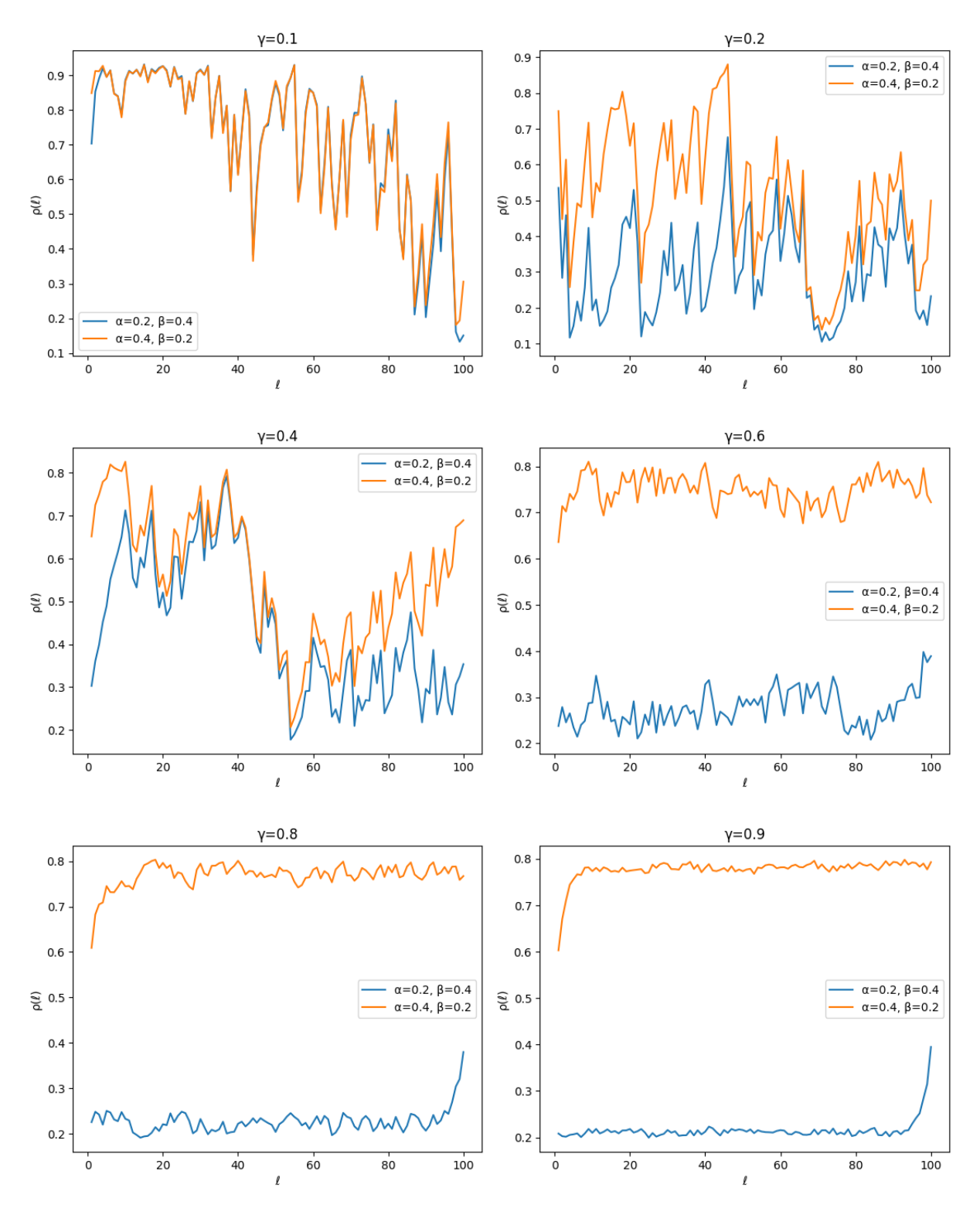


Figure 1.4: Monte-Carlo simulated density profiles at the stationary state, in the case of non-uniform, random rates for L=100. Each plot has a blue curve corresponding to $\alpha=1/5$, $\beta=2/5$ and a red curve representing $\alpha=2/5$, $\beta=1/5$, but they share the same values for the random inner rates, drawn from the uniform distribution over the interval $[\gamma,1]$ for values of γ equal to (from the top-left to the bottom-right) 0.1, 0.2, 0.4, 0.6, 0.8, 0.9. We averaged over 4×10^7 iterations.

II. k-Cluster approximations

In this chapter, we introduce the k-cluster approximations, first in general terms and then applied to the TASEP model for the cases k = 1, 2, 3, corresponding to the Mean-Field, Pair, and Triplet approximations, respectively. Our focus will be exclusively on the stationary state, analysing both the case of homogeneous rates and that of quenched sitewise disorder, with frequent comparisons to simulations. After presenting the three schemes, we will compare their numerical results with one another.

The most systematic method for closing the system of equations avoiding the aforementioned hierarchy is to factorise every k + 1–cluster probability into the (non-linear) combination of k–cluster probabilities. In other words, the probability of the configuration \underline{n} is approximated as

$$P^{t}[\underline{n}] = \frac{\prod_{i=1}^{L-(k-1)} P_{i}^{t}[n_{i} \cdots n_{i+k-1}]}{\prod_{i=2}^{L-k} P_{i}^{t}[n_{i} \cdots n_{i+k-2}]}$$

and in particular the probability of a k + 1-cluster is

$$P_{\ell}^{t}[n_{\ell}\cdots n_{\ell+k}] = \frac{P_{\ell}^{t}[n_{\ell}\cdots n_{\ell+k-1}]P_{\ell+1}^{t}[n_{\ell+1}\cdots n_{\ell+k}]}{P_{\ell+1}^{t}[n_{\ell+1}\cdots n_{\ell+k-1}]}.$$

Figure 2.1 provides a graphical representation of the k-Cluster approximation. In general, one has the freedom to choose different overlaps of neighbouring clusters [40]. As an example, with k = 3, one can use the so-called (3,1)-Cluster approximation

$$P_{\ell}^{t}[n_{\ell},n_{\ell+1},n_{\ell+2},n_{\ell+3},n_{\ell+4}] \propto \frac{P_{\ell}^{t}[n_{\ell},n_{\ell+1},n_{\ell+2}]P_{\ell+2}^{t}[n_{\ell+2},n_{\ell+3},n_{\ell+4}]}{P_{\ell+2}^{t}[n_{\ell+2}]}$$

or the (3,2)-Cluster approximation

$$P_{\ell}^t[n_{\ell},n_{\ell+1},n_{\ell+2},n_{\ell+3},n_{\ell+4}] = \frac{P_{\ell}^t[n_{\ell},n_{\ell+1},n_{\ell+2}]P_{\ell+1}^t[n_{\ell+1},n_{\ell+2},n_{\ell+3}]P_{\ell+2}^t[n_{\ell+2},n_{\ell+3},n_{\ell+4}]}{P_{\ell+1}^t[n_{\ell+1},n_{\ell+2}]P_{\ell+2}^t[n_{\ell+2},n_{\ell+3}]}.$$

For the k-Cluster approximation one has the possibility to choose k-1 different factorisations, corresponding to the k-1 possible values for the overlap — the greater the overlap the better the approximation [40]. In the present chapter, we only consider (k,k-1)-Cluster approximations, for k=1,2,3. The k-Cluster approximations for k=1,2,3 have already been applied to a TASEP in OBC to investigate both the stationary state and the dynamical transition [41] for a system with unit inner rates $r_{\ell}=1 \ \forall \ell \in \{1,\ldots,L-1\}$. Here we focus on the stationary state only, comparing the three approximations (see section 2.3.1) both for homogeneous and inhomogeneous inner rates.

Numerical Implementation

All the following approximations have been implemented using an Explicit Euler Method (EEM), consisting in approximating the time derivatives as

$$\dot{f}(t) \simeq \frac{f(t+\Delta t) - f(t)}{\Delta t},$$

¹Here and in the following, we focus on specifying the approximation of the entire configuration, as we have observed that approximating only the clusters generally does not provide sufficient information to extend the approximation to the full configuration.

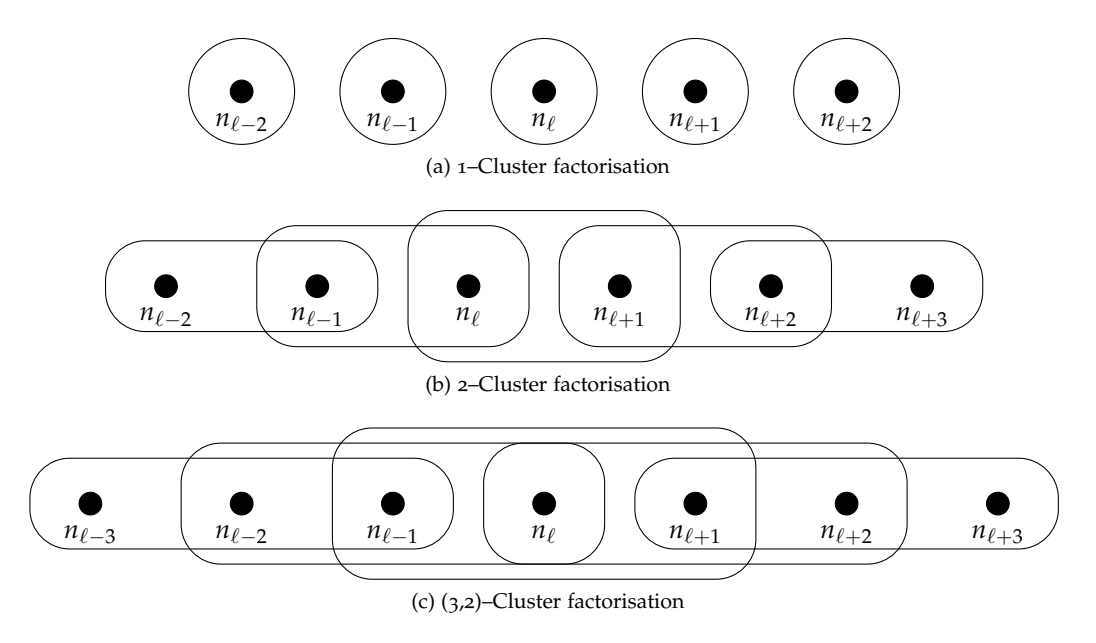


Figure 2.1: Graphical representation of the k-Cluster factorisation for (a) k = 1, (b) k = 2 and (c) k = 3. Each circle corresponds to one factor in the factorisation.

where Δt is the uniform time-spacing, given by the length of the time interval T divided by the cardinality of the temporal grid N_t . In some cases, the equation turned out to be numerically unstable for non-small enough Δt (for instance, for the Triplet approximation, L=50, $\alpha=1/5$, $\beta=2/5$ and unit inner rates the minimal value of Δt for which we observed numerical instability was $\Delta t \geq \frac{6}{5}$). In general, we use $\Delta t \leq \frac{1}{10}$, and we do not meet problems of numerical instability. Moreover, we always set the initial density at the bulk value: $\rho_\ell^0 = \rho \ \forall \ell$ (for instance, in the case $\alpha < \beta$ and $\alpha < 1/2$, we set $\rho_\ell^0 = \alpha \ \forall \ell$; instead, for the case $\beta < \alpha$ and $\beta < 1/2$, we set $\rho_\ell^0 = 1 - \beta \ \forall \ell$): this way — at least in the homogeneous case — the bulk region is already at its stationary state and, as we verified, the convergence to equilibrium is faster with respect to the case of random initial density.

2.1 The Mean-Field approximation

The Mean-Field (MF) approximation is the simplest cluster approximation (it corresponds to the 1-cluster approximation) as it amounts to assuming that the probability factorises over all the sites:

$$P^{t}[\underline{n}] = \prod_{i=1}^{L} P_{i}^{t}[n_{i}].$$

This means that the homogeneous current² $P_{\ell}^{t}[10]$ factorises as $\rho_{\ell}^{t}(1-\rho_{\ell+1}^{t})$ and the evolution of the density depends solely on the densities themselves, although through a non-linear relation:

$$\dot{\rho}_{\ell}^{t} = r_{\ell-1} \rho_{\ell-1}^{t} (1 - \rho_{\ell}^{t}) - r_{\ell} \rho_{\ell}^{t} (1 - \rho_{\ell+1}^{t}). \tag{2.1}$$

This equation can be used in order to find the density profile at any time t. Numerically, it is sufficient to make all the L variables ρ_ℓ^t evolve according to the self-consistent equation. We implemented this dynamical equation with the aforementioned EEM. With this algorithm, it can be verified that the evolution of the density profile is consistent with what described by other theories like the Domain Wall Theory [42]: by exchanging $\alpha \leftrightarrow \beta$, the velocities of the domain walls in the LD and HD phases obey $\underline{v}_{\text{LD}} = -\underline{v}_{\text{HD}}$, as figure 2.2 shows. The stationary state can be obtained by letting the equations

²We call it the 'homogeneous current' as it corresponds to J_{ℓ}^t when the inner rates are uniform and equal to one (and ℓ is an inner node).

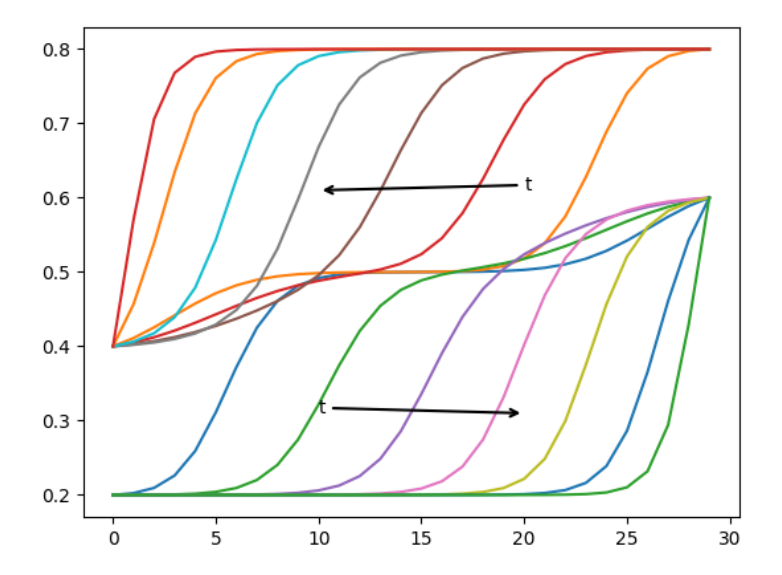


Figure 2.2: Scheme of the evolution of the density profile in the LD ($\alpha = 1/5$, $\beta = 2/5$) and HD ($\alpha = 2/5$, $\beta = 1/5$) phases at unit inner rates. The initial condition is $\rho_{\ell}^0 = \frac{1}{2} \ \forall \ell$ for both phases and the time interval is T = 130 with $N_t = 200$. The time interval between two curves is 25.

evolve for sufficiently long times. Nevertheless, below we describe an alternative strategy that is computationally faster.

2.1.1 The Mean-Field Stationary State

In the stationary state, taking the left-hand-side of equation (2.1) to be zero, we get the following recursive relation

$$\rho_{\ell} = \frac{r_{\ell-1}\rho_{\ell-1}}{r_{\ell-1}\rho_{\ell-1} + r_{\ell}(1 - \rho_{\ell+1})}.$$
(2.2)

This is a fixed point recursive relation, that can be conveniently written using the two fictitious nodes with their corresponding rates. In case of unit rates, it has been proved [43] that this equation has only one solution with the property $0 < \rho_{\ell} < 1$. Here, we do not extend the proof to the case of non-uniform rates, but we notice empirically that the density is always well defined.

Although quite rough as an approximation, the MF theory is able to capture basically all the essential features of the stationary state: it predicts the exact phase diagram 1.2 and, in general, it becomes exact when the correlations tend to zero (that is, in the bulk region and in the case $\alpha=1-\beta$, when the rates are uniform [32]). The MF density profiles for the LD and HD phases are qualitatively similar to the exact ones (see figure 2.3), but they do not exhibit any power-law correction to the exponential decay in the boundary layer, characteristic of the subphases LD-II and HD-II. Instead, it successfully predicts the power-law boundary layer for the MC phase, but with exponent 1 instead of the exact exponent 1/2 [25] (see figure 2.4). The MF results are particularly different from the exact solution in the case $\alpha=\beta$ (see figure 2.4). Here, the MF theory predicts something like the coexistence of the LD and HD phases, only separated by a 'domain wall' (i.e. a shock) which, in the limit $L\to\infty$ can occupy any position of the lattice and is instead at the centre of it for finite L. The LD phase on the left of the domain wall is characterised by a uniform density $\rho_{\rm LD}=\alpha$, while the HD phase on the right of it has a uniform density equal to $\rho_{\rm HD}=1-\alpha$. Thus, at the two extrema $\ell=1$, $\ell=L$ and (for a chain with an even number of nodes) at the centre, the values of the density correspond to the exact ones.

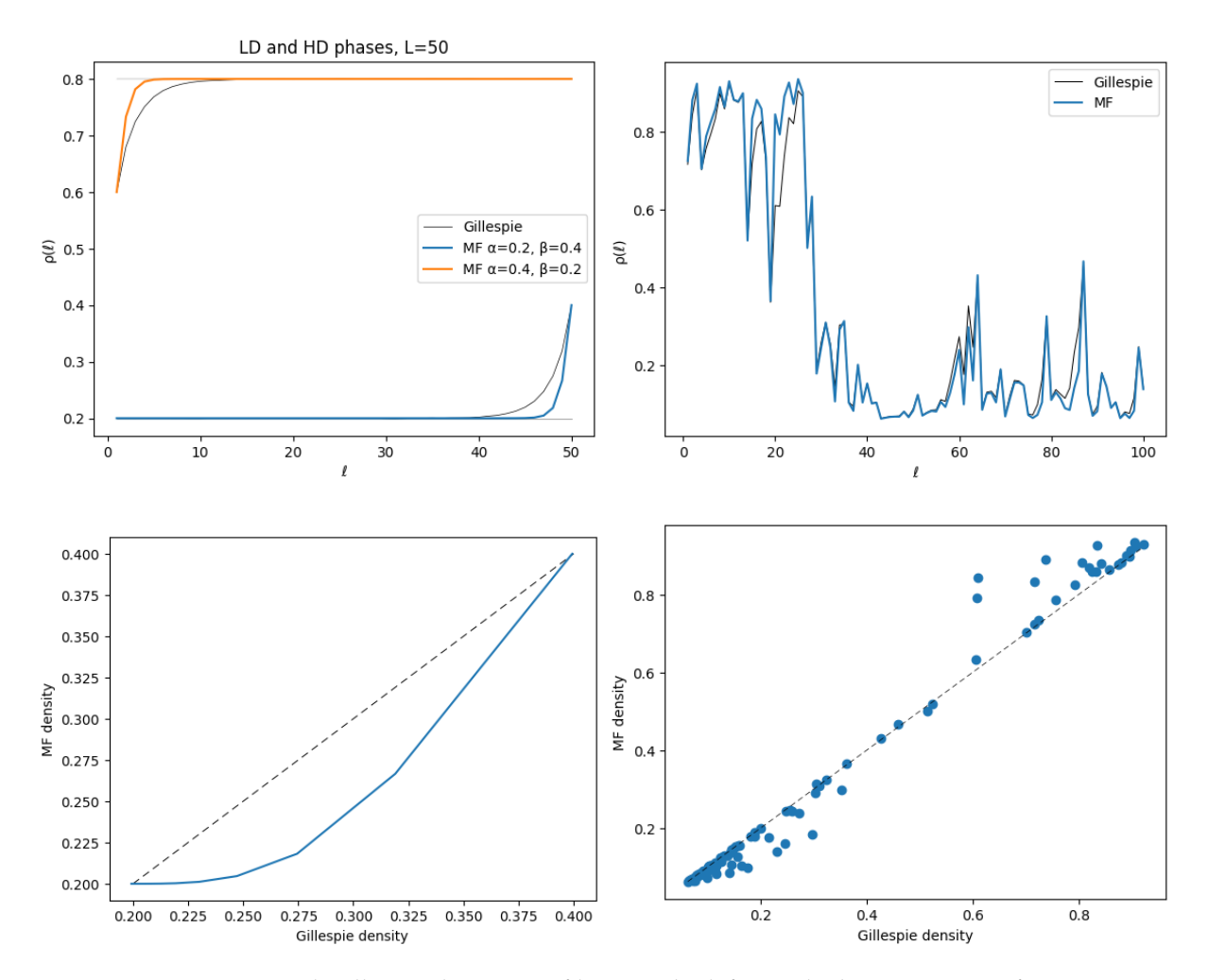


Figure 2.3: MF and Gillespie density profiles. On the left panels the rates are uniform: at the top-left, both the LD and HD phases are plotted; on the bottom-left the same density vectors calculated by means of the MF approximation and Gillespie's algorithm for the LD phase have been plotted against each other. Top-right panel shows the density profiles for random, uniformly distributed inner rates in the interval [0.6,1] for $\alpha=1/5$, $\beta=2/5$ calculated both with the MF approximation and Gillespie's algorithm. Bottom-right panel shows the same vectors, plotted one against each other.

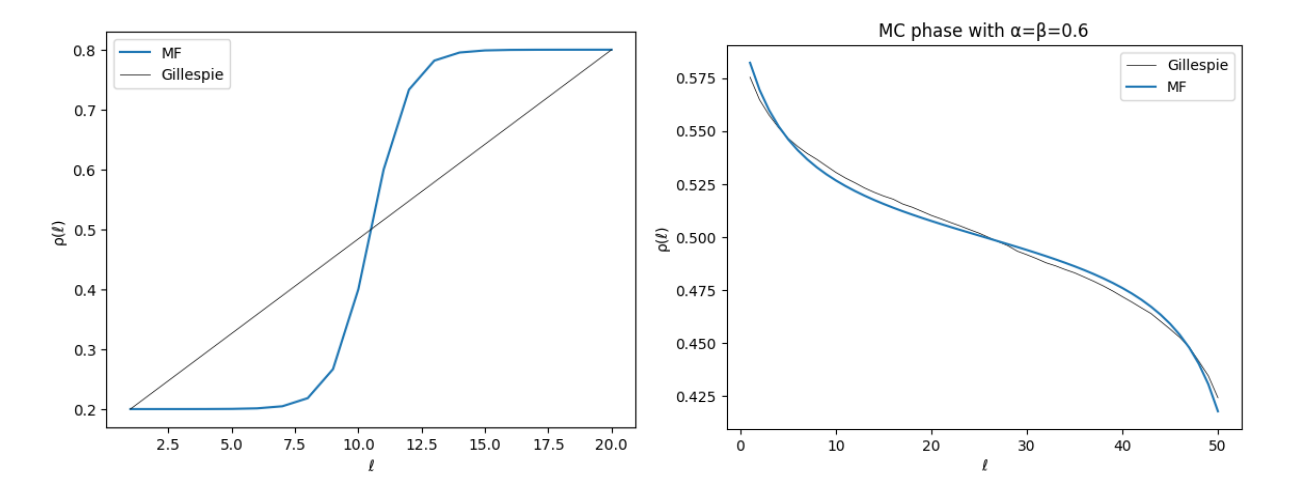


Figure 2.4: MF and Gillespie density profiles for $\alpha = \beta = 1/5$, L = 20 (left panel) and for $\alpha = \beta = 3/5$, L = 50 (right panel).

2.2 The Pair approximation

The Pair approximation (a.k.a. the 2-cluster approximation) factorises all the clusters involving more than two nodes as a product of two-node probabilities only, dividing by the overlap of one node. Thus, on the whole configuration, it comes as

$$P^{t}[\underline{n}] = \frac{\prod_{i=1}^{L-1} P_{i}^{t}[n_{i} \ n_{i+1}]}{\prod_{i=2}^{L-1} P_{i}^{t}[n_{i}]}.$$

This factorisation allows to write self-consistent equations for the two–node marginals. Consider the dynamical equation for the homogeneous current $P_{\ell}^{t}[10]$:

$$\dot{P}_{\ell}^{t}[10] = r_{\ell-1}P_{\ell-1}^{t}[100] - r_{\ell}P_{\ell}^{t}[10] + r_{\ell+1}P_{\ell}^{t}[110]
\simeq r_{\ell-1}\frac{P_{\ell-1}^{t}[10]P_{\ell}^{t}[00]}{1 - \rho_{\ell}^{t}} - r_{\ell}P_{\ell}^{t}[10] + r_{\ell+1}\frac{P_{\ell}^{t}[11]P_{\ell+1}^{t}[10]}{\rho_{\ell+1}^{t}},$$
(2.3)

where $P_{\ell}^{t}[00]$ and $P_{\ell}^{t}[11]$ can be obtained from the homogeneous current $P_{\ell}^{t}[10]$ and from the densities as

$$P_{\ell}^{t}[11] = \rho_{\ell}^{t} - P_{\ell}^{t}[10], \qquad P_{\ell}^{t}[00] = 1 - \rho_{\ell+1}^{t} - P_{\ell}^{t}[10].$$

Therefore, the system of equations for the densities and the homogeneous currents $\{P_\ell^t[10]\}_{\ell=1}^{L-1}$ is closed. One can proceed as in the case of the MF approximation in order to obtain the density profile at each time step only by evolving the densities according to equation (1.2) and the homogeneous currents according to (2.3).

For the stationary state, we developed an alternative procedure, which was inspired by the MF recursive relation (2.2) (and seems numerically faster than the dynamical algorithm).

2.2.1 The Stationary State

The recursive relation can be obtained by exploiting the translational invariance of $J = r_{\ell} P_{\ell}[10]$ at the stationary state. Indeed, taking equation (2.3) for $\dot{P}_{\ell}^{t}[10]$ and setting the left-hand-side at zero, we get

$$1 = \frac{P_{\ell}[00]}{1 - \rho_{\ell}} + \frac{P_{\ell}[11]}{\rho_{\ell+1}}.$$

As we can express any two–node marginal in terms of the density and the current simply by means of marginalisation, this gives a recursive relation, together with the translational invariance condition for *J*. Indeed

$$P_{\ell}[00] = 1 - \rho_{\ell+1} - \frac{J}{r_{\ell}}$$
 $P_{\ell}[11] = \rho_{\ell} - \frac{J}{r_{\ell}}$

and thus we obtain

$$J = r_{\ell} \frac{\rho_{\ell}(1 - \rho_{\ell}) + \rho_{\ell+1}(1 - \rho_{\ell+1}) - \rho_{\ell+1}(1 - \rho_{\ell})}{\rho_{\ell+1} + 1 - \rho_{\ell}}.$$

Considering the same equation for $\dot{P}_{\ell-1}^t[10]$,

$$r_{\ell-1} \frac{\rho_{\ell-1}(1-\rho_{\ell-1}) + \rho_{\ell}(1-\rho_{\ell}) - \rho_{\ell}(1-\rho_{\ell-1})}{\rho_{\ell} + 1 - \rho_{\ell-1}} = r_{\ell} \frac{\rho_{\ell}(1-\rho_{\ell}) + \rho_{\ell+1}(1-\rho_{\ell+1}) - \rho_{\ell+1}(1-\rho_{\ell})}{\rho_{\ell+1} + 1 - \rho_{\ell}} \quad (2.4)$$

This is a cubic equation for ρ_{ℓ} , which depends solely on $\rho_{\ell-1}$ and $\rho_{\ell+1}$. We solved it symbolically with Wolfram *Mathematica* and found that there is only one solution with the property $0 < \rho_{\ell} < 1$.

2.3 The Triplet approximation

We refer to the (3,2)-cluster approximationas the Triplet approximation. This amounts to factorise all the clusters of length greater than three, considering an overlap of length two. Thus, the Triplet approximation on the whole configuration reads

$$P^{t}[\underline{n}] = \frac{\prod_{i=1}^{L-2} P_{i}^{t}[n_{i} \ n_{i+1} \ n_{i+2}]}{\prod_{i=2}^{L-2} P_{i}^{t}[n_{i} \ n_{i+1}]}.$$

One thus needs to consider all the 4L-5 unknowns $\{\rho_\ell^t\}_{\ell=1}^L$, $\{P_\ell^t[10]\}_{\ell=1}^{L-1}$, $\{P_\ell^t[100], P_\ell^t[110]\}_{\ell=1}^{L-2}$. As usual, we developed a dynamical algorithm which evolved all the mentioned variables, according to the Triplet approximation. The dynamical equations for density and currents follow the exact equations (1.2) and (1.3); the ones for $P_\ell^t[110]$ and $P_\ell^t[100]$ are

$$\begin{split} \dot{P}_{\ell}^{t}[100] &= r_{\ell-1} P_{\ell-1}^{t}[1000] - r_{\ell} P_{\ell}^{t}[100] + r_{\ell+2} P_{\ell}^{t}[1010] \\ &= r_{\ell-1} \frac{P_{\ell-1}^{t}[100] P_{\ell}^{t}[000]}{P_{\ell}^{t}[00]} - r_{\ell} P_{\ell}^{t}[100] + r_{\ell+2} \frac{P_{\ell}^{t}[101] P_{\ell+1}^{t}[010]}{P_{\ell+1}^{t}[01]}, \\ \dot{P}_{\ell}^{t}[110] &= r_{\ell-1} P_{\ell-1}^{t}[1010] - r_{\ell+1} P_{\ell}^{t}[110] + r_{\ell+2} P_{\ell}^{t}[1110] \\ &= r_{\ell-1} \frac{P_{\ell-1}^{t}[101] P_{\ell}^{t}[010]}{P_{\ell}^{t}[01]} - r_{\ell+1} P_{\ell}^{t}[110] + r_{\ell+2} \frac{P_{\ell}^{t}[111] P_{\ell+1}^{t}[110]}{P_{\ell+1}^{t}[11]}; \end{split}$$

where variables $P_{\ell}^{t}[000]$, $P_{\ell}^{t}[001]$, $P_{\ell}^{t}[010]$, $P_{\ell}^{t}[011]$, $P_{\ell}^{t}[011]$, $P_{\ell}^{t}[111]$ can be obtained from the known set of variables $\{\rho_{\ell}^{t}, P_{\ell}^{t}[10], P_{\ell}^{t}[100], P_{\ell}^{t}[110]\}$ through marginalisation:

$$\begin{split} P_{\ell}^{t}[000] &= 1 - \rho_{\ell+2}^{t} - P_{\ell+1}^{t}[10] - P_{\ell}^{t}[100] \\ P_{\ell}^{t}[010] &= P_{\ell+1}^{t}[10] - P_{\ell}^{t}[110] \\ P_{\ell}^{t}[101] &= P_{\ell}^{t}[10] - P_{\ell}^{t}[100] \\ P_{\ell}^{t}[111] &= \rho_{\ell}^{t} - P_{\ell}^{t}[10] - P_{\ell}^{t}[110] \\ P_{\ell}^{t}[00] &= 1 - \rho_{\ell+1}^{t} - P_{\ell}^{t}[10] \\ P_{\ell}^{t}[01] &= \rho_{\ell+1}^{t} - \rho_{\ell}^{t} + P_{\ell}^{t}[10] \\ P_{\ell}^{t}[11] &= \rho_{\ell}^{t} - P_{\ell}^{t}[10]. \end{split}$$

At odds with the MF and the Pair approximations, we could not find a recursive relation for the stationary state, as the three–node marginals cannot be written in terms of solely the (translationally invariant) current and the densities.

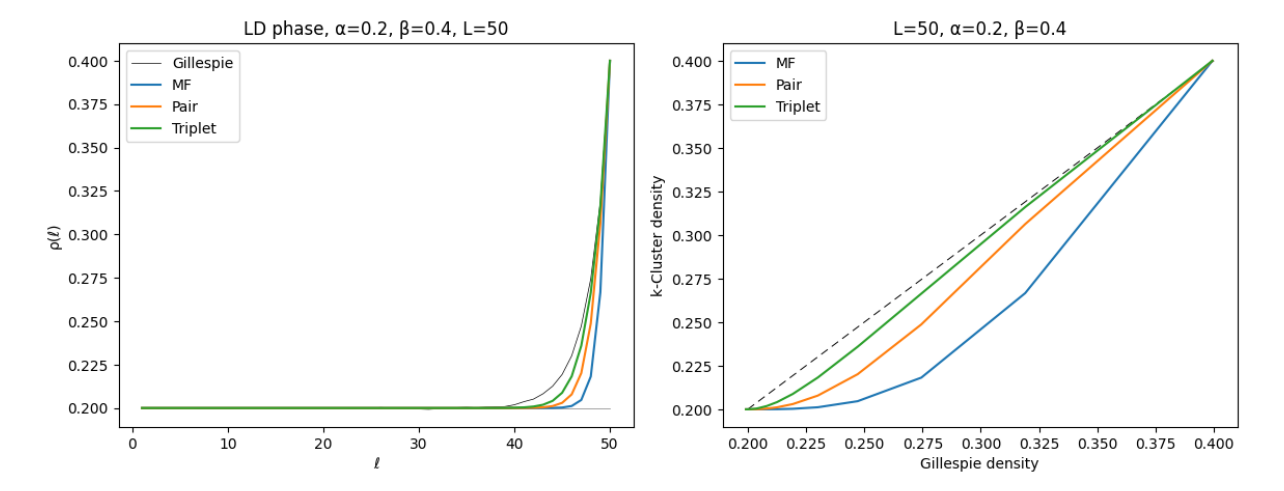


Figure 2.5: Comparison between the density profiles of a chain of length L=50 obtained by Gillespie's algorithm and 1,2,3–Cluster approximations, in the LD phase $\alpha=1/5$, $\beta=2/5$ and unit inner rates. Left panel shows the four different profiles; right panel plots the three approximated profiles against the one given by Gillespie. The black dashed line is a reference line which corresponds to the Gillespie density profile plotted against itself: the distance between the curve and the straight line is thus a measure of the distance between the Gillespie density profile and the approximated one. For the Gillespie algorithm, we averaged over 4×10^7 configurations.

2.3.1 Comparison between the 1,2,3-Cluster approximations

The three approximations give qualitatively similar results. For instance, when the inner rates are uniform and $\alpha = \beta$, they all predict the aforementioned 'coexistence' of the LD and HD phases, separated by a domain wall (differently from the exact solution which gives a linear density profile); they all yield the exponent 1 for the power-law of the MC phase (instead of the exact exponent 1/2) and none of them is able to capture the power-law correction to the boundary layer in case of the subphases LD-II, HD-II (although they present different characteristic lengths) [25, 41]. Indeed, in the k-Cluster approximation, while larger values of k improve the quality of the approximation, they are inherently limited to finite-range correlations and cannot account for long-range (infinite) correlations.

Figure 2.5 shows the comparison of the 3 considered approximations with the density vectors obtained through Gillespie's algorithm in the uniform case where all the inner rates are set to one; figures 2.6, 2.7 and 2.8 show their comparison in the case of quenched disorder. In particular, plots in figures 2.6 and 2.7 show the comparison of one density vector for each approximation to the simulated one, for rates distributed in the interval $[\gamma,1]$ at different values of γ . Instead, plot in figure 2.8 is the result of 10^3 simulations: we considered 20, equally spaced values of γ in the interval $\left[\frac{1}{10},\frac{2}{5}\right]$; for each value of γ we generate 50 vectors of rates and we run the Gillespie, MF, Pair and Triplet algorithms. Then, we take the 1-norm between the approximated and simulated density vectors, and we average over the 50 simulations for each γ . Also, we considered a relatively large lattice (L=100) so that some self-averaging effect helped noise reduction.

In all cases, the result is as expected: the Triplet approximation is better than the Pair approximation, which in turn is better than the MF approximation, both in the case of uniform inner rates and in the case of random rates.

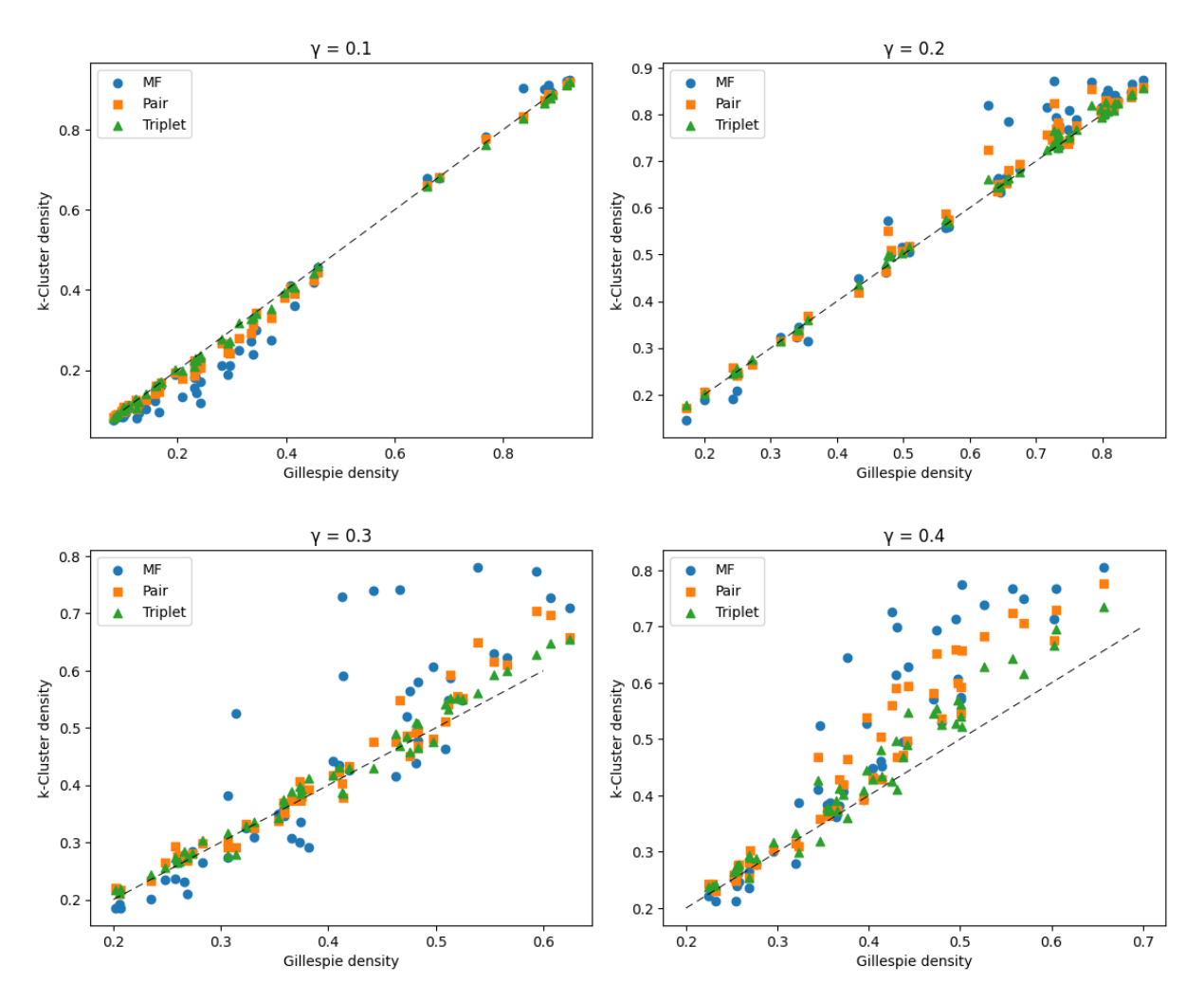


Figure 2.6: Comparison of the density profiles for various random inner rates extracted from the uniform distributions on the interval $[\gamma,1]$ for $\gamma \in \left\{\frac{1}{10},\frac{2}{10},\frac{3}{10},\frac{4}{10}\right\}$, for a chain of length L=50 and $\alpha=1/5$, $\beta=2/5$. Blue dots are the MF values, red squares correspond to the Pair approximation ones and green triangles to the Triplet's. The black dashed line is a reference line which corresponds to the Gillespie density profile plotted against itself: the distance between the dots and the straight line is thus a measure of the distance between the Gillespie density profile and the approximated one. For the Gillespie algorithm, we average over 6×10^7 configurations; for all the k-Cluster approximations we use the convergence condition that the distance (in infinity norm) between the updated density vector and the previous one was smaller than numerical precision.

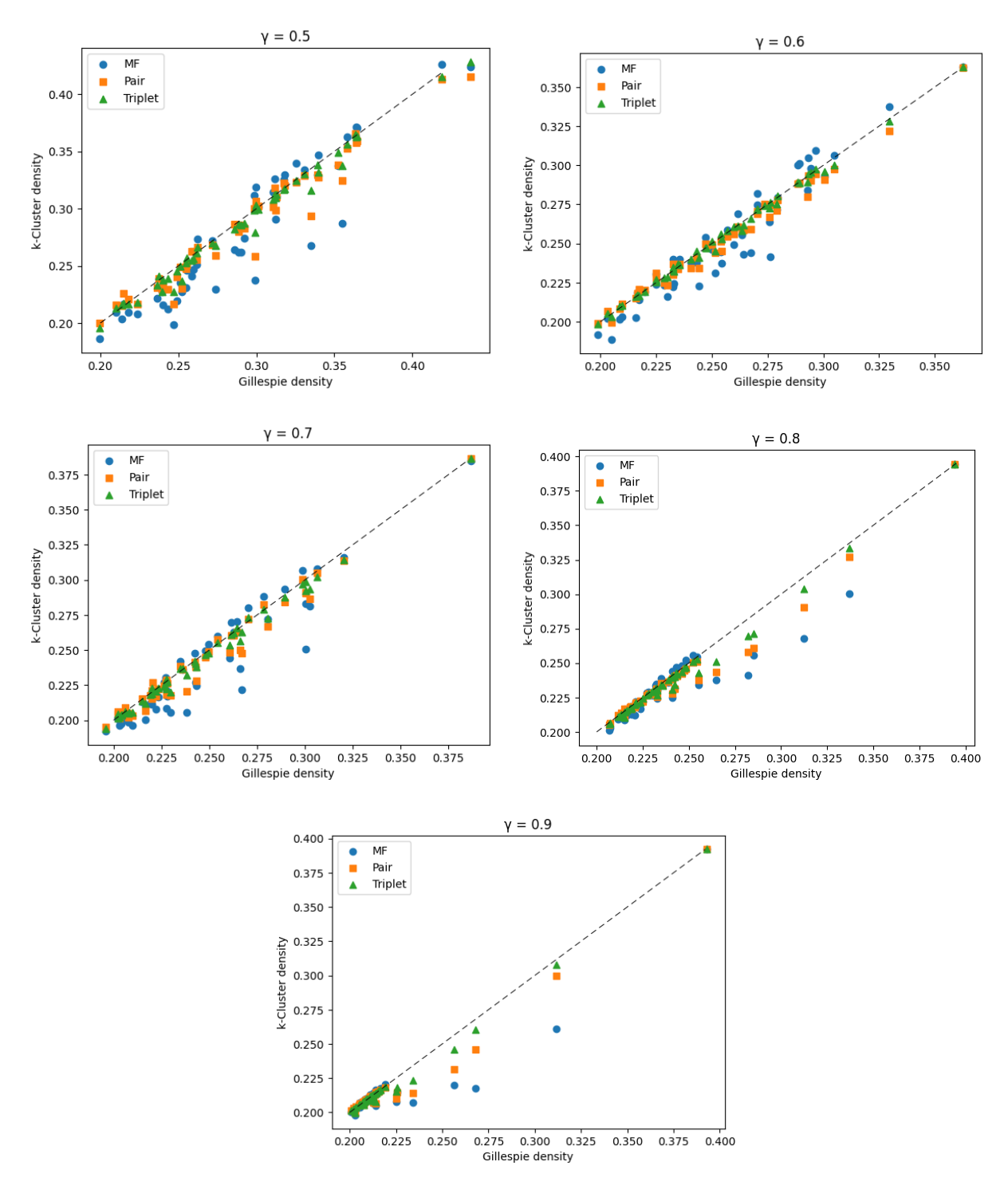


Figure 2.7: Comparison of the density profiles for various random inner rates extracted from the uniform distributions on the interval $[\gamma,1]$ for $\gamma \in \left\{\frac{5}{10},\frac{6}{10},\frac{7}{10},\frac{8}{10},\frac{9}{10}\right\}$, for a chain of length L=50 and $\alpha=1/5$, $\beta=2/5$. Blue dots are the MF values, red squares correspond to the Pair approximation ones and green triangles to the Triplet's. The black dashed line is a reference line which corresponds to the Gillespie density profile plotted against itself: the distance between the dots and the straight line is thus a measure of the distance between the Gillespie density profile and the approximated one. For the Gillespie algorithm, we average over 6×10^7 configurations; for all the k-Cluster approximations we use the convergence condition that the distance (in infinity norm) between the updated density vector and the previous one was smaller than numerical precision.

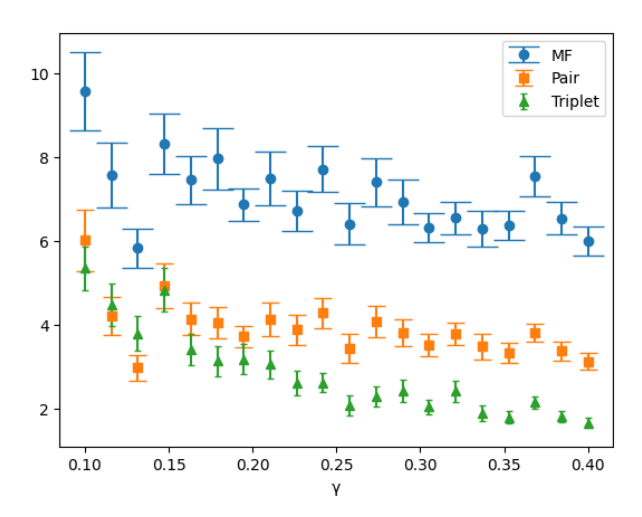


Figure 2.8: Comparison between the 1,2,3–Cluster approximations and Gillespie density profiles, at random rates drawn from the uniform distribution on the interval $[\gamma,1]$, for a chain of length L=100 and $\alpha=\beta=3/5$. Dots represent the average over 50 realizations, error bars are the mean standard deviations. For Gillespie algorithm, we averaged over 10^8 configurations for each iteration. For the MF and the Pair algorithms, we used the recursive formulas described above and iterated 6×10^3 times, while for the triplet approximation we set $T=10^3$, $N_t=5\times10^3$. We used no convergence condition, for any approximation.

III. The Car-Oriented approach

In this chapter, we briefly review the Car-Oriented Mean-Field approximation and some of its main applications in previous studies. We then extend the Car-Oriented approach to the TASEP model in the non-uniform case (such as with OBC), and to different types of approximations that resemble, in some ways, the *k*-Cluster approximations discussed earlier. Finally, we compare the results obtained from the Car-Oriented approximations with those from the *k*-Cluster approximations, and show that the former offer a (slightly) improved version of the latter.

The Car-Oriented approach takes its name from the fact that it considers the length of the space in front of a particle (a car) rather than the occupation state of a site. As a matter of fact, it considers the variables

$$P_{\ell}^{t}(m) := P_{\ell}^{t}[1\underbrace{0\cdots 0}_{m}1],$$

where the index ℓ runs from 0 to L-1 while $m\in\mathbb{N}$ corresponds to the number of unoccupied sites following site ℓ and is subject to the constraint $1\leq \ell+m\leq L$. These variables correspond to the probabilities that node ℓ is occupied and the following particle is at distance m+1, for every ℓ,m . When $m=L-\ell$, the following particle simply does not exist; when m=0 the particle in ℓ is followed by another particle in $\ell+1$ and the following hole is not specified. We will often use the short-hand notation

$$P_{\ell}^{t}(m) = P_{\ell}^{t}[10^{m}1].$$

The cardinality of this set of variables is $\mathcal{O}(L^2)$, while the k-Cluster approximations consider — for any fixed k — only $\mathcal{O}(L)$ variables. These variables are related to the density through marginalisation

$$\rho_1^t = \sum_{m=0}^{L-1} P_1^t(m), \qquad \qquad \rho_\ell^t = \sum_{m=0}^{L-\ell} P_\ell^t(m) \quad 1 < \ell < L, \qquad \qquad \rho_L^t = \sum_{m=0}^{L-1} P_{L-(m+1)}^t(m). \tag{3.1}$$

3.1 Previous studies on the Car-Oriented Mean-Field approximation

The Car-Oriented approach has already been applied to various situations: chief among them are the application to the Nagel-Schreckenberg (NaSch) model [26] (a model for vehicular traffic) and the one to TASEP with shuffled dynamics [44]. In both cases, it has been studied together with a MF-like approximation — where gaps are taken to be independent from one another — known as the Car-Oriented Mean-Field (COMF) approximation, and in Periodic Boundary Conditions at homogeneous rates. This allowed to consider translationally invariant stationary states $P(m) \equiv P_{\ell}(m) \ \forall m$ [25].

3.1.1 The COMF approximation for the NaSch model

The NaSch model extends the TASEP by allowing both discrete time evolution and variable hopping range. In this model, each particle may move up to a maximum of v_{max} sites per update (interpreted, in traffic terms, as the maximum speed), so that the hopping distance is an integer $v \in 0, 1, \ldots, v_{\text{max}}$. In addition, time is discretised into steps of length τ , which raises the issue of the update scheme: namely, the rule that determines the order in which particles are moved. In continuous-time TASEP, only one event (i.e., a configuration change) can occur in an infinitesimal interval, but in discrete time multiple events may occur within a single step. Consequently, the movement of one particle can affect the possible movement of others, making the choice of update order a critical modelling detail. The

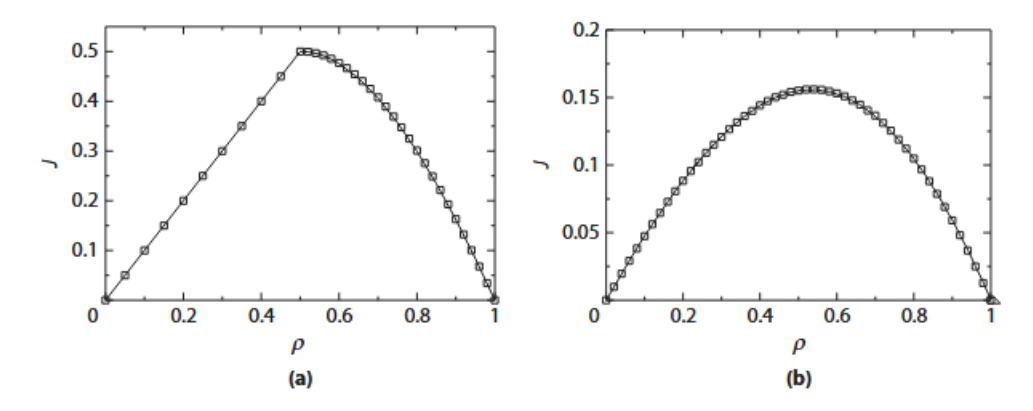


Figure 3.1: Fundamental diagram (i.e. stationary current J vs the bulk density ρ) for the shuffled dynamics in the case of uniform inner rates r=1/2 (a) and r=1 (b). Dots represent Monte-Carlo simulations; the solid line is the COMF approximation. This figure is taken from [25].

NaSch model assumes 'Parallel Dynamics', which means that all the particles are updated simultaneously. By setting $v_{\rm max}=1$, one obtains the TASEP model in discrete time with parallel updating. Moreover, the Car-Oriented approach was mainly considered in the case of periodic boundary conditions, which give a homogeneous, translational invariant stationary state. In this context, the variables of interest are the translationally invariant stationary state probabilities $P^t(v,m)$ of moving at speed v with a gap of length m in front. Under the COMF approximation, the steady state can be solved using a generating function technique [45]. In the case $v_{\rm max}=1$, the COMF approximation gives the exact result for the translational invariant stationary state. This comes not unexpected, as the COMF approximation takes into account all the relevant correlations, namely the one between nearest neighbours — for instance, through variable P(0)=P[11] (where we dropped both indices ℓ and t in order to denote the uniform stationary state). This changes if hopping beyond the nearest neighbour is allowed, that is to say in the case $v_{\rm max}>1$ and here COMF is no longer exact. Nevertheless, it yields good results because it takes into account the longer-ranged correlations at least partially. Indeed, it has been shown to give better results than the Pair approximation [9].

3.1.2 The COMF approximation for the Shuffled Dynamics

The parallel updating is not the only possible choice. Another possible updating rule is the 'Shuffled Dynamics', particularly relevant in the case of Partially Asymmetric Simple Exclusion Processes, where particles can hop in both directions and the parallel dynamics would give conflicts (i.e. particles might try to occupy the same node) whereas the shuffled dynamics would not [46]. In the shuffled update scheme, at each timestep the order in which particles are allowed to move is determined by a random permutation of the particle numbers [46, 47]. This has some dramatic consequences. First of all, the model is no longer PH symmetric: only particles are updated in a randomized sequence; holes are passive and not involved in the update process, which makes the forward and reversed dynamics fundamentally different. Second, while in general the stationary state of the TASEP with periodic boundary conditions is given by a factorised steady state, this is different for the shuffled update [25] and in fact it was shown in [47] that the master equation cannot be solved by a product Ansatz. In fact, TASEP with shuffled dynamics has not yet been solved [25]. Nevertheless, COMF [47] and Cluster approximation [48] give excellent results, for example for the fundamental diagram, as it is shown in figure 3.1.

3.2 The Car-Oriented Equation

In this section, we present the dynamical equation for our Car-Oriented variables $P_{\ell}^{t}(m)$ in OBC. This equation can be obtained marginalising the master equation, as it is shown in appendix A.2. It is convenient to define the following quantities

$$r_{-1} := 0, P_0^t(m) := P_1^t[0^m 1], P_\ell^t[10^{L-\ell-1}10] := P_\ell^t[10^{L-\ell-1}1],$$

$$r_{L+1} := 0, P_{-1}^t(m+1) := 0, P_\ell^t[10^{L-\ell}10] := 0, P_0^t(L) = P_1^t[0^L].$$

$$(3.2)$$

This way, considering as customary $r_0 = \alpha$, $r_L = \beta$, the equation can be written as

$$\dot{P}_{\ell}^{t}(m) = r_{\ell-1}P_{\ell-1}^{t}(m+1) - r_{\ell}P_{\ell}^{t}(m)(1-\delta_{m0}) + r_{\ell+m}P_{\ell}^{t}[10^{m-1}10](1-\delta_{m0}) - r_{\ell+m+1}P_{\ell}^{t}[10^{m}10], \quad (3.3)$$

where the Kronecker deltas — as well as the fictitious nodes and the other quantites defined in (3.2) — have been introduced in order to take care of all the special cases, namely $\ell = 0$, m = 0 and all the combinations of ℓ and m for which $\ell + m = L$ (notice that the first and the last terms do not involve Kronecker deltas as they appear for every value of ℓ and m). The four terms present in this equation correspond to the following physical processes.

- 1. Term $r_{\ell-1}P_{\ell-1}^t(m+1)$ corresponds to the gain of the configuration coming from the jump of the first particle to its position, i.e. to the hop of the particle from position $\ell-1$ to position ℓ , when the following occupied node is $\ell+m+1$. In case $\ell=0$, the first particle does not exist and therefore this term must be null, so we set $r_{-1}=0$.
- 2. Term $-r_{\ell}P_{\ell}^{t}(m)(1-\delta_{m0})$ corresponds to the loss of the configuration due to the jump of the first particle, i.e. to the hop of the particle from position ℓ to position $\ell+1$. In case the gap length is null, the jump is not possible.
- 3. Term $r_{\ell+m}P_{\ell}^t[10^{m-1}10](1-\delta_{m0})$ represents the gain coming from the jump of the second particle to its position, i.e. to the hop of the particle from node $\ell+m$ to node $\ell+m+1$, when the previous particle is at position ℓ . This is possible only if the length gap is non-null.
- 4. Finally, term $-r_{\ell+m+1}P_{\ell}^t[10^m10]$ represents the loss due to the jump of the last particle to the following site. In case $m=L-\ell$, the last particle does not exist and therefore this term must be null, so we set $r_{L+1}=0$.

It is important to notice that the aforementioned hierarchy of equations reflects in this description in the fact that the evolution of $P_\ell^t(m)$ involves unknowns $P_\ell^t[10^m10]$ which do not belong to our set of variables, making the system of equations not closed. Thus, it is necessary to approximate these quantities in some way that we can write them purely in terms of our variables (or marginals of them), somehow similarly to the k-Cluster approximations.

Remark. As a check of consistency, it is possible to show that the system of the Car-Oriented equations marginalises to the Continuity Equation.

Proof. For $\ell < L$, by marginalisation,

$$\dot{\rho}_{\ell}^{t} = \sum_{m=0}^{L-\ell} \dot{P}_{\ell}^{t}(m).$$

Then,

$$\begin{split} \dot{\rho}_{\ell}^{t} &= r_{\ell-1} \sum_{m=0}^{L-\ell} P_{\ell-1}^{t}(m+1) - r_{\ell} \sum_{m=0}^{L-\ell} P_{\ell}^{t}(m)(1-\delta_{m0}) + \sum_{m=0}^{L-\ell} r_{\ell+m} P_{\ell}^{t}[10^{m-1}10](1-\delta_{m0}) \\ &- \sum_{m=0}^{L-\ell} r_{\ell+m+1} P_{\ell}^{t}[10^{m}10] \end{split}$$

Now, for the first sum we translate the variable by one, for the second and the third sums we do not consider the null terms corresponding to m = 0 (they vanish due to the Kronecker delta) and for the last sum we recall that $r_{L+1} = 0$ and thus we truncate it to the term in $m = L - \ell - 1$.

$$\begin{split} \dot{\rho}_{\ell}^{t} &= r_{\ell-1} \sum_{m=1}^{L-\ell+1} P_{\ell-1}^{t}(m) - r_{\ell} \sum_{m=1}^{L-\ell} P_{\ell}^{t}(m) + \sum_{m=1}^{L-\ell} r_{\ell+m} P_{\ell}^{t}[10^{m-1}10] - \sum_{m=0}^{L-\ell-1} r_{\ell+m+1} P_{\ell}^{t}[10^{m}10] \\ &= r_{\ell-1} P_{\ell-1}^{t}[10] - r_{\ell} P_{\ell}^{t}[10] + \sum_{m=0}^{L-\ell-1} r_{\ell+m+1} P_{\ell}^{t}[10^{m}10] - \sum_{m=0}^{L-\ell-1} r_{\ell+m+1} P_{\ell}^{t}[10^{m}10] \\ &= J_{\ell-1}^{t} - J_{\ell}^{t}, \end{split}$$

which matches the continuity equation for the density at node ℓ .

For the case $\ell = L$, proceeding in the same way,

$$\dot{\rho}_{L}^{t} = \sum_{m=1}^{L} \dot{P}_{L-m}^{t}(m-1) = r_{L-1}P_{L-1}^{t}[10] - \beta \rho_{L}^{t} = J_{L-1}^{t} - J_{L}^{t},$$

which matches the continuity equation for the density at node L.

Q.E.D.

3.3 The Car-Oriented Mean-Field approximation

As we mentioned before, the COMF approximation assumes the gaps to be independent. This entails that we can write the unknowns $P_{\ell}^{t}[10^{m}10]$ appearing in equation (3.3) in the following way

$$P_{\ell}^{t}[10^{m}10] \simeq P_{\ell}^{t}[10^{m}1]P_{\ell+m+2}^{t}[0] = P_{\ell}^{t}(m)(1 - \rho_{\ell+m+2}^{t}).$$

Therefore, the COMF equation comes as

$$\dot{P}_{\ell}^{t}(m) = r_{\ell-1} P_{\ell-1}^{t}(m+1) - r_{\ell} P_{\ell}^{t}(m)(1 - \delta_{m0}) + r_{\ell+m} P_{\ell}^{t}(m-1)(1 - \rho_{\ell+m+1}^{t})(1 - \delta_{m0}) - r_{\ell+m+1} P_{\ell}^{t}(m)(1 - \rho_{\ell+m+2}^{t})$$
(3.4)

A small but rather important detail is the case $\ell = 0$, m = 1. The Car-Oriented equation (3.3) would give

$$\dot{P}_0^t(1) = -\alpha P_0^t(1) + r_1 P_1^t[10] - r_2 P_1^t[010];$$

while the COMF equation (3.4) reads

$$\dot{P}_0^t(1) = -\alpha P_0^t(1) + r_1 \rho_1^t(1 - \rho_2^t) - r_2 P_1^t(1)(1 - \rho_3^t).$$

We see that the COMF equation is just the Car-Oriented one where both $P_1^t[010]$ and $P_1^t[10]$ have been factorised. In principle the term $P_1^t[10]$ need not be factorised, as it is a marginal of our variables and indeed can be obtained as

$$P_1^t[10] = \sum_{m=1}^{L-1} P_1^t(m).$$

Nevertheless, we choose to approximate it in order to maintain the PH symmetry. Indeed, the PH symmetric of $P_1^t[10]$ is $P_{L_1}^t[10]$ and we can prove that this factorises as $\rho_{L-1}^t(1-\rho_L^t)$. Actually the proof is valid for every $\ell \in \{2, \ldots, L-1\}$, and is the following:

$$P_{\ell}^{t}[10] = \sum_{i=0}^{\ell-1} P_{i}^{t}[10^{\ell-i-1}10] = (1 - \rho_{\ell+1}^{t}) \sum_{i=0}^{\ell-1} P_{i}^{t}(\ell-i-1) = \rho_{\ell}^{t}(1 - \rho_{\ell+1}^{t}).$$
 (3.5)

This choice of factorising also $P_1^t[10]$ has the important consequence that, in every moment, the density profiles obtained with the COMF and the MF approximations are equivalent, since all the currents

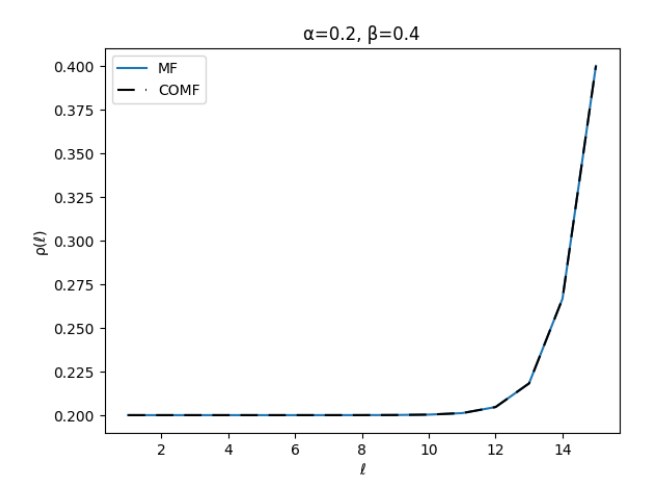


Figure 3.2: Comparison between the COMF and MF density profiles at the stationary state in the LD phase, with $\alpha = 1/5$, $\beta = 2/5$, for a chain of length L = 15.

factorise as in the MF condition, as equation (3.5) shows. Therefore, the COMF approximation gives no enhancement on the stationary state density profile with respect to the MF approximation in the case of OBC. On the other hand — as we have described at the beginning of this chapter — in the case of translational invariance the COMF theory does represent an improvement with respect to the traditional MF approximation. We conclude that such improvement is related to the translational symmetry.

This result that — at the stationary state — COMF is equivalent to MF is also confirmed numerically, as it is shown in figure 3.2.

Numerical Implementation

Since the equation (3.4) for $\dot{P}_{\ell}^t(m)$ involves the probabilities of the longer gap $P_{\ell}^t(m+1)$ and the one of the shorter gap $P_{\ell}^t(m-1)$, all the variables in our set are coupled. Therefore, in order to compute numerically the values of our variables at the stationary state, we need to evolve all of them: we shall study all the equations for any value of the index ℓ and for any value of the index ℓ . More concretely, at each time step we compute the new values of all the variables, which we use for the following time step. As in the k-Cluster approximations, we use an EEM with $\Delta t \leq \frac{1}{10}$ and an initial density equal to the bulk value of the homogeneous phase corresponding to the respective values of α and β , as it has been described at the beginning of chapter 2.

Finally, we note that, in terms of computational cost, the algorithm is slower than the standard MF approach, as it involves $\mathcal{O}(L^2)$ variables, whereas traditional MF deals with only $\mathcal{O}(L)$.

3.4 The Car-Oriented Pair approximation

The extension of the Pair approximation to the Car-Oriented approach amounts to assuming some factorisation of the kind

$$P_{\ell}^{t}[10^{m}10] \simeq \frac{P_{\ell}^{t}[10^{m}1]P_{\ell+m+1}^{t}[10]}{P_{\ell+m+1}^{t}[1]} = \frac{P_{\ell}^{t}(m)P_{\ell+m+1}^{t}[10]}{\rho_{\ell+m+1}^{t}},$$

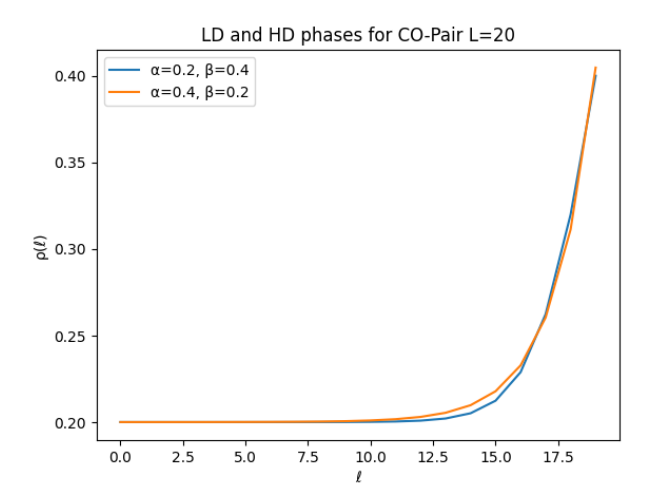


Figure 3.3: LD and HD profiles for the Car-Oriented Pair approximation, at the stationary state. The HD profile has been reversed and subtracted to 1: $\rho_{\ell}^{\text{HD}} \mapsto 1 - \rho_{L-(\ell-1)}^{\text{HD}}$. If the approximation were PH symmetric, the two profiles would perfectly overlap. The chain here is long L=20 and the values of α and β are 1/5, 2/5 for the LD phase (and they are swapped in the HD phase).

which resembles the 2-cluster approximation restricted to the particle between the two gaps. Plugging this approximation inside the Car-Oriented equation (3.3) we obtain the Car-Oriented Pair equation

$$\begin{split} \dot{P}_{\ell}^{t}(m) &= r_{\ell-1} P_{\ell-1}^{t}(m+1) - r_{\ell} P_{\ell}^{t}(m)(1-\delta_{m0}) + r_{\ell+m} \frac{P_{\ell}^{t}(m-1) P_{\ell+m}^{t}[10]}{\rho_{\ell+m}^{t}} (1-\delta_{m0}) \\ &- r_{\ell+m+1} \frac{P_{\ell}^{t}(m) P_{\ell+m+1}^{t}[10]}{\rho_{\ell+m+1}^{t}}. \end{split}$$

We also implemented this equation — in much the same way it has been described for the COMF approximation — but we realised that the PH symmetry was broken, as can be seen in figure 3.3. This can be understood by considering the quantity $P_{\ell}^{t}[1010]$, which would be mapped to

$$P_{\ell}^{t}[1010] \mapsto P_{L-(\ell+2)}^{t}[1010],$$

while our approximation gives

$$\begin{split} P_{\ell}^{t}[1010] &= \frac{P_{\ell}^{t}[101]P_{\ell+2}^{t}[10]}{\rho_{\ell+2}^{t}} \\ &\mapsto \frac{P_{L-(\ell+1)}^{t}[010]P_{L-(\ell+2)}^{t}[10]}{1-\rho_{L-(\ell+1)}^{t}} \\ &\neq \frac{P_{L-(\ell+2)}^{t}[101]P_{L-\ell}^{t}[10]}{\rho_{L-\ell}^{t}} \\ &= P_{L-(\ell+2)}^{t}[1010]. \end{split}$$

In order to restore the PH symmetry (and produce some enhancement over the cluster approximations), we built the following approximation.

3.5 The Car-Oriented Triplet approximation

The Car-Oriented Triplet approximation (COTR) is the extension of the Triplet approximation to the Car-Oriented variables. It amounts to factorise the unknowns of the Car-Oriented equation (3.3) as it is done in the (3,2)-cluster approximation but only at the node between the two gaps:

$$P_{\ell}^{t}[10^{m}10] \simeq \frac{P_{\ell}^{t}[10^{m}1]P_{\ell+m}^{t}[010]}{P_{\ell+m}^{t}[10]}.$$

The factor $P_\ell^t[010]$ does not belong to our set of Car-Oriented variables, but is just the PH symmetric version of $P_\ell^t[101]$ (more precisely, $P_\ell^t[010]$ is the PH symmetric of $P_{L-(\ell+1)}^t[101]$), which does belong to our set of variables. Hence, the need of considering, for this approximation, a set of variables that is greater than the set $\{P_\ell^t(m)\}_{\ell,m}$ considered thus far and corresponds to

$$\left\{P_{\ell}^{t}(m) := P_{\ell}^{t}[10^{m}1], H_{\ell}^{t}(m) := P_{\ell}^{t}[01^{m}0]\right\}_{\ell,m}$$

for the usual values of ℓ and m. We can extend the approximation to the full configuration in the following way

$$P^{t}[\underline{n}] = P_{1}^{t}[10^{m_{1}}1^{n_{1}}0^{m_{2}}\cdots0^{m_{k}}1^{n_{k}}0]$$

$$\simeq \frac{\prod_{i=1}^{k}P_{\ell_{i}}^{t}[10^{m_{i}}1]P_{\ell_{i}+m_{i}}^{t}[01^{n_{i}}0]}{P_{m_{1}+1}^{t}[01]\prod_{i=2}^{k}P_{\ell_{i}}^{t}[10]P_{\ell_{i}+m_{i}}^{t}[01]}$$

$$= \frac{\prod_{i=1}^{k}P_{\ell_{i}}^{t}(m_{i})H_{\ell_{i}+m_{i}}^{t}(n_{i})}{P_{m_{1}+1}^{t}[01]\prod_{i=2}^{k}P_{\ell_{i}}^{t}[10]P_{\ell_{i}+m_{i}}^{t}[01]}$$
(3.6)

where $\ell_i = 1 + \sum_{j=1}^{i-1} m_j + n_j \ \forall i \in \{1, ..., k\}$ and we assumed for simplicity that the configuration starts with $n_1 = 1$ and ends with $n_L = 0$ (in case this is not true, just consider the fictitious nodes 0 and L + 1 with $n_0 = 1$ and $n_{L+1} = 0$).

Remark. The COTR approximation is PH symmetric.

Proof. Consider the PH transformation of both members of equation (3.6). The left-hand-side transforms as

$$P_1^t[10^{m_1}1^{n_1}0^{m_2}\cdots 0^{m_k}1^{n_k}0] \mapsto P_1^t[10^{n_k}1^{m_k}\cdots 1^{m_2}0^{n_1}1^{m_1}0]; \tag{3.7}$$

while the right-hand-side becomes

$$\frac{\prod_{i=1}^{k} P_{\ell_{i}}^{t}[10^{m_{i}}1] P_{\ell_{i}+m_{i}}^{t}[01^{n_{i}}0]}{P_{m_{1}+1}^{t}[01] \prod_{i=2}^{k} P_{\ell_{i}}^{t}[10] P_{\ell_{i}+m_{i}}^{t}[01]} \mapsto \frac{\prod_{i=1}^{k} P_{L-(\ell_{i}+m_{i})}^{t}[01^{m_{i}}0] P_{L-(\ell_{i}+m_{i}+n_{i})}^{t}[10^{n_{i}}1]}{P_{L-(m_{1}+1)}^{t}[01] \prod_{i=2}^{k} P_{L-\ell_{i}}^{t}[10] P_{L-(\ell_{i}+m_{i})}^{t}[01]}.$$
(3.8)

The right-hand-side of (3.8) is nothing but the COTR factorisation of the right-hand-side of (3.7). Thus, the approximation is PH symmetric. *Q.E.D.*

Now that we have enlarged our set of variables to include variables $H_{\ell}^t(n)$, we need some dynamical equation to describe the evolution of these quantities. To ensure consistency at the boundaries, we introduce the following conventions:

$$P_{-1}^{t}[101^{n}0] := 0, \qquad H_{\ell}^{t}(L - \ell) := P_{\ell}^{t}[01^{L - \ell}], \qquad H_{\ell}^{t}(L - \ell + 1) := 0, \qquad H_{0}^{t}(L) := P_{\ell}^{t}[1^{L}]. \tag{3.9}$$

With these definitions, we can write the following (exact) evolution equation for variables $H_{\ell}^{t}(n)$:

$$\dot{H}_{\ell}^t(n) = -r_{\ell-1}P_{\ell-1}^t[101^n0] + r_{\ell}P_{\ell}^t[101^{n-1}0](1-\delta_{n0}) - r_{\ell+n}H_{\ell}^t(n)(1-\delta_{n0}) + r_{\ell+n+1}H_{\ell}^t(n+1),$$

for each $\ell \in \{0, ..., L-1\}$ and for each $n \in \{0, ..., L\}$ under the constraint $1 \le \ell + n \le L$. We can also give some physical interpretation of this equation.

- 1. Term $-r_{\ell-1}P_{\ell-1}^t[101^n0]$ represents the loss of the configuration coming from the occupation of the first hole of the cluster by some other particle, i.e. to the jump of one particle from node $\ell-1$ to node ℓ . In case $\ell=0$ the first hole does not exist, so this term must be null, so we set $r_{-1}=0$.
- 2. Term $r_\ell P_\ell^t[101^{n-1}0](1-\delta_{n0})$ represents the gain of the configuration due to the jump of the first particle to its position, i.e. to the hop of the particle from node ℓ to node $\ell+1$. This is possible only when the length of the particle-queue is non-null.
- 3. Term $-r_{\ell+n}H^t_{\ell}(n)(1-\delta_{n0})$ corresponds to the loss coming from the jump of the last particle in the queue to the following node, i.e. to the hop of the particle from node $\ell+n$ to node $\ell+n+1$. This is possible only if the length of the particle-queue is greater than zero.
- 4. The term $r_{\ell+n+1}H_{\ell}^t(n+1)$ represents the gain due to the last site becoming empty, i.e. the jump of a particle from position $\ell+n+1$ to the next site. In the case $n=L-\ell$, this final hole does not exist, so we set $r_{L+1}=0$.

Our system of Car-Oriented equations now reads

$$\begin{cases} \dot{H}_{\ell}^{t}(n) = -r_{\ell-1}P_{\ell-1}^{t}[101^{n}0] + r_{\ell}P_{\ell}^{t}[101^{n-1}0](1 - \delta_{n0}) - r_{\ell+n}H_{\ell}^{t}(n)(1 - \delta_{n0}) + r_{\ell+n+1}H_{\ell}^{t}(n+1) \\ \dot{P}_{\ell}^{t}(m) = r_{\ell-1}P_{\ell-1}^{t}(m+1) - r_{\ell}P_{\ell}^{t}(m)(1 - \delta_{m0}) + r_{\ell+m}P_{\ell}^{t}[10^{m-1}10](1 - \delta_{m0}) - r_{\ell+m+1}P_{\ell}^{t}[10^{m}10]. \end{cases}$$

The COTR approximation (3.6) implies that the unknowns in our equations can be rewritten as

$$P_{\ell}^{t}[10^{m}10] \simeq \frac{P_{\ell}^{t}(n)H_{\ell+m}^{t}(1)}{P_{\ell+m}^{t}[01]}, \qquad \qquad P_{\ell}^{t}[101^{n}0] \simeq \frac{P_{\ell}^{t}(1)H_{\ell+1}^{t}(n)}{P_{\ell+1}^{t}[01]}.$$

The introduction of variables $H_{\ell}^t(n)$ also has the relevant consequence that some of our unknowns can be obtained simply by marginalisation:

$$P_{\ell}^{t}[110] = P_{\ell+1}^{t}[10] - H_{\ell}^{t}(1) \qquad \qquad P_{\ell}^{t}[100] = P_{\ell}^{t}[10] - P_{\ell}^{t}(1).$$

Therefore, the COTR system of approximated equations is

$$\begin{cases} \dot{P}_{\ell}^{t}(0) = r_{\ell-1}P_{\ell-1}^{t}(1) - r_{\ell+1}(P_{\ell+1}^{t}[10] - H_{\ell}^{t}(1)) \\ \dot{P}_{\ell}^{t}(m) = r_{\ell-1}P_{\ell-1}^{t}(m+1) - r_{\ell}P_{\ell}^{t}(m) + r_{\ell+m}\frac{P_{\ell}^{t}(m-1)H_{\ell+m-1}^{t}(1)}{P_{\ell+m-1}^{t}[01]} - r_{\ell+m+1}\frac{P_{\ell}^{t}(m)H_{\ell+m}^{t}(1)}{P_{\ell+m}^{t}[01]} & m>0 \end{cases} \\ \dot{H}_{\ell}^{t}(0) = -r_{\ell-1}(P_{\ell-1}^{t}[10] - P_{\ell-1}^{t}(1)) + r_{\ell+1}H_{\ell}^{t}(1) \\ \dot{H}_{\ell}^{t}(n) = -r_{\ell-1}\frac{P_{\ell-1}^{t}(1)H_{\ell}^{t}(n)}{P_{\ell}^{t}[01]} + r_{\ell}\frac{P_{\ell}^{t}(1)H_{\ell+1}^{t}(n-1)}{P_{\ell+1}^{t}[01]} - r_{\ell+n}H_{\ell}^{t}(n) + r_{\ell+n+1}H_{\ell}^{t}(n+1) & n>0, \end{cases}$$

with appropriate adjustments at the border (see appendix B.1).

3.5.1 Comparison between the Car-Oriented Triplet and the Triplet approximations

After implementing the COTR approximation (in much the same way it has been described in section 3.3 for the COMF approximation), we have compared the numerical results for the COTR and the Triplet approximations in order to verify the enhancement of this new approach (which is numerically more expensive as it considers a number of variables that is $\mathcal{O}(L^2)$, while the traditional Triplet only involves $\mathcal{O}(L)$ variables). As figures 3.4 and 3.5 show, there is little difference between the COTR and the Triplet approximations in the case of uniform unit inner rates, both for the density profiles (figure 3.4) and for the profiles of the cluster probabilities (i.e. the vectors $\underline{P}^t(m)$ with components $P_\ell^t(m)$ for $\ell \in \{0, \ldots, L-m\}$). Indeed, we expect the COTR approximation to show enhancement over the Triplet one mainly in contexts where longer correlations — which the COTR approximation accounts for, at least partially — become important, i.e. in case the system favours long queues. This motivated

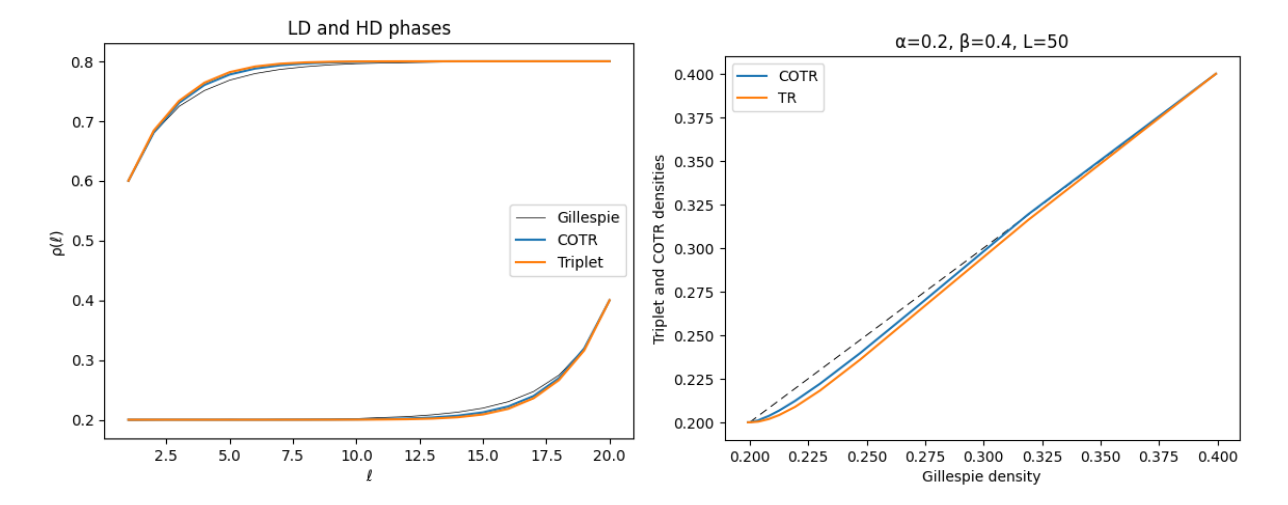


Figure 3.4: Homogeneous inner rates, comparison between the Gillespie simulation and the Triplet and COTR approximations, in the LD ($\alpha = 1/5$, $\beta = 2/5$) and HD phases ($\alpha = 2/5$ and $\beta = 1/5$), for a chain of length L = 20. On the left panel, we plot the density profiles in the LD and HD phases. On the right panel, we plot the approximated densities as a function of the simulated one. The black dashed line is the usual reference line, corresponding to the Gillespie density plotted against itself.

us to analyse the two approximations in disordered systems, particularly in the case of the type-I quenched disorder, as it has been defined in section 1.2.1. We compare the two approximations with some Gillespie simulations in two different situations: the bottleneck system and the case of random, uniformly distributed rates in the range $[\gamma, 1]$, at different values of γ .

Bottleneck with single impurity

We will study a system with an even number of lattice sites and inner rates all equal to 1, except the rate at position k = L/2. We will call the latter the 'bottleneck' and denote it by γ . We will study the density profiles obtained with our approximations and with Gillespie simulations at several values of the bottleneck.

The case of a TASEP in OBC with only one site-wise impurity at the centre of the chain has already been studied by Kolomeisky [49] for the MF approximation compared to Monte-Carlo simulations. The study shows that the MF theory is in good qualitative agreement with the simulated density profile, but it is poor at describing it quantitatively for certain values of α , β and γ .

Our results generalise this finding of Kolomeisky's to the Triplet and COTR approximations. It is however interesting, from our point of view, that the COTR approximation has shown to yield density profiles which are closer to the simulated ones with respect to the Triplet approximation at every value of the bottleneck γ and at any value of α and β , although representing a relatively small enhancement.

In order to understand the results, we developed the following argument. If γ is small enough, the total chain can be regarded as two different TASEP systems, only slightly correlated at the impurity, located at site k = L/2. There, we assume the current factorises as $J_k \simeq r_k \rho_k (1 - \rho_{k+1})$, so that we can easily identify an effective extraction rate $\beta_{\rm eff}$ at position k and an effective injection rate $\alpha_{\rm eff}$ at position k+1, given by

$$\beta_{\text{eff}} = \gamma (1 - \rho_{k+1}), \qquad \qquad \alpha_{\text{eff}} = \gamma \rho_k.$$
 (3.10)

These values of ρ_k , ρ_{k+1} depend on α , β and γ . In order to study their dependence on the bottleneck, we imagine to increase the value of γ from 0 to 1. For sufficiently small values of γ , we expect the part of the chain on the left to be in a HD phase and the one on the right to be in a LD phase (in the limit

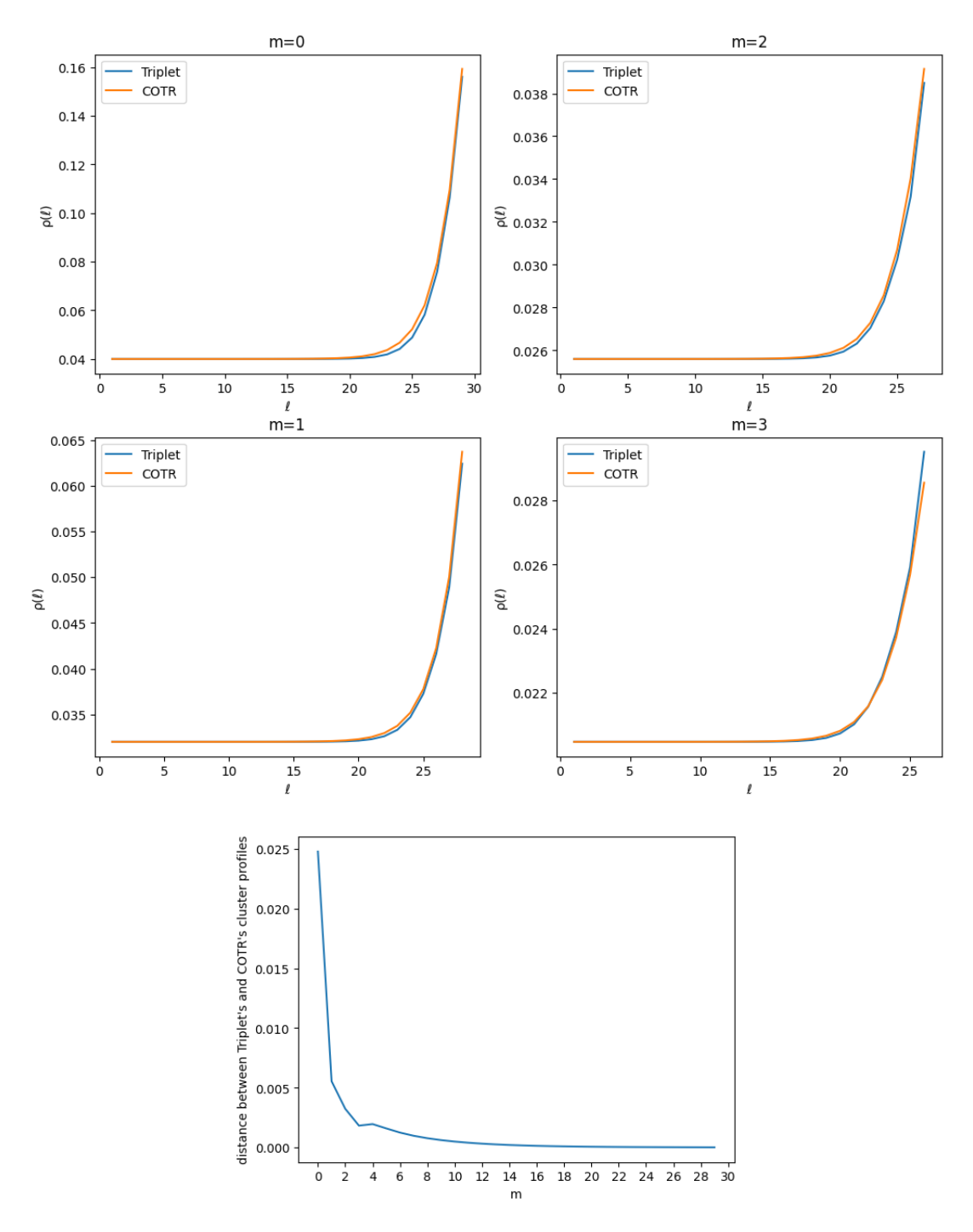


Figure 3.5: Homogeneous inner rates, comparison between the Triplet and COTR profiles for the probability $P_\ell[10^m1]$ for all ℓ and at fixed m. First four panels show the two profiles at m=0,1,2,3. Last panel shows the 1-norm distance between the profiles for every m. The length of the chain is L=30 and the injection and extraction rates are, respectively, $\alpha=1/5$, $\beta=2/5$. We notice that the distance between the COTR and the Triplet profiles vanishes as m grows. The comparison shows some change in the Triplet profile at m=3. This is due to the fact that for $m\geq 3$ Triplet includes also factors $P_\ell[000]$ in its factorisation, while for m<3 it does not.

 $\gamma \to 0^+$ the left chain is completely occupied and the right chain is totally unoccupied, if α and β are greater than zero). Thus, if L is sufficiently large, ρ_k will correspond to the HD phase bulk density $\rho_k = 1 - \beta_{\rm eff}$, while ρ_{k+1} will correspond to the LD phase bulk density $\rho_{k+1} = \alpha_{\rm eff}$. Equations (3.10) yield

$$\beta_{\text{eff}} = \alpha_{\text{eff}} = \frac{\gamma}{1+\gamma}.\tag{3.11}$$

Suppose $\alpha < \beta$ (the case $\alpha > \beta$ is just the PH symmetric of it). We know that at $\gamma = 1$ the system will be in a LD phase, so we expect that before γ approaches the value of 1, also the left chain will transition to a LD phase. This will happen as soon as $\beta_{\rm eff} > \alpha$ ($\alpha_{\rm eff} > \beta$), which gives a "critical" value of γ that can be found solving

$$\beta_{\rm eff} = \alpha$$
.

The solutions are

$$\gamma_c = \frac{-1 \pm \sqrt{1 + 4\alpha(\alpha - 1)}}{2(\alpha - 1)} \tag{3.12}$$

(if $\alpha > \beta$ just substitute α with β). At this value, we expect to see something like a domain-wall profile for our approximations and a linear one for the exact solution; so it is reasonable to expect less accuracy from our approximations when γ tends to the critical value γ_c .

When the system has transitioned to the global LD phase, the density at the right end of the left chain will be $\rho_k = \frac{\alpha(1-\alpha)}{\beta_{\rm eff}}$, which depends on γ through $\beta_{\rm eff}$. At the left end of the right chain, we have a bulk density given by

$$\rho_{k+1} = \alpha_{\text{eff}} = \gamma \rho_k = \frac{\alpha(1-\alpha)}{\alpha_{\text{eff}}}.$$

Solving for α_{eff} , we get

$$\alpha_{\rm eff} = rac{1}{2} \pm \left| \alpha - rac{1}{2}
ight|.$$

Since $\alpha < \frac{1}{2}$ by hypothesis, then

$$\alpha_{\text{eff}} = \begin{cases} \alpha \\ 1 - \alpha. \end{cases}$$

But the system must be in a LD phase, so we discard the solution $1 - \alpha > \frac{1}{2}$ and we find $\alpha_{\text{eff}} = \alpha$. This is indeed what can be observed in figure 3.6 for $\gamma \ge 1/5$.

In the case $\alpha, \beta > 1/2$, we expect the transition to happen when $\alpha_{\rm eff}$ and $\beta_{\rm eff}$ cross the value of 1/2. Here, there is only one solution of (3.12): $\gamma_c = 1$, which corresponds to the TASEP with homogeneous inner rates. Therefore, our approximation predicts that the LD phase on the left and the HD phase on the right persist up to $\gamma = 1$, when the system gets into a MC phase. This transition is predicted to be continuous from formula (3.11) (and this is confirmed by the plots in figure 3.7). Indeed, the limit for $\gamma \to 1$ gives $\alpha_{\rm eff} = \beta_{\rm eff} = 1/2$, implying

$$\rho_k = 1 - \beta_{\text{eff}} = \frac{1}{2}$$
 and $\rho_k = \alpha_{\text{eff}} = \frac{1}{2}$.

On the other hand, it is known that the bulk density of the MC phase is $\rho = 1/2$, so the transition is continuous. Moreover, it is reasonable to expect that the distance between the approximated density profiles and the simulated ones will reach a minimum at the transition, as here there is no inhomogeneity.

Numerically, we studied a chain of length L=150 for the case $\alpha<\beta$ and a chain of length L=200 for the case $\alpha>1/2$, $\beta>1/2$. Figure 3.6 collects the density profiles obtained for different values of $\gamma<1$ at $\alpha<\beta$ and $\alpha<1/2$, and figure 3.7 shows the same density profiles for $\alpha,\beta>1/2$. There is no need to investigate also the case $\beta<\alpha$ and $\beta<1/2$ as this is nothing but the PH symmetric of the case $\alpha<\beta$, $\alpha<1/2$. Our argument is in qualitatively good agreement with the numerical results,

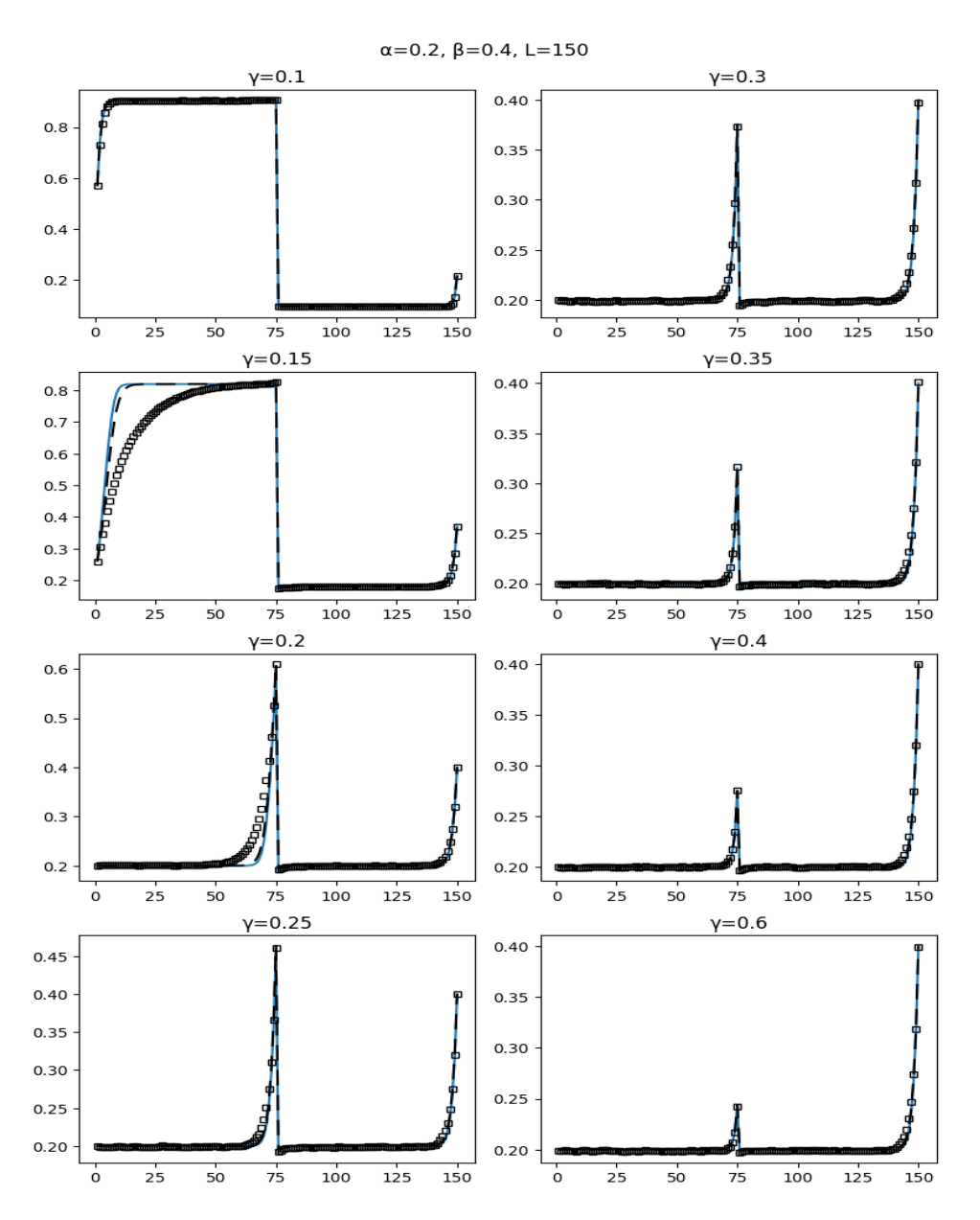


Figure 3.6: Density profiles in the presence of a single impurity with $\alpha=1/5$, $\beta=2/5$ and L=150: on the *y*-axis the value of the density, on the *x*-axis the corresponding node. The squares are the simulation results (we averaged over 3×10^8 configurations), the two lines are the Triplet (solid, blue line) and the COTR (dashed, black line) density profiles (with no convergence condition, for $T=10^4$, $N_t=10^5$), for various values of $\gamma<1$. We simulated for 8 values of γ equally spaced in the interval [0.1,0.6]. The estimated (approximate) value of γ_c is 1/4.

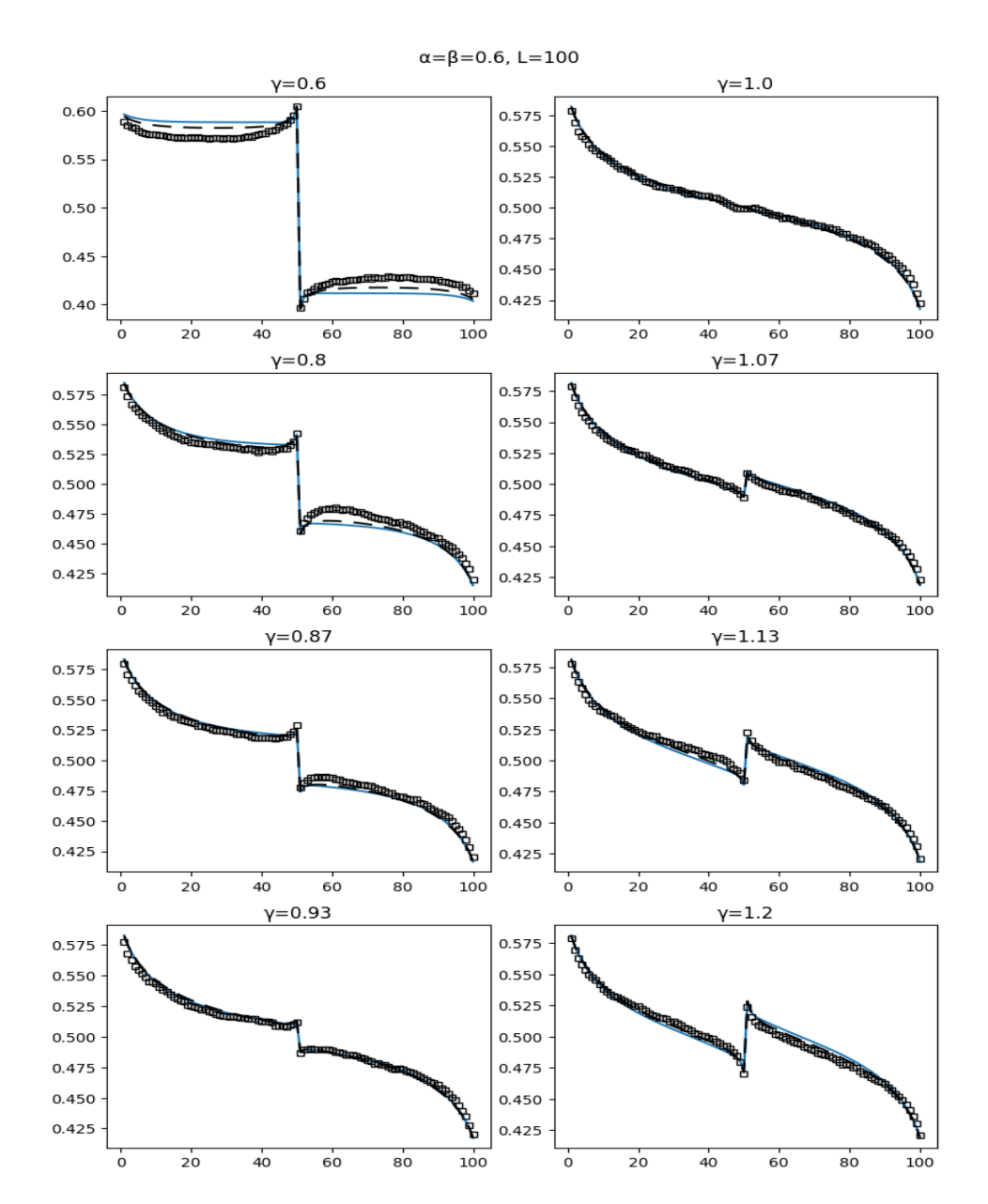


Figure 3.7: Density profiles in the presence of a single impurity with $\alpha = \beta = 3/5$ and L = 200: on the *y*-axis the value of the density, on the *x*-axis the corresponding node. The squares are the simulation results (we averaged over 3×10^8 configurations), the two lines are the Triplet (solid, blue line) and the COTR (dashed, black line) density profiles (with no convergence condition, for $T = 10^4$, $N_t = 10^5$), for various values of $\gamma < 1$. We simulated for 8 values of γ equally spaced in the interval [0.6, 1.2]. The estimated value of γ_c is 1.

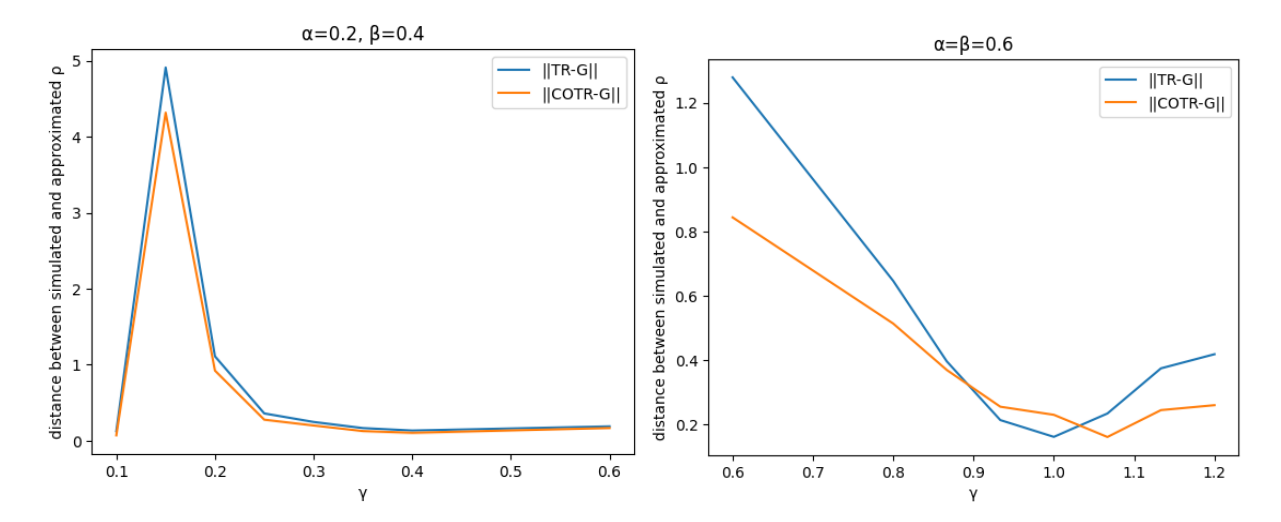


Figure 3.8: Distance in 1-norm between the Gillespie density vector and the two approximations. Left panel shows the case for $\alpha = 1/5$, $\beta = 2/5$, L = 150; right panel the one of $\alpha = \beta = 3/5$, L = 200.

although, as it could be expected, the value of γ_c for the LD phase is not very accurate (we see the transition happens between $\gamma = 0.15$ and $\gamma = 0.2$, while the approximate value of γ_c given by formula (3.12) is 0.25).

Finally, figure 3.8 shows the distance (in 1-norm) between the Gillespie density vector and the approximated ones. We notice that the COTR approximation always yields better results than the Triplet's. Also, we notice that there is a peak in both approximations at the values of γ for which the left side of the chain transitions from LD to HD, in the case α , $\beta < \frac{1}{2}$. This is in agreement with our expectation: our approximations exhibit a shock profile, while the simulated density is linear in the left chain. On the other hand, in the case α , $\beta > \frac{1}{2}$ the value of γ for which the transition to a MC phase occurs corresponds to a minimum in the distance between the simulated and approximated density profiles. This is as expected: the transition occurs at $\gamma_c = 1$, which makes all rates equal to one. We know that

the uniform case is the one in which the approximations are closest to the simulated profile.

Extended bottleneck

Figures 3.6 and 3.7 show that both the approximated density profiles are accurate in proximity of the impurity. This can be understood by considering that, at the impurity, correlations are reduced and therefore MF is already a good approximation. Thus, all the cluster approximations (and Car-Oriented cluster approximations) are accurate and therefore there is little difference between them. This motivated us to look for a bottleneck system where the presence of impurities did not bring such a steep decay of the correlations. With this spirit, we turned to the study a bottleneck where the single impurity was extended to a whole region of length $\lambda > 1$, placed at the centre of the chain, where all rates are equal to γ . We call this portion of the chain the 'slow' region and we refer to this kind of system as the 'extended bottleneck'. When γ is sufficiently small (with respect to α and β) and λ sufficiently large (with respect to the correlation length at the borders between the normal and the slow region), we expect this region to be in some sort of MC phase (in a qualitative sense), as the rate limiting step is in the bulk. Therefore, there will be some boundary layer following the impurity: thus, correlations are expected to play some major role with respect to the bottleneck with single impurity. Following the approximation above, we interpret the system as three decorrelated chains: one at the left of the slow region, one in the slow region and another one at the right of it. Moreover, we give a name to the site at the left of the slow region: we call it $j = k - \lambda/2$ (assuming λ is even). As we

neglect correlations between different regions, we factorise the current at the borders

$$J \simeq \gamma \rho_{j-1} (1 - \rho_j) \simeq \gamma \rho_{j+\lambda-1} (1 - \rho_{j+\lambda})$$

and define some effective injection and extraction rates as $\beta_{\text{eff}}^{(1)}$, $\alpha_{\text{eff}}^{(1)}$, $\beta_{\text{eff}}^{(2)}$, $\alpha_{\text{eff}}^{(2)}$ such that

$$\beta_{\text{eff}}^{(1)} = \gamma (1 - \rho_j), \qquad \alpha_{\text{eff}}^{(1)} = \gamma \rho_{j-1}, \qquad \beta_{\text{eff}}^{(2)} = \gamma (1 - \rho_{j+\lambda}), \qquad \alpha_{\text{eff}}^{(2)} = \gamma \rho_{j+\lambda-1}.$$

Now, when γ is sufficiently small, the chain on the left is expected to be in a HD phase, the one on the right in some LD phase and the one in the middle in some MC-like phase. Therefore,

$$\rho_j \simeq 1 - \beta_{\rm eff}^{(1)}, \qquad \rho_{j+\lambda} \simeq \alpha_{\rm eff}^{(2)}, \qquad J \simeq \frac{\gamma}{4} \simeq \alpha_{\rm eff}^{(2)}(1 - \alpha_{\rm eff}^{(2)}) \simeq \beta_{\rm eff}^{(1)}(1 - \beta_{\rm eff}^{(1)}),$$

where we made the same approximations already described for the case of the bottleneck with single impurity, with the further assumption that, due to the MC-like phase in the slow region, the current approached the value of $J = \frac{\gamma}{4}$. Now we can solve the equations for the effective boundary rates. Consider the equation for $\beta_{\text{eff}}^{(1)}$:

$$\beta_{\rm eff}^{(1)}(1-\beta_{\rm eff}^{(1)}) = \frac{\gamma}{4} \implies \beta_{\rm eff}^{(1)} = \frac{1}{2}(1\pm\sqrt{1-\gamma}).$$

In the limit $\gamma \to 0^+$, the negative solution tends to zero, while we expect $\beta_{\rm eff}^{(1)} > \alpha$ (the left chain is expected to be in some HD phase). Thus, we consider only the positive solution. On the other hand, $\alpha_{\rm eff}^{(2)}$ obeys the same equation and the constraint $\alpha_{\rm eff}^{(2)} < \beta$ for $\gamma \to 0^+$ forces us to choose the negative sign (the right chain is expected to be in some LD phase). Thus,

$$\beta_{eff}^{(1)} = \frac{1}{2}(1+\sqrt{1-\gamma}) \qquad \text{and} \qquad \alpha_{eff}^{(2)} = \frac{1}{2}(1-\sqrt{1-\gamma}).$$

This implies that

$$\alpha_{eff}^{(1)} = \frac{\gamma}{2}(1-\sqrt{1-\gamma}), \qquad \text{and} \qquad \beta_{eff}^1 = \frac{\gamma}{2}(1+\sqrt{1-\gamma}).$$

Now, in order to estimate the critical value of γ for which some transition occurs, we choose again to consider the case $\alpha < \beta$, $\alpha < 1/2$ (the case $\beta < \alpha$, $\beta < 1/2$ is just its PH symmetric). When $\gamma = 1$ we know the system is in the LD phase; on the other hand, when γ is sufficiently small, we expect the left chain to be in a HD phase. Thus, before γ approaches the value of 1, we expect the left part of the chain to transition from a HD phase to a LD one. This transition will occur at $\alpha = \beta_{\rm eff}^{(1)}$, so the critical value of γ can be estimated as

$$\alpha = \frac{1}{2}(1 + \sqrt{1 - \gamma_c}) \implies \gamma_c = 4\alpha(1 - \alpha)$$

(in the case $\beta < \alpha$ just substitute α with β).

Numerically, we studied again a chain of length L=150 for the case $\alpha<\beta$ (the opposite case $\beta<\alpha$ is nothing but its PH symmetric) with $\lambda=50$, at several values of $\gamma<1$. Figure 3.9 collects the simulated and approximated density profiles obtained for various values of γ and shows that, for those values of α and β , our argument is more accurate in estimating the critical value of γ_c with respect to the case of single impurity. Indeed, for $\alpha=1/5$, $\beta=2/5$ our argument gives $\gamma_c=0.64$, while simulations show that the transition occurs approximately at $\gamma=0.62$. In this case, the error is approximately 0.02; instead, in the single-impurity case, for the same values of α and β , the error is approximately 0.08. Finally, figure 3.10 shows the distance (in 1-norm) between the Gillespie density vector and the approximated ones, with particular focus on the boundary layer following the first impurity. We notice that the COTR approximation always yields better results than the Triplet's. In particular, the enhancement

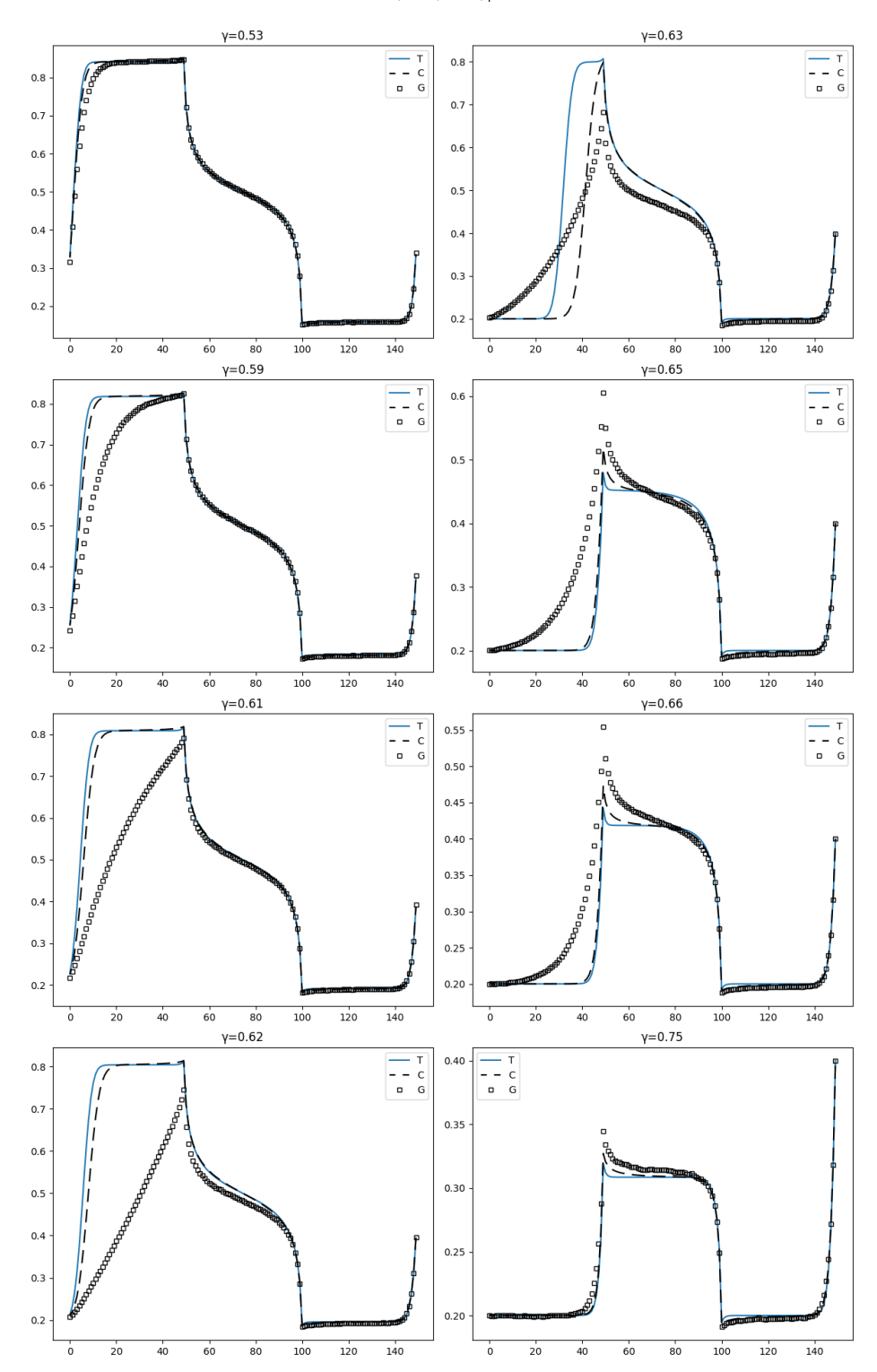


Figure 3.9: Extended bottleneck for a chain of length L=150, a slow region of size $\lambda=50$, and boundary rates $\alpha=1/5$, $\beta=2/5$. We simulated for 20 values of γ equally spaced in the interval [0.53,0.75], but we show only 8 profiles. The squares are the simulation results (we averaged over 3×10^8 configurations), the two lines are the Triplet (solid, blue line) and the COTR (dashed, black line) density profiles (with no convergence condition, for $T=10^4$, $N_t=10^5$), for various values of $\gamma<1$. The estimated value of γ_c is $\gamma_c=0.64$.

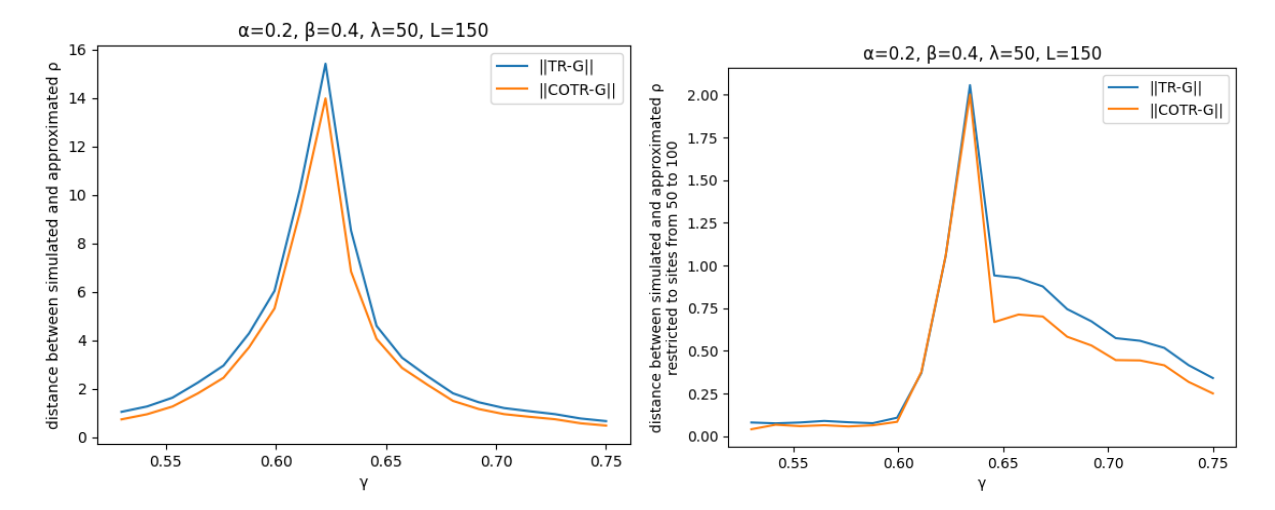


Figure 3.10: Distance in 1-norm between the simulated and approximated results for a bottleneck with extended impurity with L=150, $\lambda=50$, $\alpha=1/5$, $\beta=2/5$. Left panel shows the distance between the density vectors; right panel shows the distance between the density vectors restricted to the slow region.

is greater at the boundary layer on the left of the slow region. Here, indeed, node j is occupied with probability much greater than the following nodes and, therefore, the Car-Oriented variables $P_j[10^m1]$ play some important role.

Although some difference between the two approximations is sensible, their qualitative behaviour is essentially identical. Therefore, following the spirit of the Car-Oriented approach, we turned to the investigation of the values given by the two approximations for the probability distribution of queues of particles rather than the density. More concretely, we study the values given by the COTR and the Triplet approximations for variables $H^t_\ell(m)$, which depend on the size m of the particle-queue and on its starting position ℓ .

We start by considering the distribution of the particle-queue in the bulk. Here, due to the usual factorisation, the distribution is geometric, in the sense that

$$H_{\ell}^{t}(m) = H^{t}(m) = (1 - \rho)^{2} \rho^{m}.$$

Therefore, we expect that in a system where long correlations play some important role, as in the extended bottleneck, the Triplet approximation will not be able to capture the effect of these long correlations, and will simply display a geometric-like trend, only transitioning from one geometric distribution to another when crossing the different regions. On the other hand, if our claim that the COTR approximation is able to capture longer correlations is true, it might show some different behaviour.

Numerically, we investigated an extended bottleneck on a chain of length L=150 with $\alpha=1/5$, $\beta=2/5$ at varying γ and with an extension of the slow region equal to $\lambda=50$. We studied the values of variables $H_i(m)$ given by the two approximations, with fixed i at the centre of the left part of the chain, i.e. at site 25, and with varying m.

The Triplet approximation behaves as expected, displaying an approximately exponential decay (linear in the log–log plot). In contrast, the COTR approximation exhibits a significantly richer pattern.

This result motivates our belief in the fact that COTR is more sensitive than Triplet to long correlations and opens a route for further investigation on this difference between the two approximations. Such investigation would require comparing these numerical results with some simulations, and expanding the analytical considerations. This goes beyond the scope of the present work, but we believe it is an interesting path for future work.

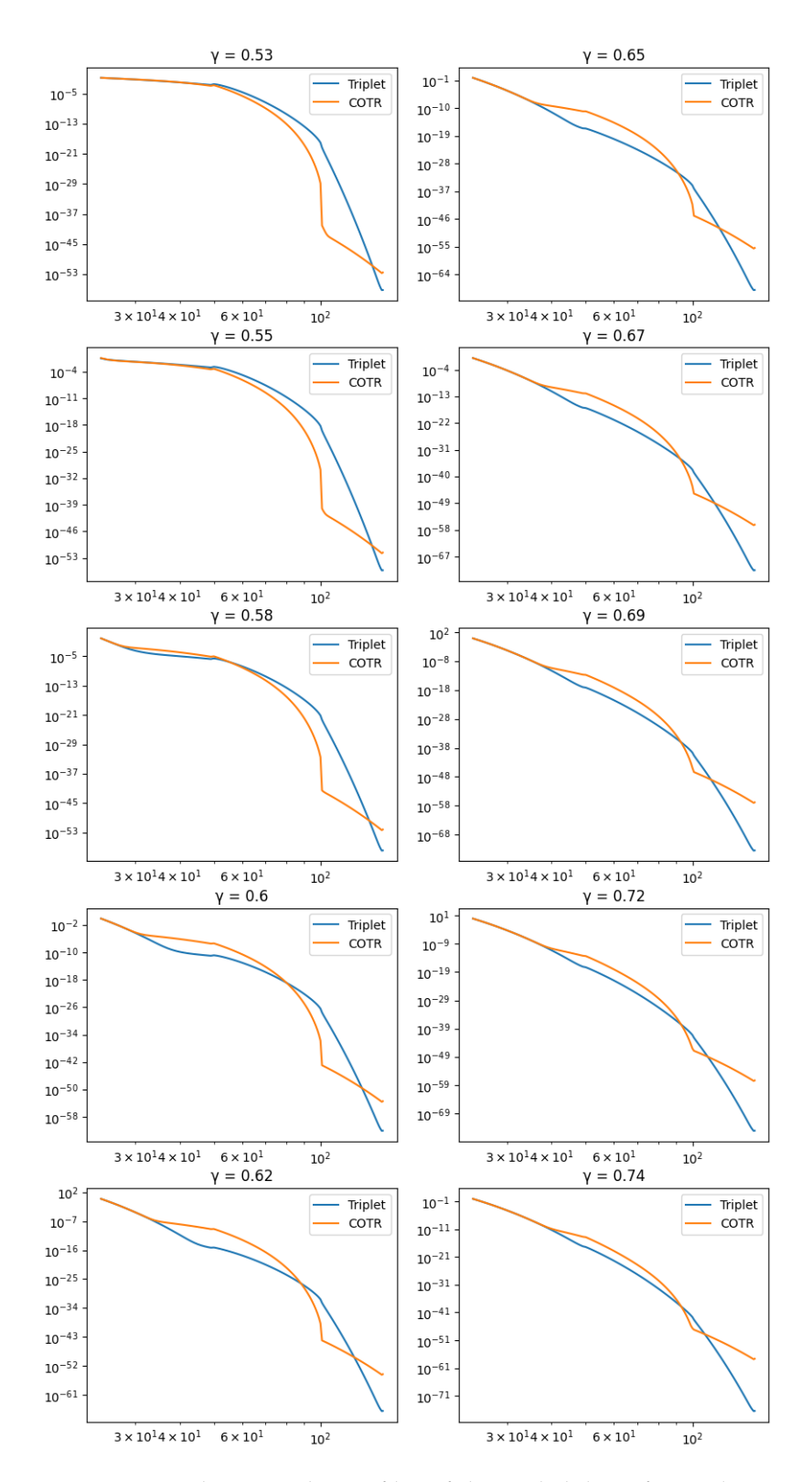


Figure 3.11: Comparison between the profiles of the probability of particle-queues given by the Triplet and the COTR approximations, in the case of an extended bottleneck with L=150, $\alpha=1/5$, $\beta=2/5$ and varying γ . On the *y*-axis, in log-scale, the values of variables $H_j(m)$ normalised with respect to $\sum_{m\geq 0} H_j(m)$ at the stationary state, with j placed at the centre of the left part of the chain (i.e. at site 25). On the *x*-axis, the value of m in log-scale.

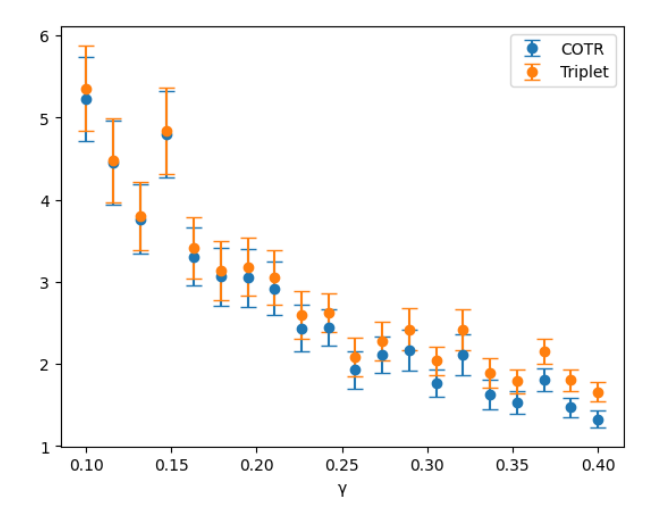


Figure 3.12: On the *x*-axis, the lower bound γ for the interval from which rates are drawn. On the *y*-axis, distances in 1-norm between the Triplet's and COTR's density profiles and Gillespie's. Dots represent the empirical average of the distance in 1-norm over 50 different realisations of inner rates; error bars represent the standard errors of such means. The size of the chain is L=100, at $\alpha=\beta=3/5$. The number of steps for the Gillespie algorithm is 10^8 for each realisation, while for the Triplet and COTR approximations we set T=1000, $N_t=5000$.

Random Uniformly Distributed Rates

We studied the quality of the COTR and the Triplet approximations in the case of random inner rates, drawn from the uniform distribution over the interval $[\gamma,1]$ at various values of γ . In order to do so, we compared the density profiles given by those approximations to the results of some Gillespie simulations. As a matter of fact, we realised 10^3 simulations and an equal number of numerical solutions given by Triplet's and COTR's algorithms. We considered 20 values of γ uniformly spaced between $\frac{1}{10}$ and $\frac{2}{5}$. For each value of γ we averaged over 50 different realisations. Also, we took a relatively large lattice (L=100) so that some self-averaging effect helped noise reduction. What we expect is that, when γ increases, the difference between the approximated density profiles and the simulated one decreases. This is indeed confirmed by our results, as it is shown in figure 3.12. It is interesting to see that in all cases the COTR distance from Gillespie's simulation is lower than that of Triplet, although the enhancement is relatively small and becomes even lower as γ decreases. Indeed, when γ is small, the high variance in the rates does not allow the growth of long queues, so the correlations are reduced.

IV. The Queue-Oriented approach

In this chapter, we present a new approach that we developed as an extension of the Car-Oriented one and that we call the 'Queue-Oriented' approach, focussing on its relation with the Car-Oriented one. We also develop an approximation, which we call the 'Queue-Oriented' approximation and compare it to the Car-Oriented Triplet approximation. Finally, we propose a further potential enhancement of the approximation, still in the Queue-Oriented framework, which we call the 'Queue-Oriented complete' approximation.

The Queue-Oriented (QO) approach is essentially an extension of the Car-Oriented approach which takes into consideration the length of the gap in front of a particle/car and the length of the following queue. The variables are thus (generalising our usual notation)

$$P_{\ell}^{t}(m,n) := P_{\ell}^{t}[10^{m}1^{n}0],$$

where $\ell \in \{1,\ldots,L-1\}$, and $m,n \in \mathbb{N}$ are subject to the constraint $1 \le \ell + m + n \le L$. The variables can be interpreted as the probability that node ℓ is occupied and that the next particle is at distance m+1 and belongs to a queue of length exactly equal to n. In case m=0, n>0 (respectively n=0, m>0), there is no hole between the particle in ℓ and the following, namely $P_\ell^t(0,n) = P_\ell^t[11^n0]$ (respectively, there is no particle between the hole in $\ell+m$ and the following, namely $P_\ell^t(m,0) = P_\ell^t[10^m0]$). In the case m=n=0, there are no particles nor holes between the initial particle in position ℓ and the final hole, so $P_\ell^t(0,0) = P_\ell^t[10]$. Moreover, due to the constraints on the values of the indices, the cases $P_0^t(0,0)$ and $P_L^t(0,0)$ are not taken into account. Actually, they can be included and interpreted as the endpoint densities, but they complicate notation and are not necessary, as they never directly appear in our equations while they can be obtained through marginalisation of the others. Indeed, the Car-Oriented variables (and thus the densities, thanks to equation (3.1)) can be obtained from the Queue-Oriented ones via marginalisation in the following way:

$$P_0^t(m) = \sum_{n=1}^{L-m} P_0^t(m,n), \qquad P_\ell^t(m) = \sum_{n=1}^{L-(\ell+m)} P_\ell^t(m,n) \quad 0 < m < L-\ell, \qquad P_\ell^t(L-\ell) = P_\ell^t(L-\ell,0),$$

for all ℓ , m such that $1 \le \ell + m \le L$. The total number of variables is $\mathcal{O}(L^3)$.

4.1 The Queue-Oriented Equation

Marginalising the Master Equation, we can obtain the dynamical equation for the QO variables $P_{\ell}^{t}(m,n)$. For convenience, we define the following quantities (similarly to how we did in the Car-Oriented scheme):

$$r_{-1} := 0 P_{-1}^{t}(m+1,n) := 0 P_{0}^{t}(m,n) = P_{1}^{t}[0^{m}1^{n}0]$$

$$r_{L+1} := 0 P_{\ell}^{t}(L-\ell,0) := P_{\ell}^{t}[10^{L-\ell}] P_{\ell}^{t}(0,L-\ell) := P_{\ell}^{t}[11^{L-\ell}] (4.1)$$

$$P_{0}^{t}(L,0) = P_{1}^{t}[0^{L}] P_{0}^{t}(0,L) = P_{1}^{t}[1^{L}] P_{\ell}^{t}(L-\ell-1,1) := P_{\ell}^{t}[10^{L-\ell-1}1]$$

so that the QO equation can be written as

$$\dot{P}_{\ell}^{t}(m,n) = \alpha P_{0}^{t}(1,n-1)\delta_{\ell 0}\delta_{m0} + r_{\ell-1}P_{\ell-1}^{t}(m+1,n) - r_{\ell}P_{\ell}^{t}(m,n)(1-\delta_{m0})
+ r_{\ell+m}P_{\ell}^{t}[10^{m-1}101^{n-1}0](1-\delta_{m0})(1-\delta_{n0})
- r_{\ell+m+n}P_{\ell}^{t}(m,n)(1-\delta_{n0})
+ r_{\ell+m+n+1}P_{\ell}^{t}(m,n+1) + \beta P_{\ell}^{t}(L-\ell-1,1)\delta_{m,L-\ell},$$
(4.2)

where the Kronecker deltas — as well as the fictitious rates and the other quantities defined in (4.1) — have been introduced in order to take care of all the special cases, namely $\ell=0$, m=0, n=0, and all the combinations of ℓ , m, n for which $\ell+m+n=L$ (notice that the second and the second-to-last terms do not involve Kronecker deltas as they appear for all combinations of ℓ , m and n, and they remain unchanged at the border). It is possible to interpret each term in this equation as a physical process, in the same way it is done in section 3.2 for the Car-Oriented equation.

Remark. As a check of consistency, it can be verified that the QO equation (4.2) marginalises to the Car-Oriented one (3.3) (and therefore to the continuity equation (1.2)).

Proof. For $m = L - \ell$, the only possible value of n is 0, so the only variable we need to consider is $P_{\ell}^{t}(L - \ell, 0) = P_{\ell}^{t}(L - \ell)$. The QO equation (4.2) reads, for this case,

$$\dot{P}_{\ell}^{t}(L-\ell,0) = r_{\ell-1}P_{\ell-1}^{t}(L-\ell+1,0) - r_{\ell}P_{\ell}^{t}(L-\ell,0) + \beta P_{\ell}^{t}(L-\ell-1,1),$$

which corresponds (thanks to the definitions in (4.1)) to

$$\dot{P}_{\ell}^{t}(L-\ell) = r_{\ell-1}P_{\ell-1}^{t}(L-\ell+1) - r_{\ell}P_{\ell}^{t}(L-\ell) + \beta P_{\ell}^{t}(L-\ell-1).$$

The latter is indeed the Car-Oriented equation (3.3) for $P_\ell^t(L-\ell)$.

For $m < L - \ell$, the marginalisation gives $P_{\ell}^{t}(m) = \sum_{n=1}^{L-(\ell+m)} P_{\ell}^{t}(m,n)$, so that the dynamical equation can be marginalised in the following way:

$$\begin{split} \sum_{n=1}^{L-(\ell+m)} \dot{P}_{\ell}^{t}(m,n) &= r_{\ell-1} \sum_{n=1}^{L-(\ell+m)} P_{\ell-1}^{t}(m+1,n) - r_{\ell} \sum_{n=1}^{L-(\ell+m)} P_{\ell}^{t}(m,n)(1-\delta_{m0}) \\ &+ r_{\ell+m} \sum_{n=1}^{L-(\ell+m)} P_{\ell}^{t}[10^{m-1}101^{n-1}0](1-\delta_{m0}) \\ &- \sum_{n=1}^{L-(\ell+m)} r_{\ell+m+n} P_{\ell}^{t}(m,n) + \sum_{n=1}^{L-(\ell+m)} r_{\ell+m+n+1} P_{\ell}^{t}(m,n+1) \end{split}$$

where we did not include the terms involving δ_{n0} as the summation only involves terms in $n \ge 1$. For the last summation, we see that the term in $n = L - (\ell + m)$ involves r_{L+1} , which is null; thus, we truncate it to $L - (\ell + m) - 1$ and we shift the index by one, obtaining

$$\sum_{n=1}^{L-(\ell+m)} r_{\ell+m+n+1} P_{\ell}^{t}(m,n+1) = \sum_{n=2}^{L-(\ell+m)} r_{\ell+m+n} P_{\ell}^{t}(m,n).$$

This way, it cancels out with the second-to-last term, leaving only $r_{\ell+m+1}P_{\ell}^t(m,1)$. All the other summations directly marginalise to the respective desired term, so that we get

$$\dot{P}_{\ell}^{t}(m) = \sum_{n=1}^{L-(\ell+m)} \dot{P}_{\ell}^{t}(m,n)
= r_{\ell-1} P_{\ell-1}^{t} [10^{m+1}1] - r_{\ell} P_{\ell}^{t} [10^{m}1] (1 - \delta_{m0}) + r_{\ell+m} P_{\ell}^{t} [10^{m-1}10] (1 - \delta_{m0}) - r_{\ell+m+1} P_{\ell}^{t}, [10^{m}10],$$

which is the Car-Oriented Equation.

Q.E.D.

4.2 The Queue-Oriented approximation

In much the same way as the Car-Oriented approach, some unknowns (i.e. variables that do not belong to the set of the QO ones $\{P_\ell^t(m,n)\}_{\ell,m,n}$) appear in the QO equation (4.2), so that the system

of equations is not closed and some approximation is needed. In particular, the unknowns are, for m, n > 0,

$$P_{\ell}^{t}[10^{m-1}101^{n-1}0].$$

There are values of ℓ , m, n for which there is no need to introduce approximations (see appendix B.2). In general, we see that any approximation that maintains the PH symmetry has to treat on equal footing indices m and n, since performing a PH transformation only entails exchanging m and n (and shifting the position index ℓ). Indeed, the PH transformation for the QO variables consists in the mappings

$$P_{\ell}^{t}(m,n) \mapsto P_{L-(\ell+m+n)}^{t}(n,m), \qquad P_{\ell}^{t}[10^{m-1}101^{n-1}0] \mapsto P_{L-(\ell+m+n)}^{t}[10^{n-1}101^{m-1}0].$$

This observation restricts the field of possible approximations to the very few that preserve the PH symmetry. One possibility is to factorise the unknowns as

$$P_{\ell}^{t}[10^{m_{1}}1^{n_{1}}0^{m_{2}}1^{n_{2}}0] \simeq \frac{P_{\ell}^{t}[10^{m_{1}}1^{n_{1}}0]P_{\ell+m_{1}+n_{1}}^{t}[10^{m_{2}}1^{n_{2}}0]}{P_{\ell+m_{1}+n_{1}}^{t}[10]} = \frac{P_{\ell}^{t}(m_{1},n_{1})P_{\ell+m_{1}+n_{1}}^{t}(m_{2},n_{2})}{P_{\ell+m_{1}+n_{1}}^{t}(0,0)},$$

entailing

$$P_{\ell}^{t}[10^{m-1}101^{n-1}0] \simeq \frac{P_{\ell}^{t}[10^{m-1}10]P_{\ell+m}^{t}[101^{n-1}0]}{P_{\ell+m}^{t}[10]} = \frac{P_{\ell}^{t}(m-1,1)P_{\ell+m}^{t}(1,n-1)}{P_{\ell+m}^{t}(0,0)},$$

which evidently consists in a PH symmetric approximation (swapping m and n only amounts to swapping the two factors in the numerator, up to translations of the position indices). This way, the QO approximated equation becomes

$$\dot{P}_{\ell}^{t}(m,n) = \alpha P_{0}^{t}(1,n-1)\delta_{\ell 0}\delta_{m0} + r_{\ell-1}P_{\ell-1}^{t}(m+1,n) - r_{\ell}P_{\ell}^{t}(m,n)(1-\delta_{m0}+\delta_{m0}\delta_{n0}) + r_{\ell+m}\frac{P_{\ell}^{t}(m-1,1)P_{\ell+m}^{t}(1,n-1)}{P_{\ell+m}^{t}(0,0)}(1-\delta_{m0})(1-\delta_{n0}) - r_{\ell+m+n}P_{\ell}^{t}(m,n)(1-\delta_{n0}) + r_{\ell+m+n+1}P_{\ell}^{t}(m,n+1) + \beta P_{\ell}^{t}(L-\ell-1,1)\delta_{m,L-\ell}.$$

$$(4.3)$$

Numerical Implementation

We implemented equation (4.3) with the usual EEM scheme. We update each variable according to its dynamical equation, and we use it for the following time step. As in the k-Cluster approximations, we use $\Delta t \leq \frac{1}{10}$ and an initial density equal to the bulk value of the homogeneous phase corresponding to the respective values of α and β , as it has been described at the beginning of chapter 2. The algorithm is slower than the Car-Oriented one, as it involves a larger number of variables (the QO variables set cardinality is $\mathcal{O}(L^3)$, the Car-Oriented one is $\mathcal{O}(L^2)$).

4.2.1 Comparison between the Queue-Oriented approximation and the Car-Oriented Triplet approximation

At the stationary state, the two density profiles (and, more in general, the cluster probabilities) we obtained with the COTR and the QO approximations are — to our surprise — equivalent. Every situation we considered (homogeneous and disordered TASEP) showed no numerical difference between the two. This is evident from the numerical results (see figure 4.1), but still has to be understood at a theoretical level. The numerical equivalence between the two approximations motivated us to seek an analytical proof of it, but we could not obtain it and leave the problem open for future work. We believe the proof could be approached by examining the QO equation in which all terms are factorised in accordance with the COTR approximation, and by demonstrating that the COTR equations satisfy the QO approximated ones, at least in the stationary state. Another possible strategy comes from noticing

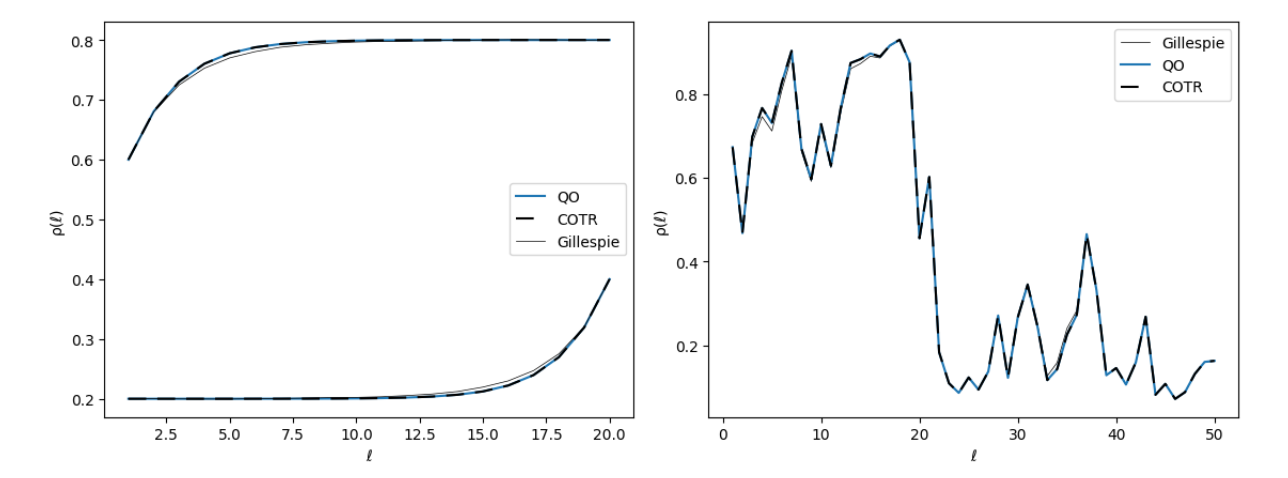


Figure 4.1: Comparison between the Gillespie, QO and COTR densities. The left panel shows the case of unit, uniform inner rates both in the LD phase ($\alpha = 1/5$, $\beta = 2/5$) and in the HD phase ($\alpha = 2/5$, $\beta = 1/5$) for a chain of length L = 20. The right panel shows the densities in the case of random rates drawn from the uniform distribution over the interval [0.1,1], for L = 50 and $\alpha = 1/5$, $\beta = 2/5$. For the Gillespie algorithm we averaged, in both cases, over 10^8 realisations; for the QO and the COTR approximations, we set T = 100, $N_t = 10^3$ for the homogeneous case and T = 500, $N_t = 5 \times 10^3$ for the inhomogeneous one, and we used the convergence condition that the updated density vector was equal to the previous one (up to numerical precision).

that, due to marginalisation, the probabilities $P_{\ell}^{t}[01^{m}0^{n}1]$ are approximated equally in the two schemes. Indeed, by marginalisation, the QO hypothesis gives

$$\begin{split} P_{\ell}^{t}[01^{m}0^{n}1] &= \sum_{\mu=1}^{\ell} \sum_{\nu=1}^{L-(\ell+n+m)} P_{\ell-\mu}^{t}[10^{\mu}1^{m}0^{n}1^{\nu}0] \\ &= \sum_{\mu=1}^{\ell} \sum_{\nu=1}^{L-(\ell+n+m)} \frac{P_{\ell-\mu}^{t}[10^{\mu}1^{m}0]P_{\ell+m}^{t}[10^{n}1^{\nu}0]}{P_{\ell+m}^{t}[10]} \\ &= \frac{P_{\ell}^{t}[01^{m}0]P_{\ell+m}^{t}[10^{n}1]}{P_{\ell+m}^{t}[10]}, \end{split}$$

which matches the COTR approximation. If one were able to show that — at least at the stationary state — the only possible way of generalising this approximation of $P_{\ell}^{t}[01^{m}0^{n}1]$ to the whole configuration was the COTR hypothesis (3.6) then the proof would be obtained.

4.3 The Queue-Oriented Complete approximation

Surprised by the aforementioned equivalence between the COTR and the QO approximations, we looked for a new approximation in order to produce a sensible enhancement over COTR approximation. In particular, we considered the following factorisation for the unknowns appearing in the QO equation (4.2):

$$P_{\ell}^{t}[10^{m_{1}}1^{n_{1}}0^{m_{2}}1^{n_{2}}0] \simeq \frac{P_{\ell}^{t}[10^{m_{1}}1^{n_{1}}0]P_{\ell+m_{1}}^{t}[01^{n_{1}}0^{m_{2}}1]P_{\ell+m_{1}+n_{1}}^{t}[10^{m_{2}}1^{n_{2}}0]}{P_{\ell+m_{1}}^{t}[01^{n_{1}}0]P_{\ell+m_{1}+n_{1}}^{t}[10^{m_{2}}1]},$$
(4.4)

which also accounts for variables $H_{\ell}^t(m,n) := P_{\ell}^t[01^m0^n1]$ — for the usual ranges of ℓ , m, and n — in addition to the $P_{\ell}^t(m,n)$ variables. Thus, the approximation above reads

$$P_{\ell}^{t}[10^{m_{1}}1^{n_{1}}0^{m_{2}}1^{n_{2}}0] = \frac{P_{\ell}^{t}(m_{1},n_{1})H_{\ell+m_{1}}^{t}(n_{1},m_{2})P_{\ell+m_{1}+n_{1}}^{t}(m_{2},n_{2})}{H_{\ell+m_{1}}^{t}(n_{1})P_{\ell+m_{1}+n_{1}}^{t}(m_{2})},$$

where the factors in the denominator are the usual Car-Oriented variables. We thus have to consider also the dynamical equation for variables $H_{\ell}^{t}(m, n)$:

$$\begin{split} \dot{H}_{\ell}^{t}(m,n) &= \dot{P}_{\ell}^{t}[01^{m}0^{n}1] \\ &= -\alpha P_{1}^{t}[0^{n}1]\delta_{m0}\delta\ell0 - r_{\ell-1}P_{\ell-1}^{t}[101^{m}0^{n}1] \\ &\quad + r_{\ell}P_{\ell}^{t}[101^{m-1}0^{n}1](1-\delta_{m0}) - r_{\ell+m}P_{\ell}^{t}[01^{m}0^{n}1](1-\delta_{m0})(1-\delta_{n0}) \\ &\quad + r_{\ell+m+n}P_{\ell}^{t}[01^{m}0^{n-1}10](1-\delta_{n0}) - r_{\ell+m+n+1}P_{\ell}^{t}[01^{m}0^{n}10] \\ &\quad + r_{\ell}P_{\ell}^{t}[10]\delta_{m0}\delta_{n0} - \beta P_{\ell}^{t}[01^{L-\ell}]\delta_{m,L-\ell} \\ &= -\alpha H_{0}^{t}(0,n)\delta_{\ell0}\delta_{m0} - r_{\ell-1}P_{\ell-1}^{t}[101^{m}0^{n}1] \\ &\quad + r_{\ell}P_{\ell}^{t}[101^{m-1}0^{n}1](1-\delta_{m0}) - r_{\ell+m}H_{\ell}^{t}(m,n)(1-\delta_{m0})(1-\delta_{n0}) \\ &\quad + r_{\ell+m+n}P_{\ell}^{t}[01^{m}0^{n-1}10](1-\delta_{n0}) - r_{\ell+m+n+1}P_{\ell}^{t}[01^{m}0^{n}10] \\ &\quad + r_{\ell}P_{\ell}^{t}(0,0)\delta_{m0}\delta_{n0} - \beta H_{\ell}^{t}(L-\ell,0)\delta_{m,L-\ell}. \end{split}$$

The number of unknowns which appear in the dynamical equation for $H^t_\ell(m,n)$ is greater than the number of unknowns that appear in the dynamical equation of the $P^t_\ell(m,n)$ variables. This can be understood by considering that, since a particle can move only if the site to the right is empty, variables $P^t_\ell(m,n)$ describe particle motion in a more natural way.

The approximation of the unknowns $P_{\ell}^{t}[101^{m}0^{n}1]$ and $P_{\ell}^{t}[01^{m}0^{n}10]$ must be consistent with the approximation in (4.4). By marginalisation, we get

$$\begin{split} P_{\ell}^{t}[101^{m}0^{n}1] &= \sum_{\nu=1}^{L-(\ell+m+n+1)} P_{\ell}^{t}[101^{m}0^{n}1^{\nu}0] \\ &= \frac{P_{\ell}^{t}(1,m)H_{\ell}^{t}(m,n)}{H_{\ell}^{t}(m)} \\ P_{\ell}^{t}[01^{m}0^{n}10] &= \sum_{\nu=1}^{\ell} P_{\ell-\nu}^{t}[10^{\nu}1^{m}0^{n}10] \\ &= \frac{H_{\ell}^{t}(m,n)P_{\ell+m}^{t}(n,1)}{P_{\ell+m}^{t}(n)}. \end{split}$$

These approximations give the following system of equations

$$\begin{split} \dot{P}_{\ell}^{t}(m,n) &= \alpha P_{0}^{t}(1,n-1)\delta_{\ell 0}\delta_{m 0} + r_{\ell-1}P_{\ell-1}^{t}(m+1,n) - r_{\ell}P_{\ell}^{t}(m,n)(1-\delta_{m 0}+\delta_{m 0}\delta_{n 0}) \\ &+ r_{\ell+m}\frac{P_{\ell}^{t}(m-1,1)H_{\ell+m-1}^{t}(1,1)P_{\ell+m}^{t}(1,n-1)}{H_{\ell+m-1}^{t}(1)P_{\ell+m}^{t}(1)}(1-\delta_{m 0})(1-\delta_{n 0}) \\ &- r_{\ell+m+n}P_{\ell}^{t}(m,n)(1-\delta_{n 0}) + r_{\ell+m+n+1}P_{\ell}^{t}(m,n+1) + \beta P_{\ell}^{t}(L-\ell-1,1)\delta_{m,L-\ell} \end{split}$$

$$(4.5a)$$

$$\dot{H}_{\ell}^{t}(m,n) = -\alpha H_{0}^{t}(0,n)\delta_{\ell 0}\delta_{m 0} - r_{\ell - 1}\frac{P_{\ell - 1}^{t}(1,m)H_{\ell}^{t}(m,n)}{H_{\ell}^{t}(m)} + r_{\ell}\frac{P_{\ell}^{t}(1,m-1)H_{\ell + 1}^{t}(m-1,n)}{H_{\ell + 1}^{t}(m-1)}(1 - \delta_{m 0})$$

$$- r_{\ell + m}H_{\ell}^{t}(m,n)(1 - \delta_{m 0})(1 - \delta_{n 0}) + r_{\ell + m + n}\frac{H_{\ell}^{t}(m,n-1)P_{\ell + m}^{t}(n-1,1)}{P_{\ell + m}^{t}(n-1)}(1 - \delta_{n 0})$$

$$- r_{\ell + m + n + 1}\frac{H_{\ell}^{t}(m,n)P_{\ell + m}^{t}(n,1)}{P_{\ell + m}^{t}(n)} + r_{\ell}P_{\ell}^{t}(0,0)\delta_{m 0}\delta_{n 0} - \beta H_{\ell}^{t}(L - \ell,0).$$

$$(4.5b)$$

We refer to this as the QO-complete approximation, which we expect to yield better results because:

- (i) it considers a greater overlap than the QO approximation (4.3) (in the sense it has been described in chapter 2);
- (ii) it enables the calculation of more variables through marginalisation, thereby avoiding approximations.

We attempted to approach the numerical implementation of the QO-complete equations (4.5), but encountered several challenges. One of the main issues was the high number of equations — particularly when accounting for all those combinations of indices ℓ , m, and n for which no approximation is needed — which made the implementation unwieldy. A numerically more systematic treatment of these variables is required, and we regard this as an important outlook for future work.

Conclusions

In this work, we investigated the non-equilibrium stationary state of an inhomogeneous TASEP using a matryoshka-like hierarchy of approximations. The innermost layer of this hierarchy consisted of a review of the well-established applications of cluster approximations to TASEP, as well as the COMF approach. We extended the latter to the case of OBC and, potentially, inhomogeneous inner rates, finding that under these conditions it becomes equivalent to the traditional MF approximation.

Building on this, we combined the Car-Oriented approach with the idea of the cluster approximation, and obtained several generalisations of the COMF approximation, which we can refer to as the Car-Oriented cluster approximations. Indeed, we argue that the methods presented in chapter 3 could represent a first sketch for a systematic generalisation of the cluster approximation to the Car-Oriented framework. However, the recipe for this generalisation is non-trivial and we expect that in many cases particular care has to be taken for some important technicalities (as illustrated by the case of the Car-Oriented Pair approximation, which we found to break the PH symmetry).

The comparisons presented in chapter 3 between the COTR and the Triplet approximations show some consistent enhancement of the Car-Oriented version over the traditional one. However, the improvement is quantitatively modest as long as the system only favours short-range correlations, and the two approximations are qualitatively very similar. It becomes more prominent in the case of quenched (sitewise) disorder, where analytical results are lacking and approximations remain the only possible strategy. Especially, it gains importance in systems that favour long correlations and when non-local variables (like the probability of a queue), rather than local variables, are considered. We believe this is an important step in the construction of this new technique of approximation, and that a more detailed study of this difference between the COTR and the Triplet approximations is needed. We regard it as an outlook for future work.

Finally, we generalise the Car-Oriented framework to the new QO approach, which considers a greater number of variables by focussing not only on gaps between particles but also on particle-queues between holes. Inspired by the cluster approximation strategy, we developed an approximation for the QO variables — ensuring preservation of the PH symmetry — and found the surprising result that, at the stationary state, it was numerically indistinguishable from the COTR approximation. This motivated us to attempt an analytical proof of their equivalence at the stationary state. We conjecture that the equivalence can be established analytically; providing a formal proof is left as an avenue for future work. We conjecture that the underlying reason for this similarity between the two approximations lies in the fact that they consider the same overlap between factors, which also entails that some variables are approximated equally, as it has been shown in section 4.2.1.

The ultimate, outermost shell of this matryoshka is the QO-complete approximation: our attempt of developing an approximation which improves COTR's. Its spirit merges on the one hand the generalisation of the cluster approximations to the Car-Oriented variables and on the other hand the QO approach. We did not include this implementation in the present work; however, we believe a numerical comparison of the COTR and QO-complete approximations would be key to understanding the behaviour of the QO variables. This remains yet another open direction for future work.

I. Derivations

A.1 From the Master Equation to the Continuity Equation

Equation (1.1) gives the formula for computing the time derivative of a cluster of length $\lambda+1$ starting in ℓ . We define $\underline{\nu}$ as the vector of variables present in the cluster: $\underline{\nu}^t \coloneqq [n_\ell^t, n_{\ell+1}^t, \dots, n_{\ell+\lambda}^t]$. Thus, we write equation (1.1) as

$$\dot{P}_{\ell}^{t}[\underline{\nu}] = \sum_{\underline{m}} P^{t}[\underline{m}] \left(\sum_{\underline{n} \setminus \underline{\nu}} \sum_{k=0}^{L} W_{\underline{n}\underline{m}}^{(k)} \right).$$

Now, the elements of the transition matrix read

(i)
$$W_{\underline{nm}}^{(0)} = \alpha \delta_{m_1,0} \left(\prod_{i>1} \delta_{n_i,m_i} \right) (2n_1 - 1)$$

(ii)
$$W_{\underline{nm}}^{(k)} = r_k \delta_{m_k,1} \delta_{m_{k+1},0} \left(\prod_{i \neq k,k+1} \delta_{m_i,n_i} \right) (n_{k+1} - n_k)$$

(iii)
$$W_{\underline{n}\underline{m}}^{(L)} = \beta \delta_{m_L,1} \left(\prod_{i < L} \delta_{n_i,m_i} \right) (1 - 2n_L).$$

Therefore,

(i) if
$$n_1 \in \underline{n} \setminus \underline{\nu} \implies \sum_{\underline{n} \setminus \underline{\nu}} W_{\underline{n}\underline{m}}^{(0)} = \alpha \delta_{m_1,0} \sum_{\underline{n} \setminus \{\underline{\nu}, n_1\}} \left(\prod_{i>1} \delta_{n_i, m_i} \right) \sum_{n_1} (2n_1 - 1) = 0$$

(ii) if
$$n_k, n_{k+1} \in \underline{n} \setminus \underline{\nu} \implies \sum_{\underline{n} \setminus \underline{\nu}} W_{\underline{n}\underline{m}}^{(k)} = r_k \delta_{m_k, 1} \delta_{m_{k+1}, 0} \sum_{\underline{n} \setminus \{\underline{\nu}, n_k, n_{k+1}\}} \left(\prod_{i \neq k, k+1} \delta_{m_i, n_i} \right) \sum_{n_k, n_{k+1}} (n_{k+1} - n_k) = 0$$

(iii) if
$$n_L \in \underline{n} \setminus \underline{\nu} \implies \sum_{\underline{n} \setminus \underline{\nu}} W_{\underline{n}\underline{m}}^{(L)} = \beta \delta_{m_L, 1} \sum_{\underline{n} \setminus \{\underline{\nu}, n_L\}} \left(\prod_{i < L} \delta_{n_i, m_i} \right) \sum_{n_L} (1 - 2n_L) = 0$$

(where by $\sum_{\underline{n}\setminus\{\underline{\nu},n_i,n_j\}}$ we mean the also variables n_i , n_j — in addition to the ones in $\underline{\nu}$ — are excluded from the summation) meaning that the only terms that survive after the summation over $\underline{n}\setminus\underline{\nu}$ are inside the cluster or at distance one from it. This is intuitive: since particles can only hop from one node to the to the next one, the variation of a configuration is due either to a hopping event in one of the two extrema of the cluster or to a hopping in some node internal to it. Therefore,

$$\dot{P}_{\ell}^{t}[\underline{\nu}] = \sum_{\underline{m}} P^{t}[\underline{m}] \left(\sum_{\underline{n} \setminus \underline{\nu}} \sum_{k=\ell-1}^{\ell+\lambda} W_{\underline{n}\underline{m}}^{(k)} \right). \tag{A.1}$$

In the case of the density, we are only interested in a cluster of length 1, so

$$\begin{split} \dot{P}_{\ell}^{t}[n_{\ell}] &= \sum_{\underline{m}} P^{t}[\underline{m}] \sum_{\underline{n} \backslash n_{\ell}} \left(W_{\underline{n}\underline{m}}^{(\ell-1)} + W_{\underline{n}\underline{m}}^{(\ell)} \right) \\ &= \begin{cases} \sum_{\underline{m}} P^{t}[\underline{m}] \sum_{\underline{n} \backslash n_{\ell}} \left[\alpha(2n_{1} - 1)\delta_{m_{1}0} \left(\prod_{i \geq 1} \delta_{m_{i},n_{i}} \right) \\ &+ r_{1}(n_{2} - n_{1})\delta_{m_{1}1}\delta_{m_{2}0} \left(\prod_{i \geq 2} \delta_{m_{i},n_{i}} \right) \right] \end{cases} & \text{if } \ell = 1 \\ &= \begin{cases} \sum_{\underline{m}} P^{t}[\underline{m}] \sum_{\underline{n} \backslash n_{\ell}} \left[r_{\ell-1}(n_{\ell} - n_{\ell-1})\delta_{m_{\ell}1}\delta_{m_{\ell+1}0} \left(\prod_{i \neq \ell-1,\ell} \delta_{m_{i},n_{i}} \right) \\ &+ r_{\ell}(n_{\ell+1} - n_{\ell})\delta_{m_{\ell}1}\delta_{m_{\ell+1}0} \left(\prod_{i \neq \ell,\ell+1} \delta_{m_{i},n_{i}} \right) \\ &\sum_{\underline{m}} P^{t}[\underline{m}] \sum_{\underline{n} \backslash n_{\ell}} \left[r_{L-1}(n_{L} - n_{L-1})\delta_{m_{L-1}1}\delta_{m_{L}0} \left(\prod_{i < L-1} \delta_{m_{i},n_{i}} \right) \\ &+ \beta(1 - 2n_{L})\delta_{m_{L}1} \left(\prod_{i \geq L} \delta_{m_{i},n_{i}} \right) \right] \end{cases} & \text{if } \ell = L. \end{cases}$$

Summing over the deltas and marginalising, we get

$$\dot{P}_{\ell}^{t}[n_{\ell}] = \begin{cases} \alpha P_{1}^{t}[0](2n_{1}-1) + r_{1}P_{1}^{t}[10](1-2n_{1}) & \text{if } \ell = 1\\ r_{\ell-1}P_{\ell-1}^{t}[10](2n_{\ell}-1) + r_{\ell}P_{\ell}^{t}[10](1-2n_{\ell}) & \text{if } 1 < \ell < L\\ r_{L-1}P_{L-1}^{t}[10](2n_{L}-1) + \beta P_{\ell}^{t}[1](1-2n_{L}) & \text{if } \ell = L. \end{cases}$$

Setting $n_{\ell} = 1$, we get the sought equation (1.1).

A.2 From the Master Equation to the Car-Oriented Equation

The Car-Oriented variables are probabilities of clusters where the first and the last variables are equal to 1, while the intermediate are 0. Thus, we consider equation (A.1), setting $n_{\ell} = n_{\ell+\lambda} = 1$, and all other variables of the cluster to zero. Moreover, we define $\mu = \lambda - 1$, which denotes the length of the gap, as customary in the Car-Oriented approach. We see that for every node $k \in \{\ell+1,\ldots,\ell+\mu-1\}$, $W_{\underline{n}\underline{m}}^{(k)} \propto n_{k+1} - n_k = 0$. Therefore, considering the cluster $\underline{\nu} = [n_{\ell} = 1, n_{\ell+1} = 0, \ldots, n_{\ell+\mu} = 0, n_{\ell+\mu+1} = 1]$, equation (A.1) becomes

$$\dot{P}_{\ell}^{t}[\underline{\nu}] = \sum_{\underline{m}} P^{t}[\underline{m}] \left(\sum_{\underline{n} \setminus \underline{\nu}} \sum_{k \in \{\ell-1, \ell, \ell+\mu, \ell+\mu+1\}} W_{\underline{n}\underline{m}}^{(k)} \right)$$
(A.2)

In the case $\mu = 0$, $W_{nm}^{(\ell)} \propto n_{\ell} - n_{\ell+1} = 0$, so it reduces to

$$\begin{split} \dot{P}_{\ell}^{t}[11] &= \sum_{\underline{m}} P^{t}[\underline{m}] \left(\sum_{\underline{n} \backslash \{n_{\ell}, n_{\ell+1}\}} W_{\underline{n}\underline{m}}^{(\ell-1)} + W_{\underline{n}\underline{m}}^{(\ell+1)} \right) \\ &= \begin{cases} \sum_{\underline{m}} P^{t}[\underline{m}] \left(\sum_{\underline{n} \backslash \{n_{1}, n_{2}\}} \alpha(2n_{1} - 1) \delta_{m_{1}0} \prod_{i > 1} \delta_{m_{i}, n_{i}} + r_{2}(n_{2} - n_{1}) \delta_{m_{2}1} \delta_{m_{3}0} \prod_{i \neq 2, 3} \delta_{m_{i}n_{i}} \right) & \text{if } \ell = 1 \\ &= \begin{cases} \sum_{\underline{m}} P^{t}[\underline{m}] \left(\sum_{\underline{n} \backslash \{n_{1}, n_{2}\}} r_{\ell-1}(n_{\ell} - n_{\ell-1}) \delta_{m_{\ell-1}1} \delta_{m_{\ell}0} \prod_{i > 1} \delta_{m_{i}, n_{i}} \\ &+ r_{\ell+1}(n_{\ell+2} - n_{\ell+1}) \delta_{m_{\ell+1}1} \delta_{m_{\ell+2}0} \prod_{i \neq \ell-1, \ell+2} \delta_{m_{i}n_{i}} \right) \\ &= \begin{cases} \sum_{\underline{m}} P^{t}[\underline{m}] \left(\sum_{\underline{n} \backslash \{n_{1}, n_{2}\}} r_{L-2}(n_{L-1} - n_{L-2}) \delta_{m_{L-2}1} \delta_{m_{L-1}0} \prod_{i \neq L-2, L-1} \delta_{m_{i}n_{i}} \\ &+ \beta(1 - 2n_{L}) \delta_{m_{L}1} \prod_{i < L} \delta_{m_{i}, n_{i}} \right) \end{cases} & \text{if } \ell = L-1 \end{cases}$$

Summing over the deltas, marginalising and setting $n_{\ell} = n_{\ell+1} = 1$, we get

$$\begin{split} \dot{P}_{\ell}^{t}(0) &\coloneqq \dot{P}_{\ell}^{t}[11] \\ &= \begin{cases} \alpha P_{1}^{t}[01] - r_{2}P_{1}^{t}[110] & \text{if } \ell = 1 \\ r_{\ell-1}P_{\ell-1}^{t}[101] - r_{\ell+1}P_{\ell}^{t}[110] & \text{if } 1 < \ell < L-1 \\ r_{L-2}P_{L-2}^{t}[101] - \beta P_{L-1}^{t}[11] & \text{if } \ell = L-1, \end{cases} \end{split}$$

which is in agreement with our equation (3.3). In case $\mu > 0$, one should consider terms $W_{\underline{n}\underline{m}}^{(\ell-1)}$, $W_{\underline{n}\underline{m}}^{(\ell)}$, $W_{\underline{n}\underline{m}}^{(\ell+\mu)}$ and $W_{\underline{n}\underline{m}}^{(\ell+\mu+1)}$. Proceeding in the same way as before, we get

$$\begin{split} &\sum_{\underline{n} \setminus \underline{\nu}} W_{\underline{n}\underline{m}}^{(\ell-1)} = \begin{cases} \alpha P_1^t[00^{\mu}1] & \text{if } \ell = 1 \\ r_{\ell-1} P_{\ell-1}^t[100^{\mu}1] & \text{if } \ell > 1, \end{cases} \\ &\sum_{\underline{n} \setminus \underline{\nu}} W_{\underline{n}\underline{m}}^{(\ell)} = r_{\ell} P_{\ell}^t[10^{\mu}1], \\ &\sum_{\underline{n} \setminus \underline{\nu}} W_{\underline{n}\underline{m}}^{(\ell+\mu)} = r_{\ell+\mu} P_{\ell}^t[10^{\mu-1}10], \\ &\sum_{\underline{n} \setminus \underline{\nu}} W_{\underline{n}\underline{m}}^{(\ell+\mu)} = \begin{cases} r_{\ell+\mu+1} P_1^t[10^{\mu}10] & \text{if } \ell + \mu < L \\ \beta P_{\ell}^t[10^{\mu}1] & \text{if } \ell + \mu = L. \end{cases} \end{split}$$

Thus, plugging these expressions in equation (A.2) the sought Car-Oriented Equation (3.3) is obtained.

II. Notes

B.1 The COTR approximation in detail

For certain values of ℓ , m, n we do not need to approximate our quantities. In our numerical implementation, we follow this scheme (where we also introduce $P_0^t(0) := \rho_1^t$, $H_0^t(0) := 1 - \rho_1^t$, $P_L^t(0) := \rho_L^t$, $H_L^t(0) := 1 - \rho_L^t$)

$$\begin{cases} \dot{P}_{\ell}^{t}(m) = r_{\ell-1}P_{\ell-1}^{t}(m+1) - r_{\ell}P_{\ell}^{t}(m)(1-\delta_{m0}) + r_{\ell+m}P_{\ell}^{t}(m-1)\pi_{\ell,m-1}^{t}(1-\delta_{m0}) - r_{\ell+m+1}P_{\ell}^{t}(m)\pi_{\ell,m}^{t} \\ \dot{H}_{\ell}^{t}(n) = -r_{\ell-1}H_{\ell}^{t}(n)\eta_{\ell,n}^{t} + r_{\ell}H_{\ell+1}^{t}(n-1)\eta_{\ell+1,n-1}^{t}(1-\delta_{n0}) - r_{\ell+n}H_{\ell}^{t}(n)(1-\delta_{n0}) + r_{\ell+n+1}H_{\ell}^{t}(n+1), \end{cases}$$

for each $\ell \in \{0, ..., L\}$, upon defining

$$\begin{split} \pi_{0,0}^t &= \frac{H_0^t(1)}{P_0^t(0)}, \\ \pi_{0,m}^t &= \frac{H_m^t(1)}{P_m^t[01]}, \\ \pi_{\ell,0}^t &= \frac{P_\ell^t[110]}{P_\ell^t(0)} = \frac{\sum_{m=0}^{\ell-1} H_m^t(\ell-m+1)}{P_\ell^t(0)}, \\ \pi_{L,0}^t &= 1, \\ \pi_{\ell,m}^t &= \frac{H_{\ell+m}^t(1)}{P_{\ell+m}^t[01]}, \\ \pi_{\ell,L-\ell-1}^t &= 1, \\ \pi_{\ell,L-\ell}^t &= 0, \\ r_{-1} &= \alpha, \\ P_{-1}^t(1) &= 1 - \rho_1^t, \\ P_{-1}^t(m) &= 0, \\ \eta_{1,n}^t &= 1, \\ \eta_{\ell,0}^t &= \frac{P_{\ell-1}^t[100]}{H_\ell^t(0)} &= \frac{\sum_{m=2}^{L-\ell+1} P_{\ell-1}^t(m)}{H_\ell^t(0)}, \\ \eta_{\ell,n}^t &= \frac{P_{\ell-1}^t(1)}{P_\ell^t[01]}, \\ \eta_{L,0}^t &= \frac{P_{\ell-1}^t(1)}{H_L^t(0)}, \\ r_{L+1} &= \beta, \\ H_L^t(1) &= \rho_L^t, \\ H_\ell^t(L-\ell+1) &= 0, \\ \end{split}$$

B.2 The Queue-Oriented approximation in detail

For certain values of ℓ , m, n it is not necessary to approximate, and indeed we avoid doing it in our numerical implementation. These cases are

(i) When $\ell = 0$, 0 < m < L and n > 0, the equation for $P_{\ell}^{t}(m, n)$ reads

$$\dot{P}_0^t(m,n) = \dot{P}_1^t[0^m 1^n 0] = -(\alpha + r_{\ell+m+n})P_0^t(m,n) + r_{\ell+m}P_1^t[0^{m-1}101^{n-1}0] - r_{\ell+m+n+1}P_0^t(m,n+1).$$

The term in $r_{\ell+m}$ in general needs to be approximated as

$$P_1^t[0^{m-1}101^{n-1}0] = \frac{P_0^t(m-1,1)P_m^t(1,n-1)}{P_m^t(0,0)}$$

except when

(a)
$$m = 1 \implies P_1^t[0^{m-1}101^{n-1}0] = P_1^t(1, n-1),$$

(b)
$$m = L - 1 \implies n = 1 \implies P_1^t[0^{m-1}101^{n-1}0] = P_1^t[0^{m-1}10] = P_0^t(m-1,1).$$

(ii) When $0 < \ell < L-1$, $0 < m < L-\ell$ and $n = L-(\ell+m)$, the equation for $\dot{P}_{\ell}^{t}(m,n)$ reads

$$\dot{P}_{\ell}^{t}(m,n) = r_{\ell-1}P_{\ell-1}^{t}(m+1,n) - (r_{\ell}+\beta)P_{\ell}^{t}(m,n) + r_{\ell+m}P_{\ell}^{t}[10^{m-1}101^{L-(\ell+m)}]$$

The quantity $P_{\ell}^{t}[10^{m-1}101^{L-(\ell+m)}]$ is normally approximated as

$$P_{\ell}^{t}[10^{m-1}101^{L-(\ell+m)}] = \frac{P_{\ell}^{t}(m-1,1)P_{\ell+m}^{t}(1,L-(\ell+m+1))}{P_{\ell+m}^{t}(0,0)}$$

except when n = 1 (i.e. $m = L - \ell - 1$), where

$$P_{\ell}^{t}[10^{m-1}101^{L-(\ell+m)}] = P_{\ell}^{t}(m-1,1).$$

B.3 Interpretation of the QO variables

We noticed it was possible to interpret the QO variables in an interesting way, by making a change of variable. Consider, instead of the usual boolean configuration $\underline{n}^t \in \{0,1\}^L$, the new configuration $\underline{s}^t \in \{0,1,\ldots,L\}^L$ where

- if the site λ is occupied then s_{λ}^t denotes the site where the cluster of particles at site λ ends, i.e. the site where the last particle of the cluster is located at time t;
- if the site λ is empty then s_{λ}^t denotes the ending site of the previous cluster of particles at time t.

In formulas,

$$s_{\lambda}^{t} = \begin{cases} \min_{i:i>\lambda \text{ and } n_{i}=0} i-1 & \text{if } n_{\lambda}=1, \\ \max_{i:i<\lambda \text{ and } n_{i}=1} i & \text{if } n_{\lambda}=0. \end{cases}$$

Moreover, we define $\min_{\varnothing} := L$, $\max_{\varnothing} := 0$, so that if there is no hole in front of the particle at site λ , then $s_{\lambda}^t = L$ and if there is no particle before the hole in site λ , then $s_{\lambda}^t = 0$. Figure B.1 shows a graphical interpretation of these variables, together with a comparison with the boolean configuration n.

Variables s interact with each other through some constraints. For example, $s_{\lambda} = \lambda$ implies $s_{\lambda+1} = s_{\lambda} = \lambda$. Figure B.2 shows the only allowed values of $s_{\lambda+1}$ once s_{λ} is fixed, for several values of s_{λ} .

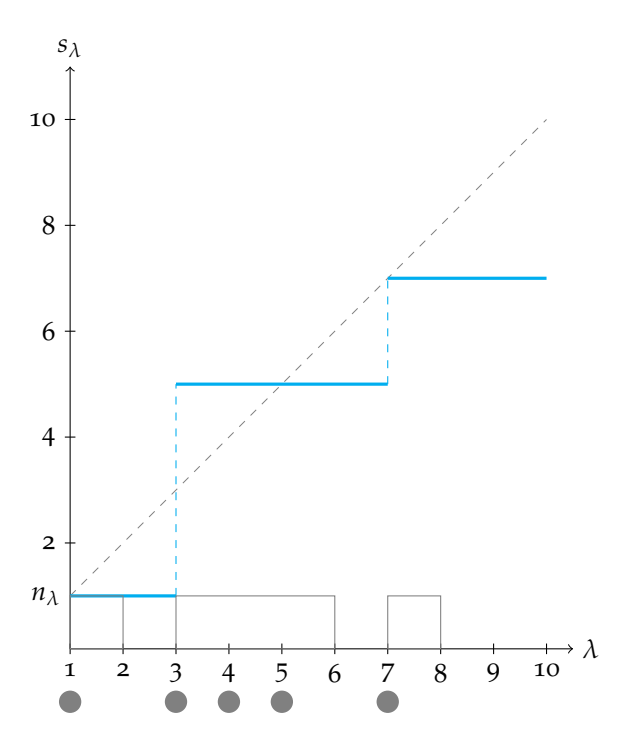


Figure B.1: Comparison between the \underline{s} and the \underline{n} configurations for a system of L=10 sites with nodes 1,3,4,5, and 7 occupied and the others empty. The \underline{s} configuration is represented by the thick blue line, while the \underline{n} configuration is represented by the gray rectangles. The gray dots below the x-axis represent the particles.

Now consider the quantity $P_{\lambda}^{t}[s_{\lambda}, s_{\lambda+1}]$. In terms of the boolean configuration, this comes as

$$\begin{split} P_{\lambda}^{t}[s_{\lambda},s_{\lambda+1}] &= \begin{cases} P_{s_{\lambda}}^{t}[10^{\lambda-s_{\lambda}}0] & \text{if } s_{\lambda} = s_{\lambda+1} < \lambda \\ P_{s_{\lambda}}^{t}[10^{\lambda-s_{\lambda}}1^{s_{\lambda+1}-\lambda}0] & \text{if } s_{\lambda} < \lambda, s_{\lambda+1} > \lambda+1 \\ P_{\lambda}^{t}[1^{s_{\lambda}-\lambda+1}0] & \text{if } s_{\lambda} \geq \lambda \end{cases} \\ &= P_{\min\{s_{\lambda},\lambda\}}^{t}[10^{\max\{\lambda-s_{\lambda},0\}}1^{\max\{s_{\lambda+1}-\lambda,0\}}0] \\ &\coloneqq P_{\ell}^{t}[10^{m}1^{n}0], \end{split}$$

which is a variable of the QO approach. The name of the approach stems from these variables, as they are able to show that the probability of a pair of variables representing two adjacent queues (where adjacent has to be understood at a site-wise level) is equivalent to the probability that a cluster of exactly m holes is followed by a cluster of exactly m particles.

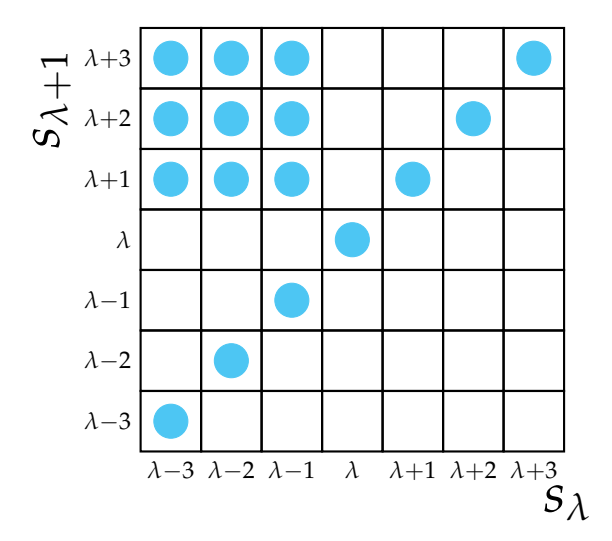


Figure B.2: Relation between variables $s_{\lambda+1}$ and s_{λ} .

Bibliography

- ¹S. G. Brush, "History of the Lenz-Ising model", Reviews of Modern Physics 39, 883 (1967).
- ²H. E. Stanley, *Introduction to phase transitions and critical phenomena* (Oxford University Press, Oxford, 1971).
- ³V. Castellano, S. Fortunato, and V. Loreto, "Statistical physics of social dynamics", Reviews of Modern Physics **81**, 591–646 (2009).
- ⁴A. G. Khachaturyan, *Theory of structural transformations in solids* (Wiley, 1983).
- ⁵J. S. Rowlinson and B. Widom, *Molecular theory of capillarity* (Clarendon Press / Oxford University Press, 1982).
- ⁶D. Poland and H. A. Scheraga, *Theory of helix–coil transitions in biopolymers* (Academic Press, 1970).
- ⁷C. T. MacDonald and J. H. Gibbs, "Concerning the kinetics of polypeptide synthesis on polyribosomes", Biopolymers 7, 707 (1969).
- ⁸C. T. MacDonald, J. H. Gibbs, and A. C. Pipkin, "Kinetics of biopolymerization on nucleic acid templates", Biopolymers **6**, 1 (1968).
- ⁹A. Schadschneider and M. Schreckenberg, "Car-oriented mean-field theory for traffic flow models", Journal of Physics A: Mathematical and General **30**, L69–L75 (1997).
- ¹⁰J. R. Buchan and I. Stansfield, "Halting a cellular production line: responses to ribosomal pausing during translation", Biochemical Society Transactions 35, 1600–1605 (2007).
- ¹¹T. Tuller et al., "An evolutionarily conserved mechanism for controlling the efficiency of protein translation", Cell **141**, 344–354 (2010).
- ¹²A. R. Buskirk and R. Green, "Ribosome pausing, arrest and rescue in bacteria and eukaryotes", Phil. Trans. R. Soc. B **372**, 20160183 (2017).
- ¹³A. G. Johnson, R. Grosely, A. N. Petrov, and J. D. Puglisi, "Dynamics of IRES-mediated translation", Philosophical Transactions of the Royal Society B (2017).
- ¹⁴R. J. Jackson, C. U. T. Hellen, and T. V. Pestova, "The mechanism of eukaryotic translation initiation and principles of its regulation", Nature Reviews Molecular Cell Biology **11**, 113–127 (2010).
- ¹⁵E. Svidritskiy, G. Demo, A. B. Loveland, C. Xu, and A. A. Korostelev, "Extensive ribosome and RF2 rearrangements during translation termination", eLife **8**, e46850 (2019).
- ¹⁶D. J. Young and N. R. Guydosh, "Rebirth of the translational machinery: the importance of recycling ribosomes", BioEssays 44, e2100269 (2022).
- ¹⁷G. W. Lakatos and T. Chou, "Totally asymmetric exclusion processes with particles of arbitrary size", Journal of Physics A **36**, 2027 (2003).
- ¹⁸T. Chou, "Ribosome recycling, diffusion, and mRNA loop formation in translational regulation", Biophysical Journal **85**, 755–773 (2003).
- ¹⁹H. Zur and T. Tuller, "Ribosome recycling induces optimal translation rate at low ribosomal availability", Journal of the Royal Society Interface 11 (2014).
- ²⁰R. Lipowsky, S. Klumpp, and T. M. Nieuwenhuizen, "Random walks of cytoskeletal motors in open and closed compartments", Physical Review Letters **87**, 108101 (2001).
- ²¹F. Spitzer, "Interaction of markov processes", Advances in Mathematics **5**, 256 (1970).
- ²²J. T. MacDonald, J. H. Gibbs, and A. C. Pipkin, "Kinetics of biopolymerization on nucleic acid templates", Biopolymers **6**, 1 (1968).

- ²³T. Chou, "Kinetics and thermodynamics across single-file membrane channels", Physical Review Letters **80**, 85 (1998).
- ²⁴B. Widom, J. L. Viovy, and A. D. Defontaines, "Repton model of gel electrophoresis and diffusion", Journal de Physique I 1, 1759 (1991).
- ²⁵A. Schadschneider, D. Chowdhury, and K. Nishinari, *Stochastic transport in complex systems* (Elsevier, Amsterdam, 2011).
- ²⁶K. Nagel and M. Schreckenberg, "A cellular automaton model for freeway traffic", Journal de Physique I **2**, 2221 (1992).
- ²⁷P. Wagner, "How human drivers control their vehicle", European Physical Journal B 52, 427 (2006).
- ²⁸C. Arita and A. Schadschneider, "Exclusive queueing processes and their application to traffic systems", Journal of Statistical Mechanics: Theory and Experiment, Po7013 (2014).
- ²⁹M. Morandotti and F. Solombrino, "Mean-field analysis of multipopulation dynamics with label switching", SIAM Journal on Mathematical Analysis **52**, 1427–1462 (2020).
- ³⁰L. Ambrosio, M. Fornasier, M. Morandotti, and G. Savaré, "Spatially inhomogeneous evolutionary games", Communications on Pure and Applied Mathematics **74**, 1353–1402 (2021).
- ³¹B. Derrida, E. Domany, and D. Mukamel, "An exact solution of a one-dimensional asymmetric exclusion model with open boundaries", Journal of Statistical Physics **69**, 667–687 (1992).
- ³²B. Derrida, M. R. Evans, V. Hakim, and V. Pasquier, "Exact solution of a 1d asymmetric exclusion model using a matrix formulation", Journal of Physics A **26**, 1493 (1993).
- ³³J. Krug, "Boundary-induced phase transitions in driven diffusive systems", Physical Review Letters **67**, 1882 (1991).
- ³⁴J. Krug, "Phase separation in disordered exclusion models", Brazilian Journal of Physics **30**, 97 (2000).
- ³⁵J. Krug, "Particlewise disorder in exclusion processes", in *Traffic and granular flow '97*, edited by M. Schreckenberg and D. E. Wolf (Springer, Singapore, 1998), p. 285.
- ³⁶Z. Csahok and T. Vicsek, "Lattice gas model with quenched disorder", Journal of Physics A **27**, L591 (1994).
- ³⁷G. Tripathy and M. Barma, "Driven lattice gases with quenched disorder: exact results and different macroscopic regimes", Physical Review E **58**, 1911 (1998).
- ³⁸M. Bengrine, A. Benyoussef, H. Ez-Zahraouy, and F. Mhirech, "Asymmetric exclusion models with quenched disorder", Physics Letters A **253**, 135 (1999).
- ³⁹D. T. Gillespie, "Exact stochastic simulation of coupled chemical reactions", The Journal of Physical Chemistry **81**, 2340–2361 (1977).
- ⁴⁰D. ben Avraham and J. Köhler, "Mean-field (n, m)–cluster approximation for lattice models", Physical Review A **45**, 8358 (1992).
- ⁴¹A. Pelizzola and M. Pretti, "Cluster approximations for the tasep: stationary state and dynamical transition", European Physical Journal B **90**, 183 (2017).
- ⁴²A. Pelizzola, M. Pretti, and F. Puccioni, "Dynamical transitions in a one-dimensional Katz–Lebowitz–Spohn model", Entropy **21**, 1028 (2019).
- ⁴³D. Botto, A. Pelizzola, M. Pretti, and M. Zamparo, "Dynamical transition in the TASEP with Langmuir kinetics: mean-field theory", Journal of Physics A: Mathematical and Theoretical **52**, 045001 (2019).
- ⁴⁴M. Wölki, A. Schadschneider, and M. Schreckenberg, "Asymmetric exclusion processes with shuffled dynamics", Journal of Physics A **39**, 33 (2006).
- ⁴⁵A. Schadschneider and M. Schreckenberg, "Car-oriented mean-field theory for traffic flow models", Journal of Physics A **30**, L69 (1997).
- ⁴⁶A. Keßel, H. Klüpfel, J. Wahle, and M. Schreckenberg, "Microscopic simulation of pedestrian crowd motion", in *Pedestrian and evacuation dynamics*, edited by M. Schreckenberg and S. Sharma, check exact reference [1260] (Springer, 2001), p. 193.

- ⁴⁷M. Wölki, A. Schadschneider, and M. Schreckenberg, "Asymmetric exclusion processes with shuffled dynamics", Journal of Physics A **39**, 33 (2006).
- ⁴⁸D. A. Smith and R. E. Wilson, "Dynamical pair approximation for cellular automata with shuffled update", Journal of Physics A **40**, 2651 (2007).
- ⁴⁹A. B. Kolomeisky, "Asymmetric simple exclusion model with local inhomogeneity", Journal of Physics A: Mathematical and General **31**, 1153 (1998).